

# **INVESTIGATION OF VPS33B DEFICIENCY IN MOUSE AND MAN**

By

Holly Smith

A thesis submitted to  
The University of Birmingham  
for the degree of  
DOCTOR OF PHILOSOPHY

College of Medicine & Dentistry  
The University of Birmingham  
March 2012

UNIVERSITY OF  
BIRMINGHAM

**University of Birmingham Research Archive**

**e-theses repository**

This unpublished thesis/dissertation is copyright of the author and/or third parties. The intellectual property rights of the author or third parties in respect of this work are as defined by The Copyright Designs and Patents Act 1988 or as modified by any successor legislation.

Any use made of information contained in this thesis/dissertation must be in accordance with that legislation and must be properly acknowledged. Further distribution or reproduction in any format is prohibited without the permission of the copyright holder.

## **Abstract**

Arthrogryposis, renal dysfunction and cholestasis (ARC) syndrome is a severe multisystem disorder caused by mutations in *VPS33B* and *VIPAR*. A splice site mutation, VPS33B c.1225+5 G>C, was identified in a patient with attenuated ARC phenotype. Modelling of this mutation and missense mutations indicated that VPS33B-VIPAR interaction and co-localisation at recycling-endosome like structures is necessary for their function.

Development of a murine ARC model began with ubiquitous removal of Vps33b, and in parallel, its homologue Vps33a. Both resulted in embryonic lethality between E7.5 and E8.5.

A good ARC phenocopy was obtained the liver specific Vps33b knockout, *Vps33b<sup>fl/fl</sup>-AlpfCre*. Bile acid levels were increased in comparison to control and the apical proteins CEA and BSEP were mislocalised, with the distribution similar to that in ARC livers. In contrast, a *Vps33b<sup>fl/fl</sup>-Pf4Cre* mouse did not result in a good ARC platelet phenocopy, with  $\alpha$ -granules found present. They did however present with a mild platelet phenotype, with defects in stable aggregate formation under shear conditions and deficiencies in the  $\alpha$ -granule proteins VWF and PF4, giving possible insights into the bleeding diathesis in patients.

In conclusion, this work has produced suitable ARC models for further study of Vps33b function and provides a platform for the future development of gene therapy and drug treatments.

## **Acknowledgements**

I would firstly like to thank members of the Medical and Molecular Genetics Department and the Platelet Group at The University of Birmingham, particularly to the past and present members of the Gissen group: Ania Straatman-Iwanowska, Danai Bem, Christopher Bruce, Blerida Banushi and Andrew Cullinane for all of their help throughout my project. Thank you to Craig Hughes, Steve Thomas and Alex Borgognone for teaching me the techniques required for investigation of platelet function. I am also thankful to Paloma Garcia for her help with stem cell culture techniques. A big thank you also goes to Jenny Ullah, without whom the management of my project would not have been possible.

I would like to thank Paul Gissen and Steve Watson for supervising the project and their continued support throughout. I would also like to acknowledge the Medical Research Council for funding the research.

Finally, I would like to thank my family and friends for their constant encouragement and support.



## **Table of Contents**

<b>Abstract</b>	<b>I</b>
<b>Table of Contents</b>	<b>III</b>
<b>List of Figures</b>	<b>IX</b>
<b>List of Tables</b>	<b>IX</b>
<b>Abbreviations</b>	<b>X</b>
 <b>CHAPTER 1 - INTRODUCTION</b>	 <b>1</b>
<b>1.1 ARC syndrome</b>	<b>2</b>
<b>1.2 VPS33B and VIPAR</b>	<b>2</b>
<b>1.3 Cell polarity</b>	<b>3</b>
<b>1.4 Protein Transport</b>	<b>4</b>
<b>1.5 Protein Sorting</b>	<b>6</b>
1.5.1 Basolateral sorting motifs	8
1.5.2 Apical sorting motifs	9
1.5.3 PDZ motif	10
<b>1.6 Fusion of vesicles to the correct membrane</b>	<b>10</b>
1.6.1 Transport of vesicles – cytoskeleton and motor proteins	11
1.6.2 Tethering factors	13
1.6.3 SNARES	18
1.6.4 SM proteins	19
1.6.5 Rab proteins	22
<b>1.7 Apical junctional complexes</b>	<b>24</b>
1.7.1 Tight junctions	24
1.7.2 Adherens junctions	25
<b>1.8 The AJC and epithelial polarisation in ARC syndrome</b>	<b>28</b>
<b>1.9 Animal models of Vipar, Vps33b and its homologue Vps33a</b>	<b>30</b>
1.9.1 VPS33A models	31
1.9.2 VPS33B and VIPAR models	32
<b>1.10 The Liver</b>	<b>36</b>
1.10.1 The importance of hepatocyte polarity in liver development/function	38
1.10.2 Apical hepatocyte transporters	39

1.10.3 Cholestatic liver disease	40
1.10.4 ARC liver	42
<b>1.11 Platelets</b>	<b>46</b>
1.11.1 Platelet storage granules	47
1.11.2 $\alpha$ -granules and platelet function	51
1.11.3 Storage pool diseases linked to defective trafficking and vesicle fusion	52
1.11.4 ARC syndrome platelets	56
<b>1.12 Thesis Aims</b>	<b>59</b>
 <b>CHAPTER 2 – MATERIALS AND METHODS</b>	 <b>60</b>
<b>2.1 ARC-LOVD Database</b>	<b>61</b>
<b>2.2 Protein structure predictions of VPS33B and VIPAR</b>	<b>61</b>
<b>2.3 Patients and controls</b>	<b>61</b>
<b>2.4 Extraction of DNA from cells and tissue</b>	<b>62</b>
<b>2.5 Polymerase Chain Reaction (PCR)</b>	<b>62</b>
<b>2.6 Agarose gel electrophoresis</b>	<b>63</b>
<b>2.7 Sequencing of DNA</b>	<b>64</b>
2.7.1 Exo-SAP reaction	64
2.7.2 Sequencing reaction	65
2.7.3 Sample precipitation	65
2.7.4 Sequencing analysis	66
<b>2.8 RNA extraction</b>	<b>66</b>
<b>2.9 DNA and RNA quantification</b>	<b>67</b>
<b>2.10 RNA analysis</b>	<b>68</b>
2.10.1 Reverse Transcription	68
2.10.2 Sequencing of cDNA	69
<b>2.11 Techniques for identification of complex mutations</b>	<b>69</b>
2.11.1 Platinum Taq	69
2.11.2 Gel extraction	70
2.11.3 Long range PCR	70
2.11.4 Nested primers	71
2.11.5 3'-RACE	71
2.11.6 Quantitative Real-time PCR using genomic DNA	72
<b>2.12 Cloning of Vps33b cDNA for sequencing</b>	<b>74</b>
2.12.1 Ligation reaction	74

2.12.2 Bacterial transformation	74
2.12.3 Colony Selection	75
2.12.4 Miniprep	75
2.12.5 Sequencing a plasmid	76
2.12.6 Site Directed Mutagenesis	76
<b>2.13 Co-overexpression studies</b>	<b>77</b>
2.13.1 Cell Culture	77
2.13.2 Transfection	78
2.13.3 Fixation and staining	78
2.13.4 Immunofluorescence confocal Microscopy	78
<b>2.14 Protein extraction</b>	<b>79</b>
<b>2.15 Western Blotting</b>	<b>79</b>
2.15.1 Protein quantification	79
2.15.2 SDS-PAGE	80
2.15.3 Protein Transfer	81
2.15.4 Immunoblotting	82
2.15.5 Detection	82
2.15.6 Stripping and Re-probing	83
2.15.7 Densitometry	83
<b>2.16 Mouse strains</b>	<b>83</b>
<b>2.17 Animal Husbandry</b>	<b>84</b>
<b>2.18 Timed matings</b>	<b>85</b>
2.18.1 Embryo extraction and genotyping	85
2.18.2 Dissection of E7.5	86
2.18.3 Dissection of E8.5-9.5	86
<b>2.19 Establishing ES cell lines from blastocysts</b>	<b>86</b>
2.19.1 Mouse Embryonic Fibroblast (MEF) feeder cell preparation	86
2.19.2 E3.5 blastocyst extraction	87
2.19.3 ES cell culture	87
2.19.4 ES cell transfection with Cre-containing plasmid	88
<b>2.20 Analysis of Liver function</b>	<b>89</b>
2.20.1 Blood extraction for plasma protein analysis	89
2.20.2 Electrospray mass spectrometry of bile acids	89
2.20.3 Fixation and processing of liver samples	89
2.20.4 Immunohistochemistry	89
2.20.5 Immunofluorescent staining	90
<b>2.21 Analysis of platelets and megakaryocytes</b>	<b>91</b>
2.21.1 Megakaryocyte culture	91
2.21.2 Bleeding time tests	92
2.21.3 Platelet count and Mean Platelet Volume	93

2.21.4 Spleen measurement	93
2.21.5 Mouse platelet preparation	93
2.21.6 $\alpha$ -granule secretion analysis by Flow Cytometry	94
2.21.7 Aggregometry and dense granule secretion	94
2.21.8 <i>In vitro</i> flow assay	95
2.22.9 Platelet preparation for EM	96
 <b>CHAPTER 3 – ASSOCIATIONS AMONG GENOTYPE, CLINICAL PHENOTYPE AND INTRACELLULAR LOCALISATION OF TRAFFICKING PROTEINS IN ARC SYNDROME</b>	 <b>97</b>
<b>3.1 Introduction</b>	<b>98</b>
<b>3.2 Aims and methodology</b>	<b>99</b>
<b>3.3 Results</b>	<b>100</b>
3.3.1 ARC-LOVD Database Construction	100
3.3.2 New Variants	101
3.3.3 Database Analysis	103
3.3.4 Identification of patients with an attenuated ARC phenotype	105
3.3.5 Mutation identification in Patient AB	108
3.3.6 Mutation identification in Patient CD	109
3.3.7 Characterisation of the donor splice site mutation in Patient AB and Patient CD	111
3.3.8 Genotype-phenotype correlation, VPS33B-VIPAR complex formation	113
3.3.9 Interaction of VPS33B and VIPAR with the core HOPS complex protein VPS18	117
<b>3.4 Conclusions</b>	<b>119</b>
3.4.1 VPS33B and VIPAR co-localisation is disrupted when severe ARC phenotype mutations are modelled	119
3.4.2 Identification of an attenuated phenotype, and partial VPS33B-VIPAR co-localisation	119
3.4.3 VPS33B and VIPAR interaction with the HOPS complex protein, VPS18	120
 <b>CHAPTER 4 - VPS33A AND VPS33B MOUSE MODELS</b>	 <b>121</b>
<b>4.1 Introduction</b>	<b>122</b>
<b>4.2 Methodology - Developing Vps33a and Vps33b deficient mice</b>	<b>126</b>
<b>4.3 Results</b>	<b>128</b>
4.3.1 Ubiquitous <i>Vps33a</i> <sup>-/-</sup> and <i>Vps33b</i> <sup>fl/fl</sup> - <i>PgkCre</i> mice are embryonically lethal	128
4.3.2 Determining time-point of lethality	129
4.3.3 Isolation of embryonic stem cells from knockout blastocysts	135
<b>4.4 Discussion</b>	<b>135</b>
 <b>CHAPTER 5 - A LIVER-SPECIFIC VPS33B CONDITIONAL KNOCKOUT MOUSE</b>	 <b>140</b>

<b>5.1 Introduction and overview</b>	<b>141</b>
<b>5.2 Aims</b>	<b>141</b>
<b>5.3 Results</b>	<b>142</b>
5.3.1 Developing a liver-specific Vps33b conditional knockout mouse	142
5.3.2 <i>Vps33b<sup>fl/fl</sup></i> - <i>Alb</i> Cre liver function tests	143
5.3.3 Developing a second liver specific Vps33b conditional knockout mouse	145
5.3.4 <i>Vps33b<sup>fl/fl</sup></i> - <i>Alfp</i> Cre liver function tests	145
5.3.5 Localisation of liver proteins in <i>Vps33b<sup>fl/fl</sup></i> - <i>Alfp</i> Cre mice	147
<b>5.4 Discussion</b>	<b>150</b>
5.4.1 Is the <i>Vps33b<sup>fl/fl</sup></i> - <i>Alfp</i> Cre mouse a phenocopy of the ARC liver?	151
 <b>CHAPTER 6 - A MEGAKARYOCTYE AND PLATELET-SPECIFIC VPS33B CONDITIONAL KNOCKOUT MOUSE</b>	 <b>154</b>
<b>6.1 Introduction and overview</b>	<b>155</b>
<b>6.2 Methodology</b>	<b>156</b>
<b>6.3 Results</b>	<b>156</b>
6.3.1 Megakaryocyte Vps33b levels in <i>Vps33b<sup>fl/fl</sup></i> - <i>Pf4</i> Cre mice	156
6.3.2 Analysis of platelet count, volume and spleen size	157
6.3.3 Electron microscopy of platelets	159
6.3.4 Bleeding time test	159
6.3.5 Aggregation and dense granule secretion	164
6.3.6 Shear assay to assess thrombus formation under stress	166
6.3.7 Immunoblotting for the presence of α-granule proteins	168
<b>6.4 Discussion</b>	<b>170</b>
6.4.1 Characterisation of the platelets from <i>Vps33b<sup>fl/fl</sup></i> - <i>Pf4</i> Cre mouse	170
6.4.2 Development of the mouse model - a good model for ARC platelets?	172
6.4.3 Why a mild phenotype in <i>Vps33b<sup>fl/fl</sup></i> - <i>Pf4</i> Cre platelets?	172
 <b>CHAPTER 7 – DISCUSSION</b>	 <b>174</b>
<b>7.1 Development of an ARC-LOVD database provides a central resource for researchers and clinicians</b>	<b>175</b>
<b>7.2 Mutation analysis in <i>VPS33B</i> and <i>VIPAR</i> identifies a genotype-phenotype correlation</b>	<b>175</b>
<b>7.3 Vps33b and its homologue, Vps33a, are necessary for murine development</b>	<b>177</b>
<b>7.4 Use of <i>Alfp</i>-Cre for removal of Vps33b from murine liver results in a suitable ARC phenocopy</b>	<b>178</b>
<b>7.5 A megakaryocyte and platelet specific Vps33b conditional knockout mouse results in a mild α-granule defect</b>	<b>179</b>

<b>7.6 Future Experiments</b>	<b>180</b>
<b>7.7 Final thoughts</b>	<b>180</b>
<b>APPENDICES</b>	<b>182</b>
<b>APPENDIX 1</b>	<b>183</b>
Antibodies and dilutions used for immunoblotting	186
Antibodies and dilutions used for immunofluorescence microscopy	187
antibodies and dilutions used for immunohistochemistry	187
<b>APPENDIX 2</b>	<b>188</b>
<b>REFERENCES</b>	<b>189</b>
<b>MANUSCRIPTS AND PEER REVIEWED PAPERS</b>	<b>211</b>

## List of Figures

Figure 1.1 Planes of polarisation and an overview of protein trafficking in polarised epithelial cells	5
Figure 1.2 The location of tethering complexes in eukaryotic cells	14
Figure 1.3 Predicted CORVET and HOPS subunit composition and HOPS switching	17
Figure 1.4 SNAREpin formation and SM binding models	21
Figure 1.5 Molecular composition of tight and adherens junctions	27
Figure 1.6 Hepatocytes	37
Figure 1.7 Staining of apical proteins in control and ARC liver	45
Figure 1.8 Electron microscopy images of platelets	50
Figure 1.9 Immunofluorescence localisation of VPS33B with vesicle/organelle markers	58
Figure 3.1 ARC-LOVD database content analysis.	104
Figure 3.2 Patients with attenuated ARC syndrome.	107
Figure 3.3 Characterisation of the heterozygous deletion mutation in Patient AB	110
Figure 3.4 Characterisation of the heterozygous splice site mutation in Patient AB	112
Figure 3.5 VPS33B and VIPAR interaction	115
Figure 3.6 Ultrastructural localisation of VPS33B, VPS33B(c.1225+5G>C), VIPAR and VPS18 constructs	116
Figure 3.7 VPS33B and VIPAR interaction with VPS18	118
Figure 4.1 Murine <i>Vps33a</i> and murine <i>Vps33b</i> inactivation in the mouse germline.	127
Figure 4.2 E9.5 Morphology of <i>Vps33a</i> Embryos,	132
Figure 4.3 E9.5 Morphology of <i>Vps33b</i> Embryos,	134
Figure 4.4 Blastocyst outgrowth at 3 days after isolation.	Error! Bookmark not defined.
Figure 4.5 Murine development between E7-E9	130
Figure 5.1 <i>Vps33b<sup>fl/fl</sup></i> - <i>AlbCre</i> Liver characterisation	144
Figure 5.2 <i>Vps33b<sup>fl/fl</sup></i> - <i>AlfpCre</i> Liver characterisation	146
Figure 5.3 Immunohistochemical analysis of protein localisation in mouse liver	148
Figure 5.4 Immunohistochemical and immunofluorescent analysis of BSEP localisation in mouse liver	149
Figure 6.1 Immunoblot for <i>Vps33b</i> , platelet count, mean platelet volume and spleen mass	158
Figure 6.2 Ultrastructural analysis of platelets	160
Figure 6.3 Bleeding time test	161
Figure 6.4 Flow cytometry to assess P-selectin expression on the platelet membrane	163
Figure 6.5 Aggregation and dense granule secretion in response to thrombin and collagen	165
Figure 6.6 In vitro shear assay images and protein quantification	167
Figure 6.7 Immunoblotting and densitometry of $\alpha$ -granule proteins.	169

## List of Tables

Table 1.1 Summary of <i>Vps33a</i> , <i>Vps33b</i> and <i>Vipar</i> model organisms	35
Table 3.1 Novel Pathogenic <i>VPS33B</i> and <i>VIPAR</i> variants listed in ARC database	102
Table 4.1 Genotypes of offspring from <i>Vps33a<sup>+/-</sup></i> x <i>Vps33a<sup>+/-</sup></i> matings and offspring positive for <i>Pgk-Cre</i> from <i>Vps33b<sup>+/-</sup></i> x <i>Vps33b<sup>+/-</sup></i> - <i>PgkCre</i> matings.	128
Table 4.2 Genotypes of offspring from <i>Vps33a<sup>+/-</sup></i> x <i>Vps33a<sup>+/-</sup></i> timed matings.	131
Table 4.3 Genotypes of offspring from <i>Vps33b<sup>+/-</sup></i> x <i>Vps33b<sup>+/-</sup></i> - <i>PgkCre</i> timed matings.	133

## **Abbreviations**

AP	Adaptor Protein
ALT	ALanine Transaminase
AJC	Apical Junctional Complexes
ARC	Arthrogryposis, Renal dysfunction and Cholestasis
AST	ASpartate Transaminase
BEACH	Beige mouse, and Chediak Higashi syndrome
BSEP	Bile Salt Exporter Pump
BLOC	Biogenesis of Lysosome related Organelles Complex
CLIP-170	CAP-GLY domain containing Linker Protein 170
CEA	Carinoembryonic Early Antigen
CHS	Chediak Hiagshi Syndrome
CORVET	Class C cOre Vacuole/Endosome Tethering
COPI	Coatomer Protein Complex-I
COPII	Coatomer Protein Complex-II
CRE	Common Recycling Endosome
CCDS	Consensus CoDing Sequences
EE	Early Endosome
EM	Electron Microscopy
ER	Endoplasmic Reticulum
ECM	ExtraCellular Matrix
gGT	gamma-Glutamyl Transpeptidase
GPI	GlycoPhosphatidyl-Inositol
GPS	Grey Platelet Syndrome
HPS	Hermansky Pudlak Syndrome
HOPS	HOmotypic Protein Sorting
HEAT	Huntington, Elongation Factor 3, PR65/ATOR
IQGAP	IQ motif containing GTPase Activating Protein
JAM	Junctional Adhesion Molecules
LE	Late Endosome
LDLR	Low Density Lipoprotein Receptor
LYST	LYSosomal Trafficking regulator
MDCK	Madin Darby Canine Kidney cells
MT	microtubule
MVB	Multi Vesicular Bodies
MDR1	MultiDrug Resistance protein 1
MDR2	MultiDrug Resistance protein 2
MDR3	MultiDrug Resistance protein 3
MRP2	MultiDrug Resistance-associated Protein 2
MRP3	Multidrug Resistance-associated Protein 3



MRP4	Multidrug Resistance-associated Protein 4
NHERF-1	Na <sup>+</sup> /H <sup>+</sup> exchanger regulatory factors-1
NSF	N-ethylmaleimide Sensitive Fusion
OATP	Organic Anion Transporting Polypeptide
OCT1	Organic Cation Transporter
PDZ	postsynaptic density protein PSD-95/SAP-90, Disc-large DLG and zona occludens ZO-1
Pgk	Phosphoglycerate kinase
ATP8B1	phospholipid-transporting ATPase IC
PM	Plasma Membrane
PF4	Platelet Factor 4
+TIPs	plus-end-tracking protein
LLC-PK1	porcine kidney epithelial cells
PFIC	Progressive Familial Intrahepatic Cholestasis
WIF-B9	rat hepatoma/human fibroblast hybrid cells
SM	Sec1/Munc18
NTCP	Sodium/Taurocholate Co-transporting Peptide
SNARE	Soluble NSF Attachment protein Receptors
$\alpha$ SNAP	Soluble NSF attachment proteins
SPE-39	SPERMATogenesis defective 39
TJ	Tight Junction
TGN	Trans-Golgi Network
VPS33B	Vacuolar Protein Sorting-associated protein 33B
VSV-G	vesicular stomatitis virus G-protein
VWF	von Willebrands Factor
VIPAR	VPS33B Interacting Protein, Apical-basolateral polarity Regulator

# **CHAPTER 1 - INTRODUCTION**

### **1.1 ARC syndrome**

Arthrogryposis, Renal dysfunction and Cholestasis (ARC) syndrome (MIM 208085) is an autosomal recessive multisystem disorder caused by mutations in *VPS33B* (Vacuolar Protein Sorting-associated protein 33B) and *VIPAR* (VPS33B Interacting Protein, Apical-basolateral polarity Regulator)(Gissen et al. 2004)(Cullinane et al. 2010). The first cases of ARC syndrome were reported in 1973 and 1979 by Lutz-Richner and Landolt, and Nezelof et al. (Lutz-Richner & Landolt 1973)(Nezelof et al. 1979). ARC syndrome patients characteristically present with neonatal cholestatic jaundice, renal tubular acidosis, variable degree of joint contractures and a severe failure to thrive (Gissen et al. 2006). Most patients fail to survive past the first year of life despite medical intervention as a result of recurrent infections leading to dehydration and acidosis (Abu-Sa'da et al. 2005). Other features include ichthyosis- dry scaly or flaky skin, a platelet  $\alpha$ -granule storage defect (Deal et al. 1990) and mild dysmorphic features such as large hands, low set ears and sloping forehead. Corpus callosum dysgenesis (at least 20%), cardiac defects and deafness have also been reported (Gissen et al. 2006).

### **1.2 VPS33B and VIPAR**

Mutations in *VPS33B* and *VIPAR* have been found to be causative for ARC syndrome (Gissen et al. 2004)(Cullinane et al. 2010). VPS33B is a 617 amino acid protein containing a Sec1-like domain spanning the entire protein (Carim et al. 2000). It is a member of the Sec1/Munc18 (SM) family of proteins, which are known to directly interact with SNAREs (Soluble NSF Attachment protein Receptors) and aid SNARE complex formation leading to tethering and fusion of organellar membranes (Gallwitz & Reinhard Jahn 2003).

*VIPAR* has 2 protein coding sequences within the Consensus CoDing Sequences (CCDS) database (<http://www.ncbi.nlm.nih.gov/CCDS/CcdsBrowse>), resulting in proteins of 480 or 493 amino acids in size, and contains a golgin A5 domain in the C-terminal domain identified using the Pfam database. Golgins were originally identified as golgi-localised proteins (Fritzler et al. 1993) which contain a shared rod-like motif containing long coiled-coil regions (Burkhard et al. 2001). They are responsible for structural support of the golgi cisternae and have also been shown to be involved in membrane tethering (Barr & Short 2003). They are proposed to allow the movement of vesicles through the golgi by a series of tethering and release events (Sinka et al. 2008). They carry out this function by interacting with Rabs (Hayes et al. 2009)(Yu & Hughson 2010), small GTPases involved in intracellular trafficking, discussed in section 1.6.5.

In ARC syndrome it has been found that apical proteins in polarised epithelial cells, such as Bile Salt Exporter Pump (BSEP) and CarcinoEmbryonic Antigen (CEA) within hepatocytes, are mislocalised (Gissen et al. 2004)(Cullinane et al. 2010). Additionally, further defects involved in cell polarity have been identified. In order to understand why in ARC syndrome a deficiency in VPS33B or *VIPAR* may cause the phenotype observed, and how it is the hope to determine this by developing a model organism, cell polarity and protein trafficking must first be understood.

### **1.3 Cell polarity**

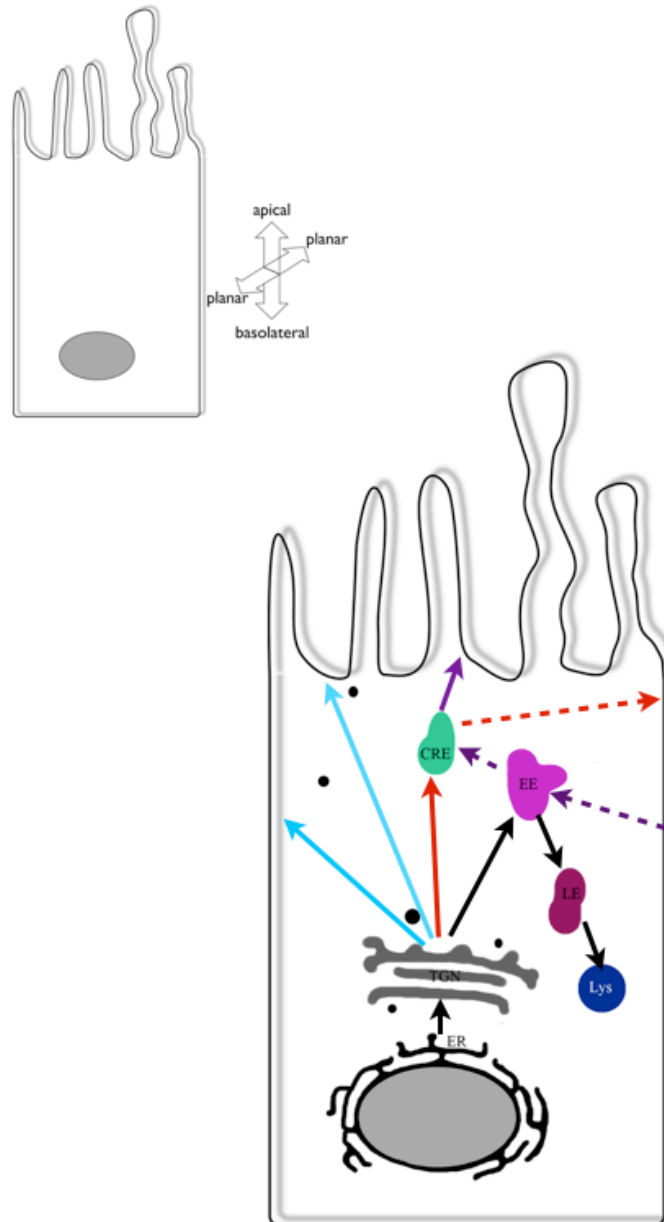
Cell polarity is the ability of cells to maintain an asymmetric distribution of molecules in order to confine specific activities to distinct areas of the cell (Carmosino et al. 2010). For example, in the liver it is necessary for hepatocytes to be polarised in order to produce and excrete bile. The apical membrane forms the bile canaliculi and is modified specifically for

bile constituent excretion. The lateral surfaces contact one another forming junctional complexes (adherens and tight) to provide a barrier between the blood and bile, and the basal membrane contacts the blood for uptake of many different molecules such as cholesterol, removal of which is required to prevent accumulation of cholesterol in the body and to produce bile.

Within polarised cells there exists two planes of polarisation (figure 1.1), planar cell polarity (Axelrod 2009) not discussed here, and perpendicular to this, apical-basolateral polarity. There are complex mechanisms responsible for establishment of apical-basolateral cell polarity, and many layers of regulation are required. Proteins must be correctly targeted to the relevant membrane within specific vesicles, the membrane domains must be defined in order for the vesicles to reach their destination, and extrinsic cues must be received in order for the cell to be orientated in the correct manner (Mellman & Nelson 2008).

#### **1.4 Protein Transport**

Transport of proteins through the epithelial cell requires careful regulation in order for the cell to function correctly and maintain apical-basolateral polarity. Major breakthroughs in protein transport were made by George E. Palade for which he received a Nobel Prize in 1974 (Palade 1975). The aim of his work was to identify and discern the function of the tiny structures within cells. Palade developed an in vivo autoradiographic technique suitable for electron microscopy (EM) (Caro & Palade 1964). The synthesis, intracellular transport, storage and secretion of proteins in the guinea pig was studied by injecting a DL-leucine-4,5- $H^3$  label, which was integrated into newly synthesised proteins. By fixing the pancreas at time-points



**Figure 1.1 Planes of polarisation and an overview of protein trafficking in polarised epithelial cells**

There exists 2 planes of polarisation within an epithelial cell, planar and apical-basolateral polarity.

Newly synthesised proteins undergo folding in the endoplasmic reticulum (ER), and are transported to the trans-Golgi network (TGN) where post-translational modifications occur. From the TGN proteins may be trafficked directly to apical and basolateral surfaces (blue arrows), sorted to the correct membrane in common recycling endosomes (CRE), or undergo transcytosis from the basolateral to apical surfaces (purple arrows). Proteins destined for degradation traffic through early and late endosomes (EE and LE) to the lysosomes (Lys)

Adapted from (Schuck & Simons 2004)

ranging from 5 minutes to 15 hours, protein progression through the pancreatic exocrine cells was observed. This work led to a model of the secretory process, which holds strong today. Along with work from other groups organelles and vesicles involved in protein transport within polarised cell have been characterised (figure 1.1).

### **1.5 Protein Sorting**

Within cells there are 3 major sites of protein sorting: the golgi, endosomes and the plasma membrane (PM)(Mellman & Nelson 2008). Intermediate vesicles which allow transport between these structures are formed by Coatamer Protein Complex-I (COPI) and Coatamer Protein Complex-II (COPII) originally identified in yeast, responsible for golgi-ER and ER-golgi transport respectively (Novick et al. 1980)(Hosobuchi et al. 1992)(Lee et al. 2004). Additionally, the Adaptor Protein (AP)-clathrin complexes, first identified in 1969 in guinea pig brain synaptosomes (Kanaseki & Kadota 1969), are a major component of protein sorting responsible for transport between golgi, endosomes and plasma membrane. These coat proteins are recruited to the donor membrane, select specific cargo for the vesicle and form a scaffold which allows the vesicles to bud from the donor membrane, the coat is then shed (Robinson 2004). The complexes are ubiquitous to all cells, however polarised cells have further adapted to allow sorting of proteins to different membrane domains. One adaptor protein, AP-1B, identified within polarised cells is definitively involved in the sorting of proteins to the basolateral membrane (Ohno et al. 1999).

AP-complexes are heterotetramers and together with other proteins recognise and bind specific protein motifs allowing the sorting and correct targeting of proteins. There have been 4 AP-complexes identified to date, AP-1 to AP-4. AP complexes 1-4 are composed of 2 large

subunits ( $\gamma$ ,  $\alpha$ ,  $\delta$ , and  $\epsilon$  respectively) and  $\beta$ 1-4, a medium-sized  $\mu$  subunit and a small  $\sigma$  subunit (Robinson & Bonifacino 2001). The AP complex subunits are collectively known as adaptins. The  $\mu$  adaptin subunits promote protein sorting by binding to tyrosine-based or di-leucine based peptide sorting motifs (Nakatsu & Ohno 2003).

AP-1B an epithelial cell-specific variant of AP-1 contains a  $\mu$ 1B subunit in the place of the ubiquitous  $\mu$ 1A subunit. In the first study carried out to determine the role of AP-1B, porcine kidney epithelial (LLC-PK1) cells were used as they do not express the subunit  $\mu$ 1B (Fölsch et al. 1999). It was found that Low Density Lipoprotein Receptor (LDLR) was localised in the apical membrane in these cells but in the basolateral membrane in Madin Darby Canine Kidney (MDCK) cells. When  $\mu$ 1B was stably introduced into the LLC-PK1 cells, LDLR localisation was then restricted to the basolateral membrane. The same observation was made with the transferrin receptor, another basolateral PM protein, indicating that AP-1B plays a critical role in the targeting of proteins to the basolateral membrane (Fölsch et al. 1999). An AP-1B deficient mouse was created by the knockout of *Ap1m2*. This mouse developed spontaneous chronic colitis and was found to have defects in trafficking of cytokine receptors in the gut epithelial cells, with them being mistargeted to the apical instead of the basolateral membrane (Takahashi et al. 2011), thus supporting results from studies using cell lines. Hepatocytes do not express the epithelial specific variant of AP-1 in higher mammals, instead appearing to sort their proteins at multivesicular bodies and the basolateral membrane rather than the TGN, adding an extra layer of complexity to the understanding of apical-basolateral polarity establishment and maintenance (Matter & Mellman 1994)(Ohno et al. 1999).

Mutations in AP-3 have been found to cause Hermansky Pudlak Syndrome (HPS), a rare autosomal recessive disorder characterised by oculocutaneous albinism and bleeding problems due to a dense granule storage disease (Dell'Angelica et al. 1999) discussed in section 1.11.3.



AP-3 has also been found to interact with HOMotypic Protein Sorting (HOPS) complex proteins in yeast (Angers & Merz 2009). There is ongoing debate as to whether VPS33B and VIPAR, deficiencies of which cause ARC syndrome, form part of the mammalian equivalent of the HOPS complex, discussed in section 1.6.2 and 1.9, which has also been shown to interact with AP-3 (Zlatic et al. 2011).

### **1.5.1 Basolateral sorting motifs**

In 1986, Mostov et al. found that by deleting a motif on polymeric immunoglobulin-A receptor, the basolateral protein was mislocalised to the apical membrane (Mostov et al. 1986). Subsequently, in 1991 they found that if this motif was transferred to apically localised proteins they would be mislocalised to the basolateral membrane (Casanova et al. 1991). Specific basolateral motifs were eventually identified and were found to be very similar to endocytic motifs (Weisz & Rodriguez-Boulant 2009). Motifs recognised by clathrin adaptors and AP-complexes include tyrosine, leucine or di-leucine based sorting motifs found on cytoplasmically exposed regions (Fölsch et al. 2009). Basolateral sorting signals are normally dominant over apical sorting signals (Matter & Mellman 1994), therefore in most cases a basolateral signal must be absent in order for proteins to be trafficked apically.

### **1.5.2 Apical sorting motifs**

Apical sorting is complex and has proven more difficult to elucidate than basolateral sorting. Proteins are either trafficked directly (vectorial route) to the apical membrane (Weisz & Rodriguez-Boulan 2009), or indirectly via the basolateral membrane (transcytotic route) (Bonilha et al. 1997). Apical sorting signals may be contained within any of the domains of the protein; cytoplasmic, membrane or luminal domains and the sorting signal within the protein is contributed to by the lipid, carbohydrate or protein components (Fölsch et al. 2009). Examples of known apical sorting signals include O- and N- glycans, which are added post-translationally to the extracellular domains of proteins. They are important in targeting of these proteins to the apical membrane (Vagin et al. 2009). For example, the removal of N-glycans from BSEP significantly decreased its abundance within the apical membrane (Mochizuki et al. 2007). Also, the addition of N-glycans to endoplasmic reticulum (ER)- or basolaterally-localised proteins was shown to redistribute the modified proteins to the apical membrane (Vagin et al. 2009). A second group of apical targeting signals first characterised in the 1980's by Ferguson and Williams (Ferguson & Williams 1988) is the GlycosylPhosphatidyl-Inositol (GPI) anchor. It is a post-translational modification, located at the C-terminus of proteins (Paulick & Bertozzi 2008). This modification anchors proteins to the outer leaflet of the plasma membrane, and since many GPI-anchored proteins are apically located it has been proposed as an apical-targeting signal. Addition of this modification onto secreted proteins resulted in an apical localisation (Lisanti et al. 1989).

### **1.5.3 PDZ motif**

In addition to apical and basolateral sorting signals contained within proteins, there are also components which allow retention within the membrane. PDZ proteins (their name deriving from the first three proteins in which this domain was identified; postsynaptic density protein PSD-95/SAP-90, Disc-large DLG and zona occludens ZO-1 (Kennedy 1995)) anchored at the target membrane contain PDZ domains. These domains recognise 5 amino acid motifs usually found at the C-terminus of proteins destined for the apical or basolateral membrane (Brône & Eggermont 2005). Interaction of the PDZ protein with the 5 amino acid motif allows the trafficked protein to be retained at the target membrane. PDZ proteins may be specifically located at the apical or basolateral membrane, for example the PDZ protein, Na<sup>+</sup>/H<sup>+</sup> exchanger regulatory factors-1 (NHERF-1), is located at the apical brush-border of epithelial cells and affects membrane expression and localisation of its interacting proteins including a wide range of ion channels and transporters such as Npt2 (Brône & Eggermont 2005). In *NHERF-1*<sup>-/-</sup> mice, Npt2, normally apically located in renal proximal tubule cells, is instead found in intracellular vesicles reducing expression in the membrane resulting in a phosphate wasting phenotype (Shenolikar et al. 2002).

### **1.6 Fusion of vesicles to the correct membrane**

Sorting of apical and basolateral membrane proteins into vesicles at the TGN and the recycling endosome is the first step necessary to get proteins to their target membrane. The vesicles must be coupled to a movement mechanism, to physically transport them to their target membrane. In addition to this they require fusion machinery at the membrane to allow them to dock and fuse at the correct location. Movement is mediated by the cytoskeleton and

motors. Docking and fusion is mediated by tethering factors, Soluble NSF Attachment protein (SNAP) REceptors, SNAREs, small Rab GTPases and Sec1/Munc18 family members.

### **1.6.1 Transport of vesicles – cytoskeleton and motor proteins**

In order to be transported throughout the cell, vesicles must rely on motor proteins to tether them to and transport them along the microtubules and actin filaments. In 1994 it was demonstrated that microtubule motors were required for both apical and basolateral transport within MDCK cells (Lafont et al. 1994). Previous to this it was believed that transport to the basolateral membranes occurred by diffusion and was microtubule and actin independent (Rindler et al. 1987). Cells were treated with a drug that causes depolymerisation of microtubules, Nocodazole, and apical and basolateral trafficking was measured by monitoring levels of Hemagglutinin and vesicular stomatitis virus G-protein (VSV-G) respectively. Transport of both was blocked by Nocodazole treatment.

The majority of microtubules (MTs) form small oligomers (nucleate) and then rapidly extend from microtubule organising centres (MTOCs) and centrosomes. In non-polarised cells such as fibroblasts they remain anchored here (Mellman & Nelson 2008). In epithelial cells however, most MTs align along the apical-basolateral axis of the cell, with the slow-growing minus end towards the apical domain, and the fast growing plus-end towards the basolateral (Müsch 2004). Microtubule-based transport to both the apical and basolateral membranes is dependent on different motors. Kinesins typically traffic towards the fast-growing plus-end at the basolateral membrane, and dyneins towards the minus-end and thus target the apical membrane (Li & Gundersen 2008). For example, transport of rhodopsin-bearing vesicles in photoreceptors within the eye utilises a dynein light-chain, Tctex-1, which interacts with the

C-terminus of the transmembrane protein rhodopsin for trafficking to the apical membrane (Tai et al. 1999).

Actin filaments have also been implicated in vesicle movement, but are shorter than microtubules. They are composed of G-actin monomers which polymerise in a polarised manner, with growth more rapid at the plus-end (Li & Gundersen 2008). Myosins are involved in vesicle trafficking along actin filaments through their tail domains, and Myosin I, II, V and VI are the most important in trafficking within polarised epithelial cells (Durrbach et al. 2000)(Au et al. 2007)(Müller et al. 2008). Myosin II regulatory light chain for example was identified in a yeast two-hybrid screen of rat liver as a binding partner for BSEP, MultiDrug Resistance protein 1 (MDR1) and MultiDrug Resistance protein 2 (MDR2)—proteins found in the apical membrane of hepatocytes (Chan et al. 2005). It was shown that by blocking myosinII with Blebbistatin, a compound that stabilises myosinII in an actin detached state, newly synthesised BSEP appearance at the apical surface was significantly impaired, suggesting that myosinII is required for its trafficking to the apical membrane.

Filamentous actin forms a sheet underneath the plasma membrane in eukaryotic cells, known as the actin cortex, and is dense enough to restrict vesicles from the plasma membrane. Capture of microtubules at the cortex, referred to as cortical capture, results in the stabilisation of microtubules (Li & Gundersen 2008). Proteins are present at this juncture which link microtubules and actin to allow vesicle transfer from one to the other and subsequent transport to the PM (Watanabe et al. 2004). Proteins involved include plus-end-tracking protein (+TIPs) proteins which bind to the + ends of microtubules such as CAP-GLY domain containing linker protein 170 (CLIP-170), and proteins associated with the actin cortex such as IQ motif containing GTPase activating protein (IQGAP), an essential protein for cytoskeleton reorganisation (Briggs & Sacks 2003). IQGAP1 interacts directly with

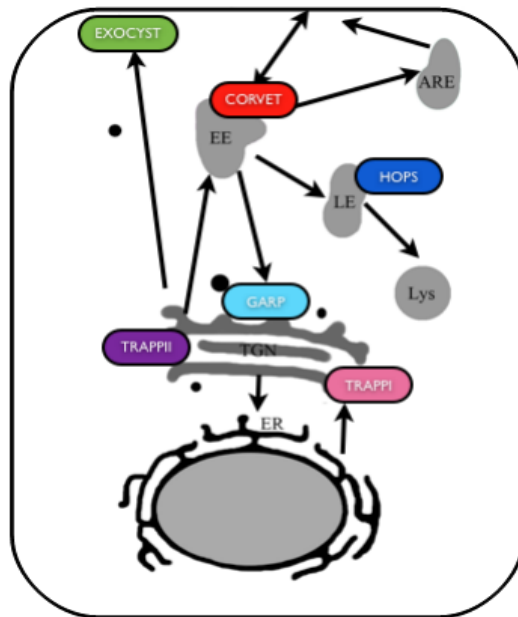
[12]

Adenomatous Polyposis Coli (APC) linking it to the actin cortex, and together they are required for the formation of a complex with CLIP-170. CLIP-170 is a +TIP, and interaction with IQGAP1 allows the capture of microtubules providing a link between the cortical actin and microtubules.

Once vesicles have been transported to the correct destination the next important step is for the recognition of cargo at the recipient end. A multitude of different factors are involved, beginning with tethering factors.

### **1.6.2 Tethering factors**

Before vesicles come into contact with their target membrane and undergo SNARE mediated fusion, tethering factors may act as an initial connection and act as facilitators of membrane recognition (Sztul & Lupashin 2006). In vitro reconstitution of SNARE-mediated vesicle fusion is slow (Ohya et al. 2009) and SNARE complex assembly has been shown to be accelerated by tethering factors (Shorter et al. 2002). This may be due to some vesicles arriving with their coats intact possibly obscuring SNAREs and therefore requiring another mode for tethering (Zink et al. 2009). Tethers are able to interact with Rab GTPases to capture vesicles before SNARE action (Behnia & Munro 2005). Tethering factors fall into 2 categories: long coiled-coil tethers and multiprotein complexes (Yu & Hughson 2010).



**Figure 1.2 The location of tethering complexes in eukaryotic cells**

The location of multisubunit tethering complexes involved in vesicle trafficking are shown. CORVET- class C core vacuole/endosome tethering complex, GARP - Golgi-associated retrograde protein complex, HOPS- homotypic fusion and vacuole protein sorting (or class C vacuolar protein sorting) complex, TRAPP- transport protein particle.

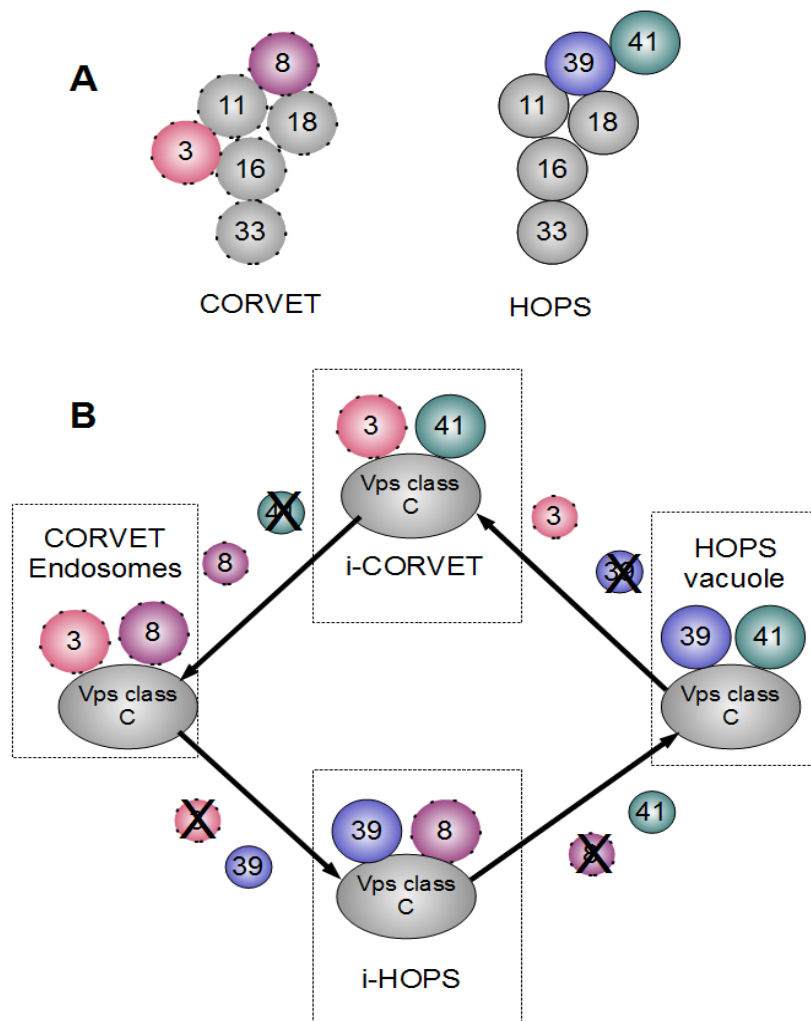
Adapted from (Yu & Hughson 2010)

Coiled-coil tethers, including golgins, are characterised by long regions of homodimeric, parallel coiled-coil motifs forming long, extended rod-like structures (Burkhard et al. 2001). This structure allows coiled-coil tethers to bridge the gap between membranes, and their role is demonstrated by the p115 and cis-Golgi matrix protein (GM130) model. In vitro and in vivo studies suggest a critical role for P115 in tethering or fusion (Waters et al. 1992)(Seemann et al. 2000)(Yu & Hughson 2010). It resides on COPI vesicles and binds GM130 found on cis-golgi (Sönnichsen et al. 1998). It is proposed that p115 binds GM130, linking COPI vesicles to golgi elements in order to facilitate fusion (Sztul & Lupashin 2006). Blocking P115 or GM130 function resulted in defective trafficking of VSV-G from ER to golgi (Seemann et al. 2000).

Tethering multiprotein complexes act at specific locations (Figure 1.2), for example the HOMotypic fusion and vacuole Protein Sorting (HOPS) and Class C core vacuole/endosome tethering (CORVET) complexes in yeast act at the vacuole and endosomes respectively. The core protein components of these complexes were first identified due to a loss of vacuole in yeast (Raymond et al. 1992)(Wada et al. 1992) and these complexes are essential for the biogenesis and maturation of late endosomes and vacuoles (Nickerson et al. 2009). Through in vitro reconstitution of proteolysosomes resembling vacuoles, it has been shown that HOPS is required for tethering and fusion of these vesicles, its action dependent on the presence of a combination of Ypt7- a Rab GTPase and SNARE proteins (Wickner 2010).



In yeast, HOPS and CORVET complexes contain a common set of 4 class C Vps genes originally identified in yeast mutants without vacuoles, Vps11, Vps16, Vps18 and Vps33 (Raymond et al. 1992)(Wada et al. 1992). These complexes are of particular interest as VPS33B and VIPAR are homologues of yeast Vps33 and Vps16 respectively, core components of HOPS and CORVET complexes. In yeast, the HOPS and CORVET complexes are well defined, each complex contains 2 additional proteins, Vps39 and Vps41 in the HOPS complex and Vps3 and Vps8 in the CORVET complex (Seals et al. 2000)(Peplowska et al. 2007). The organisation of proteins within the HOPS complex in yeast has been investigated and its predicted composition detailed (Figure 1.3A)(Ostrowicz et al. 2010)(Plemel et al. 2011). Peplowska et al. have found that the HOPS and CORVET complexes are able to convert into one another via intermediates of these complexes in a directed manner, and thus suggests a link to organelle identity and Rab GTPase switching (Figure 1.3B)(Peplowska et al. 2007). In metazoans the HOPS complex is less well defined, and an equivalent to the CORVET complex is yet to be reported. In metazoans there are 2 homologues of the yeast HOPS and CORVET core protein Vps33 which in humans share 51% similarity, designated VPS33A and VPS33B (Gissen et al. 2005). Vps33a and Vps33b animal models, discussed in section 1.9, have presented different phenotypes with protein function shown to be non-redundant thus implying they are required at different trafficking steps. Yeast Vps16 also contains 2 homologues in metazoans, in humans known as VPS16 and a more distant homologue VIPAR. It has been found in *Drosophila* (Pulipparacharuvil et al. 2005) and human embryonic kidney (HEK293) cells (Cullinane et al. 2010) that Vps33a interacts with Vps16a and not Vps16b, and Vps33b interacts with Vps16b (VIPAR in humans) but not Vps16a. In *C. elegans*, this was found not to be the case as Spe-39 was found to interact with both Vps33b and Vps33a (Zhu et al. 2009). The interactions of these proteins



**Figure 1.3 Predicted CORVET and HOPS subunit composition and HOPS switching**

- A. Predicted HOPS and CORVET subunit interactions determined by a combination of co-immunoprecipitation and yeast-2-hybrid experiments. Adapted from (Ostrowicz et al. 2010)(Plemel et al. 2011)
- B. A model for the conversion of the multisubunit complexes HOPS and CORVET and their intermediates, iHOPS and iCORVET suggesting that these complexes are dynamic. Adapted from (Peplowska et al. 2007)

with other HOPS and CORVET complex proteins remains poorly defined, however in *Drosophila* it was found that Vps33a interacts with a homologue of Vps18, Dor, suggesting that Vps33a might form part of the metazoan HOPS complex (Sevrioukov et al. 1999).

### 1.6.3 SNARES

In the 1980's Novick and Schekman identified the first SNARE proteins: Sec17, Sec 20 and Sec22, using temperature sensitive *Saccharomyces cerevisiae* trafficking mutants (Novick et al. 1980). SNAREs are a superfamily consisting of 36 members in humans and 25 in yeast (Jahn & Scheller 2006). SNARE proteins contain a conserved motif of 60-70 amino acids made up of heptad repeats (Kloepper et al. 2007). These motifs form coiled-coils of 4  $\alpha$ -helices and are classified according to which conserved amino acid they have within the central '0' layer, either 1 of 3 glutamine residues (Qa-, Qb- or Qc-) or an arginine residue (R-) (Bock et al. 2001). Q-SNAREs are predominantly found on the target membrane and thus used to be known as t-SNAREs, R-SNAREs on the vesicle and were otherwise known as v-SNAREs. One of each of the 4 classifications of SNARE are required to form a hetero-oligomeric trans-SNAREpin which provides the energy to allow fusion of vesicles (Figure 1.4A) (Südhof & Rothman 2009). One SNARE complex has been shown to be sufficient for membrane fusion (van den Bogaart et al. 2010) In 1996 it was found that N-ethylmaleimide Sensitive Fusion (NSF) protein and Soluble NSF Attachment Protein ( $\alpha$ SNAP) were required for recycling of SNAREs, allowing dissociation of SNAREpins thus priming SNAREs for the next round of binding, but were not required for docking or fusion (Mayer et al. 1996). In 1993, Sollner and Rothman introduced the SNARE hypothesis suggesting that SNAREs were sufficient to confer specific binding (Söllner et al. 1993). However, it was subsequently found

in a series of studies that binding of vesicles was much more promiscuous and other factors must be involved (Waters & Hughson 2000).

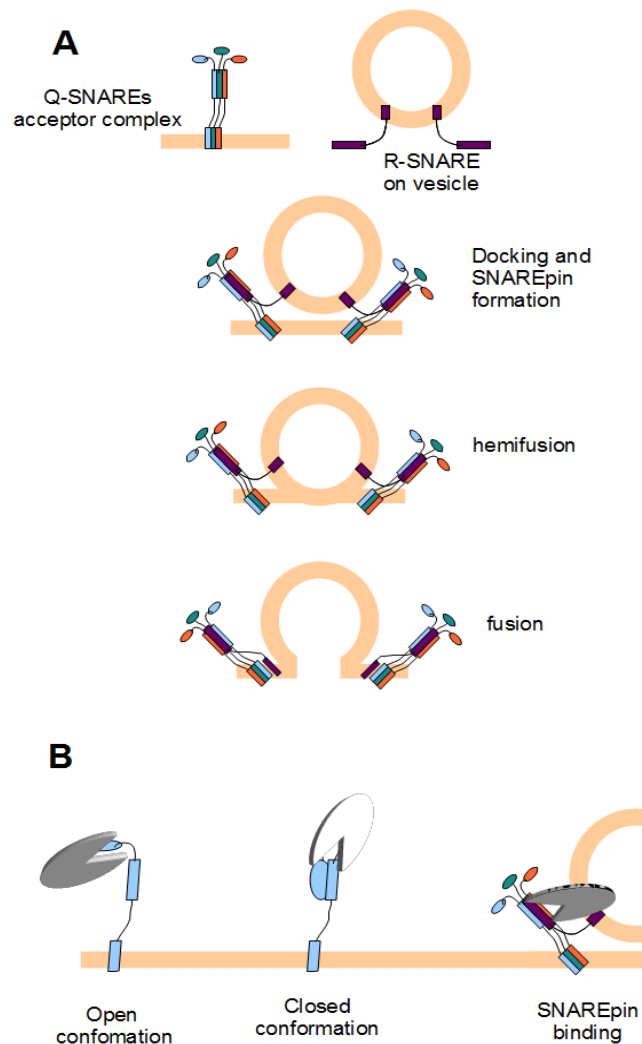
Specific apical and basolateral localisation of Q-SNAREs are critical for polarity. Syntaxin 3 is found on the apical membrane and syntaxin 4 on the basolateral membrane in all cell types (Low et al. 1996) (Weimbs et al. 1997). When syntaxin 3 was mislocalised by altering its apical targeting FMDE motif (named after the first 4 amino acids) in the N-terminal domain, it was found that syntaxin 3 was localised in both the apical and basolateral membranes in MDCK cells (Sharma et al. 2006). As a result of this, p75, an apical membrane protein was found in the basolateral membrane of mutants, indicating that syntaxin 3 allows the p75-positive vesicle to become fusion competent. Overall epithelial polarity was also affected and this was tested by monitoring trans-epithelial electrical resistance (TEER) - a measure of tight junction reformation after reintroduction of calcium to cells growing in calcium free media. The TEER peak, an indication of tight junction formation, was delayed by approximately 10 hours. Wild type MDCK cells grown in 3D culture form cysts, with the apical membrane facing a single lumen. In syntaxin3 knockdown cells, tight junctions could not be detected and a lumen did not form giving a tumour-like structure. This indicates that syntaxin3 plays an important role in apical-basolateral polarity and SNAREs may contribute to fusion specificity (Sharma et al. 2006).

#### **1.6.4 SM proteins**

VPS33B is a member of the Sec1/Munc18 (SM) family of which there are seven SM family proteins in vertebrates. Their structure is highly conserved, consisting of 3 domains making an arched shape protein with a cavity on one side and a groove on the other, both of which have been implicated in SNARE interaction (Misura et al. 2000). SM proteins have been

shown to bind individual Q-SNAREs, for example when bound to its cognate SM protein Tlg2p adopts a closed conformation preventing SNAREpin formation (Furgason et al. 2009), suggesting a negative regulatory role for SM proteins. However it has also been shown that SM proteins are as important as SNAREs in membrane fusion events with deletion of Munc18-1 blocking exocytosis at synapses (Verhage et al. 2000) and has more severe consequences than deleting its interacting SNAREs, synaptobrevin or SNAP-25. This suggests that the role of SM proteins is not purely inhibitory but that they also have an important stimulatory role. This is confirmed by many studies including a multitude of different organisms showing that a loss of function of SM proteins leads to an accumulation of vesicles (Novick & Schekman 1979)(Hosono et al. 1992)(Harrison et al. 1994). SM proteins have been found to interact via their N-terminus with an N-terminal peptide sequence within syntaxins (Yamaguchi et al. 2002). In this way the SM proteins are able to bind to the open conformation of the syntaxin but leave the arch-shaped part of the protein to bind to the SNAREpin (figure 1.4B) (Dulubova et al. 2007).

Studies in *S. cerevisiae* indicate that the role of SM proteins in vesicle fusion go further than SNAREpin formation. A wide range of sec1 mutants were constructed using site-directed mutagenesis and random mutations (Hashizume et al. 2009). The mutants could be separated into 2 groups depending on their phenotype. Group 1 mutants did not form SNARE complexes or fuse suggesting a role for Sec1p in vesicle docking and SNAREpin formation. The second group were able to dock and form SNAREpins, however the vesicles could not fuse, suggesting a role for SM proteins in vesicle fusion. Supporting findings were made when Vps33p in yeast was found to be required for pore opening, the last stage of vesicle fusion, after the hemifusion of vesicle membranes (Pieren et al. 2010). Vacuoles isolated from yeast were found to maintain 70% of the lipid mixing activity but only 6% of content mixing



**Figure 1.4 SNAREpin formation and SM binding models**

- A. 3 Q-SNAREs on a target membrane come into contact with an R-SNARE on a vesicle. The vesicle is able to dock through loose interaction of the Q-SNAREs with the R-SNARE. These are then able to ‘zip-up’ to form a tight SNARE-pin, and mixing of the membranes- ‘hemifusion’, and pore opening- ‘fusion’ may then occur. Adapted from (Jahn & Scheller 2006).
- B. SM proteins have been found to bind Q-SNAREs in an open conformation thought to aid SNAREpin formation or less commonly in a closed conformation. SM proteins also bind the SNAREpin. Adapted from (Südhof & Rothman 2009)

ability when Vps33p was inactive indicative of a pore opening defect.

### **1.6.5 Rab proteins**

There are over 60 Rab genes in the human genome, they are members of the Ras superfamily of GTPases and are conserved in all eukaryotes. Some Rabs are ubiquitously expressed whereas others are tissue specific, such as Rab17 in epithelia (Stenmark & Olkkonen 2001). Rabs are located in the cytoplasm or on cytoplasmic face of specific intracellular membranes allowing them to carry out their functions. Rabs specifically involved in maintenance of apical-basolateral polarity are Rab11a, Rab11b, Rab25 and Rab8a (Casanova et al. 1999)(Wang et al. 2000)(Roland et al. 2011) . Rab11a is known to function at the apical recycling endosome and investigations using cell lines found that in Rab11a GTP deficient mutants, basolateral trafficking is not affected but apical recycling and transcytosis of IgA is (Casanova et al. 1999).

Rab localisation is influenced by their state, they cycle between a guanosine triphosphate (GTP) bound or guanine diphosphate (GDP) bound conformation, with the GTP bound being considered 'active'. GDP/GTP exchange factors (GEFs) mediate the exchange of GDP to GTP on the Rab (Stenmark & Olkkonen 2001).

In its GTP bound state Rabs are able to bind their effectors. Rabs perform their function by recruiting a variety of different effectors at different stages in membrane transport. They have roles in cargo selection, vesicle transport, tethering and fusion (Hutagalung & Novick 2011). Rab9 can recruit cargo through its effector TIP47. When TIP47 is directly bound to Rab9-GTP, TIP47 has increased affinity for its cargo, mannose-6-phosphate receptors (M6PR). TIP47 directly links M6PR and Rab9, allowing Rab9 to direct the M6PR receptors from

endosomes to the TGN (Carroll et al. 2001). Trafficking of vesicles via Rab effectors is due to Rabs ability to interact with motor proteins that act on microtubules. Rab11 for example recruits myosinVb through its effector FIP2, allowing regulation of plasma membrane recycling (Hales et al. 2002). Rabs are also involved in SNARE mediated vesicle fusion by interaction with effectors that influence SNARE function, for example by interaction with tethers, SM proteins or directly with the SNAREs themselves (Hutagalung & Novick 2011). One such example is the interaction of the yeast Rab Ypt7p and tethering complex HOPS during vacuole formation (Seals et al. 2000). Reconstitution of HOPS-directed fusion of proteoliposomes by Wickner and colleagues (Stroupe et al. 2006)(Mima et al. 2008)(Stroupe et al. 2009)(Wickner 2010) found that the fusion of vesicles was dependent on the presence of the HOPS complex. Ypt7p was shown to be essential for reconstituted fusion under conditions when HOPS could not bind to membrane lipids, for example when Vps41p was phosphorylated (Hickey et al. 2009). This suggests the key role for Ypt7 is to bind HOPS to the vesicle membrane. They also found that the HOPS complex and the yeast Rab, Ypt7, were not sufficient for stable tethering but also required 3 of the 4 SNARE proteins. Upon trans-SNARE formation HOPS prevents the disassembly of trans-SNARE complexes and allows membrane fusion (Xu et al 2010).

Sorting and targeting of proteins to the apical and basolateral membranes, and fusion of the transport vesicles at the correct membrane is important in maintaining apical-basolateral polarity. The complexes and structures which define these domains also need to be understood to give an overview of apical-basolateral polarity.



## **1.7 Apical junctional complexes**

In ARC syndrome, defects in junctions joining epithelial cells have been identified (Cullinane et al. 2010). Epithelial cells are polarised cells and provide tissues with selective barrier against the external environment. They perform this function by contacting neighbouring cells via tight junctions and adherens junctions collectively known as apical junctional complexes (AJC).

### **1.7.1 Tight junctions**

Tight junctions (TJ) are present at the most apical part of the AJC and were first observed by Farquhar and Palade in 1963 (Farquhar & Palade 1963). The tight junction forms a continuous belt separating the apical and basolateral membrane domains (Förster 2008). TJs are composed of three transmembrane proteins which form part of the tight junction, occludin, claudins and junctional adhesion molecules (JAMs)(figure 1.5)(Aktories & Barbieri 2005). Occludin and claudins homodimerise to form tight cell-cell contacts, thus allowing TJs to fulfil their role.

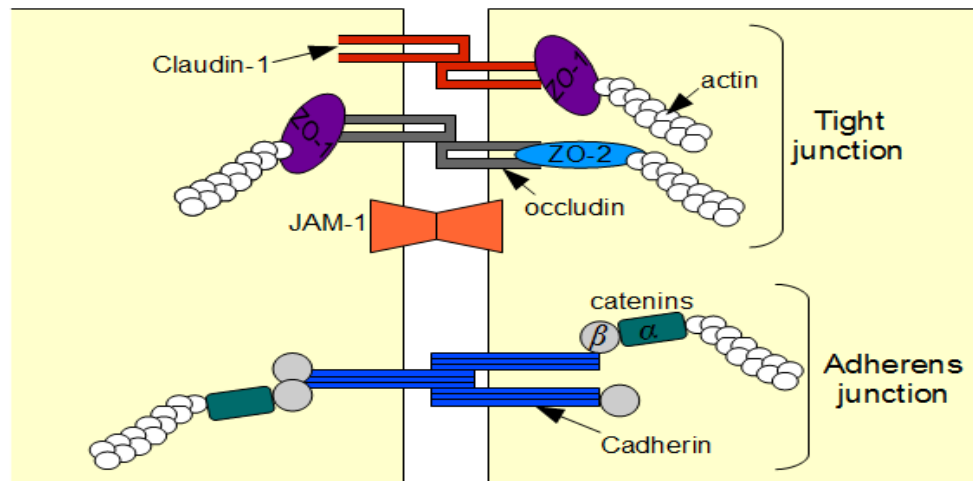
Tight junctions have 3 functions; to form a tight seal between epithelial cells and therefore block the movement of ions through the paracellular space, regulate the diffusion of solutes with size and charge selectivity through the paracellular space thus providing a 'gate' function (Powell 1981) and provide a 'fence' which separates and prevents the mixing of apical and basolateral membrane components. Purification of TJ-enriched membrane from rodent livers allowed the identification of the first TJ-associated protein Zona Occludins-1 (ZO-1) (Stevenson et al. 1986). ZO-1 is one of the cytoplasmic adapter proteins, including ZO-2 and ZO-3 responsible for linking the tight junction transmembrane proteins to the actin cytoskeleton, thought to be key for its 'fence' function (Förster 2008).

Claudins are tetraspanning membrane proteins and there are multiple subtypes, 24 in humans and mouse have been identified to date, and different epithelial cells have different combinations of these claudins (Förster 2008). Mouse models have been used to further elucidate the requirements of these different claudins, and is good example of how genetically modified mice have been used to understand protein function in multicellular organisms (Gupta & Ryan 2010). For example, claudin-1 knockout mice died at birth due to a skin barrier defect with water loss, indicating that claudin-1 is important for skin integrity (Furuse et al. 2002). This is supported by patients with mutations in Claudin-1 presenting with neonatal ichthyosis and sclerosing cholangitis (Hadj-Rabia et al. 2004).

### **1.7.2 Adherens junctions**

Adherens junctions (AJ) are a defining feature of epithelial sheets (Fristrom 1988) and are found basolaterally to the TJ, just below the apical surface (Wang & Margolis 2007). They are composed of members of the cadherin superfamily, E-cadherin in the case of epithelial cells, which are membrane spanning proteins that interact with the cadherins on neighbouring cells. Cadherins transdimerise in a calcium dependent manner and form weak homophilic cell-cell contacts (Baum & Georgiou 2011). In this way they are able to form a tight adhesive belt around the cell. The cytoplasmic tail of cadherins connects to multiple intracellular proteins allowing wide reaching functions (Hartsock & Nelson 2008). These proteins include members of the catenin superfamily which make up the adherens junction and include p120-,  $\alpha$ - and  $\beta$ -catenin (Harris & Tepass 2010). Roles of the adherens junctions include cell-cell adhesion, attachment to and regulation of the actin cytoskeleton, intracellular signalling and transcriptional regulation (Hartsock & Nelson 2008).

E-cadherin is a key protein in epithelial cells, with it being required for morphogenesis, epithelial function and as a tumour suppressor (Lock & Stow 2005). Its localisation is dynamic and it is trafficked to the AJ via Rab11 positive endosomes (Le et al. 1999)(Lock & Stow 2005). In one study depleting E-cadherin resulted in defective TJ formation, but found that maintenance of the TJ was not affected (Capaldo & Macara 2007).



**Figure 1.5 Molecular composition of tight and adherens junctions**

Three transmembrane proteins make up the tight junction, the claudins, occludin and JAM-1 which seal the space between cells preventing paracellular diffusion. These proteins connect to the actin cytoskeleton via ZO-1 and ZO-2. Adherens junctions found just below the tight junctions consist of the transmembrane protein cadherin which transdimerise to form a tight belt around the cell. These proteins interact with the actin cytoskeleton via  $\alpha$ - and  $\beta$ -catenins. Adapted from (Förster 2008).

### **1.8 The AJC and epithelial polarisation in ARC syndrome**

ARC syndrome has been associated with abnormalities in polarised epithelial cells particularly in the liver and kidney (Cullinane et al. 2010). Mislocalisation of apical membrane proteins to the cytoplasm or basolateral membrane, for example Carcinoembryonic antigen (CEA) and Bile Salt Exporter Pump (BSEP), has been found in hepatocytes and renal tubular cells in VPS33B and VIPAR deficient patients (Gissen et al. 2004)(Cullinane et al. 2010). Other apical proteins such as MRP2 remain correctly localised. Investigations using Vps33b- and Vipar-deficient mouse inner medullary collecting duct (mIMCD-3) cells by Cullinane et al. confirmed the mislocalisation of apical proteins (Cullinane et al. 2010). When Vipar- and Vps33b-deficient mIMCD-3 cells were transfected with an apical p75 neurotrophin receptor protein it was found that p75 was mislocalised to the basolateral membrane. In addition, if protein synthesis was blocked in the mIMCD knockdown cells, levels of p75 on the membrane dropped suggesting that for some reason the stability of p75 is reduced. As VPS33B and VIPAR form a complex, shown to partially co-localise with Rab11a – a marker for apical recycling endosomes. It was proposed that defective recycling of p75 is responsible for the reduction of its level at the membrane.

In both Vps33b- and Vipar-deficient mIMCD-3 cells, Cullinane et al. found that apical junctional complexes (AJC) were disrupted, with tight junctions showing reduced complexity by freeze-fracture electron microscopy (Cullinane et al. 2010). Epithelial cell polarity is characterised by the presence of AJCs and when these are disrupted epithelial polarity is lost (Etienne-Manneville 2008). AJC proteins were abnormally expressed in the knockdown cells with E-cadherin and Claudin-1 levels at the AJC being reduced. Disruption of the AJC led to loss of a columnar appearance of cells to a more flattened appearance. In addition, mIMCD-3 cells no longer grew in a uniformed monolayer but instead grew in multi-layered structures. It

was suggested that this might be due to a loss in the knockdown cells of contact-inhibition (Cullinane et al. 2010). Contact inhibition is required for cells growing in a monolayer to become quiescent when they reach confluence to prevent overgrowth and it has been suggested in several studies that E-cadherin adhesion is required for this growth inhibition in epithelial cells (Takahashi & Suzuki 1996)(Croix et al. 1998).

The ability of epithelia to form lumina is a central architectural characteristic of most organs (Schlüter & Margolis 2009). Simple assays modelling cyst and tube formation can be used to assess the ability of epithelial cells to polarise. In a cyst formation assay, cells are embedded in extracellular matrix (ECM) where the cells polarise resulting in the formation of a large hollow lumen (Schlüter & Margolis 2009). It has been found that lumen formation is related to apical membrane biogenesis (Lubarsky & Krasnow 2003). Defects in polarity can result in multiple-lumen or no-lumen phenotypes. Epithelial cells grown in 3D collagen gel can also form tubules when cells extend out from a cyst, repolarise and form a lumen connecting to the cyst (Leung-Hagesteijn et al. 2005). Vps33b- and Vipar-knockdown cells were unable to form tubular structures in gels (Cullinane et al. 2010). Together this data suggests that VPS33B and VIPAR are involved in the establishment and maintenance of apical-basolateral polarity in epithelial cells.

In the case of ARC syndrome, a complex multisystem disorder in which apical-basolateral polarity is defective, model organisms would be useful to learn more about the function of VPS33B and VIPAR in cellular trafficking and organ development and function.

### **1.9 Animal models of Vipar, Vps33b and its homologue Vps33a**

In metazoans there are 2 homologues of the yeast vacuolar protein-sorting protein Vps33p, Vps33a and Vps33b (Pevsner et al. 1996). Human VPS33B and VIPAR share 31% identity and 51% similarity, with an insertion of 31aa which is present in VPS33B but not VPS33A (Gissen et al. 2005). Mutations in *VPS33B* have been found in patients with ARC syndrome. Although *VPS33A* has been suggested as a candidate gene for Hermansky Pudlak Syndrome, no mutations have been identified in human *VPS33A* (Suzuki et al. 2003). *VIPAR* is a distant homologue of yeast *vps16*, mutations in which also result in ARC syndrome (Cullinane et al. 2010). Studies using model organisms have been undertaken in order to try and delineate the roles of these proteins and determine whether in metazoans these form part of an equivalent HOPS or CORVET complex. The models used so far will be discussed.

In *Saccharomyces cerevisiae*, genetic screens identified 41 Vacuolar Protein Sorting (VPS) genes involved in delivery of cargo to the yeast vacuole (Novick et al. 1980). Cells with a deletion of the VPS genes *Vps33*, *Vps18*, *Vps11* or *Vps16* (Woolford et al. 1990)(Preston et al. 1991)(Horazdovsky & Emr 1993) caused a severe ‘no vacuole’ phenotype, and were named Vps Class C genes. In addition to the ‘no vacuole’ phenotype, deletion of *Vps33* revealed defects in fusion events at the late endosome (Subramanian et al. 2004). In yeast, Vps33p and Vps16 are core components of the HOPS complex and CORVET complex along with the remaining 2 class C VPS proteins Vps18 and Vps11, which act at the vacuole and endosomes respectively (Peplowska et al. 2007).

### 1.9.1 VPS33A models

*Drosophila* - In *Drosophila carnation* has been identified as the homologue of human *VPS33A*. Studies have looked at the role of the protein product of *car*, Car/Vps33A, in *Drosophila* (Sevrioukov et al. 1999)(Akbar et al. 2009). A mutation in *car* which led to an almost complete deletion of the Vps33A protein resulted in lethality at the second instar stage (larval stage in development of *Drosophila*). This indicates Vps33A is important for larval development of the fly (Akbar et al. 2009). Due to lethality, knockout of Vps33A was restricted to the eye. *Car* was shown to be necessary for biogenesis of pigment granules, a lysosome-related organelle within the eye (Akbar et al. 2009). Loss of Vps33A also resulted in defective delivery of endosomal contents to lysosomes. As a consequence, endocytosed receptors and ligands accumulated in late endosomes. It was found *dVps33b* could not rescue the *car* phenotype indicating that Vps33A and Vps33B are not redundant in *Drosophila*.

It was demonstrated by Sevrioukov et al. that Vps33A interacts with Deep-orange (Dor) a homologue of the yeast core HOPS complex protein, Vps18 (Sevrioukov et al. 1999). The HOPS complex in yeast is required for the fusion of autophagosomes with vacuoles in yeast (Rieder & Emr 1997). Accumulation of autophagosome-like organelles was observed in *car* mutants supporting a role for Vps33A in autophagosome-lysosome fusion in *Drosophila*. Degeneration of the photoreceptor neurons was detected which is an important observation as neurodegeneration is a common result of lysosome dysfunction (Akbar et al. 2009).

*Mouse* - The first mammalian mutation to be identified in *Vps33a* was a spontaneous missense mutation *p.Asp251Glu* in the *buff* mouse (Suzuki et al. 2003). Reduced coat-colour pigmentation due to reduced size and number of melanosomes and a dense granule platelet defect was detected. In contrast to the dense granule defect seen in *buff* platelets, ARC patients with mutations in *VPS33B* have a platelet  $\alpha$ -granule biogenesis disorder (Lo et al.



2005). Lysosomal function in the *buff* mouse initially was thought to be unaffected. However, in a study on bladder urothelium it was found that there was a defect in the endocytic degradation of uroplakin (Guo et al. 2009). The fusion of uroplakin-degrading multi-vesicular bodies to lysosomes was defective, indicating that Vps33a may play a role in this fusion event. Standardised behavioural tests were carried out on the *buff* mouse and significant motor deficits were found in tests such as grip strength and righting reflex, worsening with age (Chintala et al. 2009). A progressive loss of Purkinje cells was found, suggesting a role for Vps33a in maintenance but not formation of Purkinje cells. In conclusion, it appears that Vps33a in the mouse is required for the formation of melanosomes (Suzuki et al. 2003), the maintenance of Purkinje cells (Chintala et al. 2009) and may act in the endocytic degradation pathway (Akbar et al. 2009).

### **1.9.2 VPS33B and VIPAR models**

*C. elegans* – In 2009, Zhu et al. published work using *C. elegans* and RNAi experiments to investigate the function of Spermatogenesis defective protein 39 (SPE-39)(VIPAR homologue)(Zhu et al. 2009). Previously it had been found that in *C. elegans* spermatogenesis is defective in *spe-39* mutant (Zhu & L'Hernault 2003). It was confirmed that this phenotype was also observed when knocking down expression of Vps33b but not Vps33a by RNAi. Defective cell division and membranous organelle defects were observed. Processing of internalised yolk proteins and degradation of endocytosed substrates in oocytes and coelomocytes (macrophage-like scavengers) respectively, were also found to be defective in *C. elegans* suggesting a function for SPE-39 in endosomal/lysosomal trafficking pathways (Zhu et al. 2009). An interaction between SPE-39 and both VPS33A and VPS33B was

reported by Zhu et al. an interaction not observed in *Drosophila* or HEK293 cells (Pulipparacharuvil et al. 2005)(Zhu et al. 2009)(Cullinane et al. 2010).

*Drosophila* – Pulipparacharuvil et al. 2005 found that dVps33A interacts with dVps16A, and dVps33b interacts with dVps16b (now known as full-of-bacteria – a homologue of human VIPAR)(Pulipparacharuvil et al. 2005). An investigation of the *full-of-bacteria (fob)* gene has recently been reported in *Drosophila*. In this homozygous *fob* null allele, a defect in phagosome fusion with lysosomes was reported in hemocytes (fly macrophages) when challenged with non-pathogenic bacteria (Akbar et al. 2011). The same was observed with a Vps33b knockdown by RNAi, suggesting the 2 proteins work together in this process. The endocytic trafficking of ligands was unaffected unlike the *car* mutant. Starvation induced autophagy that requires fusion with lysosomes was also not affected suggesting a very specific role for *fob* and dVps33b in phagosome-lysosome fusion. VPS33B in humans has also been shown necessary for phagosome-lysosome fusion in macrophages and that the *M. Tuberculosis* protein PtpA inhibits this fusion by dephosphorylating VPS33B (Bach et al. 2008).

*Zebrafish* – Zebrafish morpholinos have been used to further investigate the role of Vps33b and Vipar in development. Abnormal liver biliary tract development with a reduced number of terminal branches was observed in zebrafish larvae after treatment with morpholino oligonucleotides used to knock down expression of both Vps33b and Vipar (Matthews et al. 2005)(Cullinane et al. 2010). Bile excretion was reduced when monitored by using PED6, a compound that becomes fluorescent after cleavage by a phospholipase enzyme in the liver cells, and then is excreted as part of bile into the hepatobiliary ductal system (Matthews et al. 2005). Keratin immunostaining was also abnormal consistent with the abnormal development of terminal biliary ductules. Cytoplasmic vesicles were present within Vps33b deficient [33]

biliary epithelial cells, suggesting the defect in biliary tract development may be due to a defect in vesicle sorting (Matthews et al. 2005).

No Vps33b or Vipar mouse models have yet been reported. In this thesis, the development of mouse models of Vps33a and Vps33b deficiencies are described. These mouse models were created in order to investigate the function of the two genes within the mammalian system.

Disrupted gene	Organism	Phenotype
<i>vps33</i> treatment with the mutagenic agent, ethyl methanesulfonate	Yeast	<ul style="list-style-type: none"> <li>• 'no vacuole' phenotype</li> <li>• Defective endosomal fusion</li> </ul>
<i>carnation (Vps33a)</i> null allele using P element	<i>Drosophila</i>	<ul style="list-style-type: none"> <li>• Lethal at second instar stage</li> <li>• defective biogenesis of pigment granules in the eye</li> <li>• accumulation of autophagosomes (defective fusion with lysosomes)</li> </ul>
<i>Vps33a</i> , spontaneous mutation	<i>buff</i> mouse	<ul style="list-style-type: none"> <li>• Reduced size and number of melanosomes</li> <li>• dense granule defect in platelets</li> <li>• defective fusion of uroplakin-degrading multi-vesicular bodies to lysosomes</li> </ul>
<i>Vps33b</i> <i>RNAi</i>	Nematode, <i>C. elegans</i>	<ul style="list-style-type: none"> <li>• Defective spermatogenesis – associated with defects in formation of membranous organelles</li> </ul>
<i>Vps33b</i> <i>RNAi</i>	<i>Drosophila</i>	<ul style="list-style-type: none"> <li>• Defective fusion of phagosomes with lysosomes</li> </ul>
<i>Vps33b</i> Morpholino	Zebrafish	<ul style="list-style-type: none"> <li>• abnormal biliary tract development</li> <li>• Reduced bile excretion</li> </ul>
<i>Vps16</i> treatment with the mutagenic agent, ethyl methanesulfonate	Yeast	<ul style="list-style-type: none"> <li>• 'no vacuole' phenotype</li> </ul>
<i>spe-39 (VIPAR)</i> induced mutation due to treatment with the mutagenic agent ethyl methanesulfonate or ultraviolet irradiation	Nematode, <i>C. elegans</i>	<ul style="list-style-type: none"> <li>• Defective fusion of membranous organelles required for sperm function</li> <li>• Defective clearance of endocytosed substrates in macrophage-like cells and oocytes</li> </ul>
<i>fob (VIPAR)</i> targeted mutagenesis using ends-out homologous recombination	<i>Drosophila</i>	<ul style="list-style-type: none"> <li>• Defective fusion of phagosomes with lysosomes</li> </ul>
<i>Vipar</i> morpholino	Zebrafish	<ul style="list-style-type: none"> <li>• abnormal biliary tract development and accumulation of vesicles in biliary epithelial cells</li> <li>• Reduced bile excretion</li> </ul>

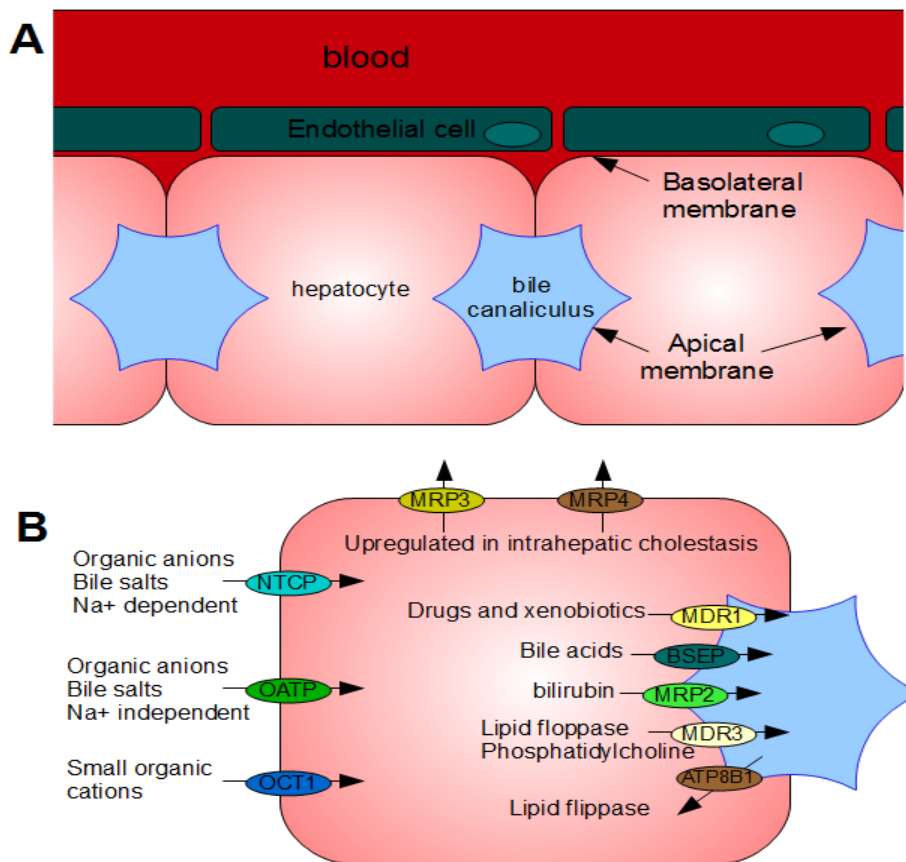
**Table 1.1 Summary of Vps33a, Vps33b and Vipar model organisms**

The method of production, model organism used and phenotype observed is listed.

### **1.10 The Liver**

Cholestasis is a cardinal feature of ARC syndrome, and is due to a defect in bile export- a function of the primary liver cell, the hepatocyte. The liver is the largest visceral organ in mammals, and is composed of 7 distinct cell types including: hepatocytes, sinusoidal endothelial cells, kupffer cells, hepatic stellate cells, biliary epithelial cells, pit (natural killer) cells and hepatic dendritic cells (Ishibashi et al. 2009). It carries out a great many functions including bile synthesis, glycogen storage, plasma protein synthesis and hormone production. It also extracts and metabolises multiple nutrients, xenobiotics and old cells brought in from the gastrointestinal tract via portal circulation.

Hepatocytes, otherwise known as liver parenchymal cells, are large polygonal cells that make up 80% of the mass/volume of the liver and compose 60% of all cell content within this organ (Tanaka et al. 2011). Hepatocytes are polarised cells, with the apical membrane modified specifically for bile constituent excretion into the bile canaliculi (Nicolaou et al. 2012), and the basolateral surfaces which consist of 2 parts: the membrane where hepatocytes contact one another, forming junctional complexes (adherens, tight and gap) to provide a barrier between the blood and bile, and the membrane which contacts the blood forming spaces known as sinusoids (Figure 1.6A). Hepatocytes are not simple bipolar cells such as the proximal tubule kidney epithelial cells. They do not have a singular apical-basolateral polarity but instead have a punctate plasma membrane (figure 1.6A) (Wilton & Matthews 1996), which allows the formation of a large branched network of bile canaliculi.



**Figure 1.6 Hepatocytes**

A. Hepatocyte polarity - hepatocytes are not simple bipolar cells but instead have multiple apical surfaces which allow the formation of a large branched network of bile canaliculi

B. Transporters found in the apical and basolateral membranes of hepatocytes and their substrates. Arrows indicate the direction of transport. In the basolateral membrane - Sodium/Taurocholate Co-transporting Peptide (NTCP), Organic Anion Transporting Polypeptide (OATP) Organic Cation Transporter (OCT1). Efflux pumps in the basolateral membrane include Multidrug Resistance-associated Protein 3 and 4 (MRP3, MRP4). Apical (canalicular) efflux pumps of the hepatocyte comprise bile-salt export pump (BSEP), Multidrug resistance-associated protein 2, and MultiDrug Resistance protein 1 and 3 (MRP2, MDR1 and MDR3), and phospholipid-transporting ATPase IC (ATP8B1). Adapted from (Giacomini et al. 2010).

A major role of hepatocytes is to produce bile, which is secreted via the biliary duct system into the intestine for the emulsification of fats. In addition it is an important route for elimination of drugs, toxins and metabolic products such as cholesterol and bilirubin (Trauner & Boyer 2003). Bile canaliculi are the terminal ductules of the intrahepatic biliary tree, and are found at the apical surface of the hepatocytes where bile is secreted. These canaliculi join to form the Canals of Hering which are lined with cholangiocytes – cells which alter the constituents of the primary canicular bile, then bile ductules, intrahepatic bile ducts and finally the common bile duct, where the bile exits the liver for storage in the gall bladder before release into the small intestine (Arias et al. 2009). Many of the organic constituents of bile such as bile acids are reabsorbed (up to 95%) in the small intestine and then taken back to the liver in the portal vein. Bile salts are then reabsorbed at the basolateral side of the hepatocytes, allowing the circulation and reuse of these bile constituents. This is known as enterohepatic circulation (Hofmann 1999).

#### **1.10.1 The importance of hepatocyte polarity in liver development/function**

Apical junctional complexes in hepatocytes demarcate the bile canaliculi, they form a barrier between the blood and bile allowing the maintenance of concentration gradients between the two (Boyer 1980) and act as a physical barrier to separate the apical and basolateral domains in order to allow polarisation of hepatocytes (Son et al. 2009). In zebrafish hepatocyte polarisation coincides with development of the vasculature and biliary tree, suggesting hepatocyte polarisation may be required for the formation of these structures during liver development (Sakaguchi et al. 2008). It has also been shown that disruption of apical trafficking of ABC transporters in hepatocytes results in a failure of bile canaliculi to form in rat hepatoma/human fibroblast hybrid (WIF-B9) cells, a polarised hepatic epithelial cell line

(Wakabayashi et al. 2006), demonstrating the necessity for correct apical localisation of proteins during canalicular formation in the liver. Disrupted liver architecture and disruption of the bile ducts is a characteristic of many common liver diseases such as hepatitis and non-alcoholic fatty liver disease. Better understanding of the molecular mechanisms underlying biliary development can be gained by the investigation of rare single-gene disorders, such as progressive familial intrahepatic cholestasis (Cagle 2010), disorders which are associated with bile duct hypoplasia.

### **1.10.2 Apical hepatocyte transporters**

Apical and basolateral surfaces of the hepatocyte contain different transporters for uptake and secretion of bile constituents. Bile salt secretion occurs against a steep concentration gradient at the apical membrane, and relies on members of the ATP-binding cassette (ABC) superfamily (Nicolaou et al. 2012). ABCB11 (otherwise known as the Bile Salt Exporter Pump - BSEP) is a member of this superfamily and transports monovalent bile salts across the apical membrane. It is trafficked to the apical membrane via a Rab11a recycling endosomes (Wakabayashi et al. 2004).

The apical ABC transporter Multidrug Resistance-associated Protein 2 (MRP2) transports products including organic anions and their conjugates (bilirubin)(Nicolaou et al. 2012). MRP2 contains a PDZ binding motif thought to aid its targeting to the apical membrane (C-terminal phosphorylation). NHERF-1, a PDZ protein has been shown to influence the level of MRP2 at the apical membrane (Li et al. 2010).

MultiDrug Resistance protein 1 (MDR1 - otherwise known as ABCB1) is also found on the apical membrane and transports drugs and xenobiotics into the bile (Cascorbi 2011). In



contrast to BSEP, MDR1 has been shown to be transported directly from the golgi to the apical membrane (Sai et al. 1999).

MultiDrug Resistance protein 3 (MDR3) is a lipid floppase, transporting phosphatidylcholine from the inner to the outer leaflet of the canalicular membrane, where it is extracted by bile acids (Jacquemin 2001)(Davit-Spraul et al. 2009). It plays an important role in reducing the cytolytic action of bile acids (Elferink & Beuers 2011).

ATP8B1 (FIC1) is a lipid flippase also found at the apical membrane and plays the opposite role to MDR3, (Groen et al. 2011) moving phosphatidylserine from the outer to the inner leaflet, and is thought to counteract the destabilisation of the canalicular membrane when MDR3 flops phosphatidylcholine.

### **1.10.3 Cholestatic liver disease**

Cholestatic liver disease is a term that describes any condition in which the flow of bile from the liver is disrupted. Cholestatic diseases can be divided into two main groups, extrahepatic cholestasis which occurs outside the liver (and is secondary to disrupted bile flow via bile ducts) and intrahepatic which occurs inside the liver and can occur due to maldevelopment of intrahepatic bile ducts and/or abnormal transport of bile out of hepatocytes across the canalicular membrane. Both groups of cholestatic disorders have many different causes such as infection, single gene disorders, congenital malformations and maternal drug exposure. One of the cardinal features of ARC syndrome is intrahepatic cholestasis.

Genetic causes of intrahepatic cholestasis include mutations in many genes, some of which may have a known function in bile transport but the role of many others has not been delineated (Jansen & Sturm 2003). For example, Progressive Familial Intrahepatic Cholestasis

(PFIC) is a group of autosomal recessive diseases caused by mutations in various canalicular transporter proteins. PFIC Type 1 is caused by mutations in *ATP8B1*, encoding the lipid flippase at the canalicular membrane (Bull et al. 1997). PFIC type 2 by mutations in the *ABCB11* gene (also known as *BSEP*)(Strautnieks et al. 1998) and type 3 by mutations in *MDR3*, the lipid floppase (de Vree et al. 1998). Due to the differences in the function of the affected genes, and differing severity dependent on the patient mutation, there is a large scope of clinical variability between patients.

In addition to defects in apical proteins, mutations in tight junction proteins, Claudin-1 and ZO-2 have been shown to cause 2 forms of intrahepatic cholestasis. Neonatal sclerosing cholangitis-ichthyosis syndrome is an autosomal recessive disorder caused by mutations in claudin-1. Patients present with jaundice, itching and acholic (absent bile, pale in colour) stool. It is a severe condition characterised by inflammation and fibrosis of intra- and extrahepatic bile ducts (Hadj-Rabia et al. 2004) leading to liver cirrhosis and liver failure. Some patients however, were found to have intrahepatic biliary hypoplasia on liver biopsy, which a similar histological appearance to the patients with PFIC1 and PFIC2. The pathophysiology underlying this condition is unclear but it is believed that a loss of cell polarity and paracellular leakage of bile secondary to abnormal development of tight junction may result from loss of claudin-1, which is a tight junction constituent protein (Paganelli et al. 2011)(Grosse et al. 2011).

Patients with familial hypercholanaemia, an autosomal recessive disorder were found to contain mutations in ZO-2, which links transmembrane junctional proteins with actin cytoskeleton (Carlton et al. 2003). The disease is characterised by elevated serum bile acids, itching and fat malabsorption (Carlton et al. 2003). Mutations in ZO-2 were also proposed to increase paracellular permeability to bile acids allowing movement from the bile to the blood

through the paracellular space. A variety of different possible mechanisms were proposed for this including the failure of claudin to anchor properly, or changes in the conformation of claudin pores (Carlton et al. 2004).

#### **1.10.4 ARC liver**

Lutz-Richner and Landholt in 1973 were the first to report ARC syndrome, and in 1979 a second family were reported by Nezelof et al. (Lutz-Richner & Landolt 1973)(Nezelof et al. 1979). Due to the different histological observations made when examining the livers from these patients, they were considered to represent 2 different clinical disorders. The first group had paucity of intrahepatic bile ducts and giant cell transformation of hepatocytes, and the second had pigment deposition in hepatocytes and cholestasis. However, in 1994 Horslen et al. suggested that the phenotypes were a variation within a single syndrome. This was due to the identification of a patient presenting with the cardinal features of ARC syndrome, but an overlap between the 2 liver pathologies previously reported, with cholestasis, lipofuscin deposition and intrahepatic biliary hypoplasia observed (Horslen et al. 1994).

One of the cardinal features of ARC syndrome is neonatal cholestatic jaundice. 14 out of 15 ARC patients analysed in one study (Gissen et al. 2006) had non-excreting biliary isotope studies, suggesting biliary obstruction or severe intrahepatic cholestasis. Bilirubin is the end degradation product of haeme and is often used as a marker of abnormal biliary excretion. It is normally excreted into the bile by MRP2 (ABCC2), an apical protein (Trauner & Boyer 2003). When the liver is damaged or bile ductular system is occluded, bilirubin levels in the blood increase resulting in jaundice (Carlton et al. 2004). ARC patients present with conjugated hyperbilirubinaemia. Bilirubin, a breakdown product of haeme, is delivered to the liver in its unconjugated form. Here it is conjugated with glucuronic acid making it water

soluble. If uptake of bilirubin by the liver is impaired or there is a defect in bilirubin conjugation, unconjugated bilirubin levels in the blood are raised; if excretion from the liver is impaired, conjugated bilirubin levels are increased (Carlton et al. 2004). In the case of ARC syndrome the levels of conjugated bilirubin are increased in the blood suggesting a secretion defect. Additional markers typically used to assess liver damage found that ARC patients show low gamma-glutamyl transpeptidase (gGT) activity and normal to slightly increased ALanine Transaminase (ALT) and ASpartate Transaminase (AST). gGT is a protein found in the membrane or many tissues, most notably the liver. Elevated serum gGT levels can be indicative of diseases of the liver, biliary system or the pancreas. ALT and AST are enzymes also found within liver cells, if cells are damaged these proteins are released into the blood, and are therefore also used to identify possible liver damage.

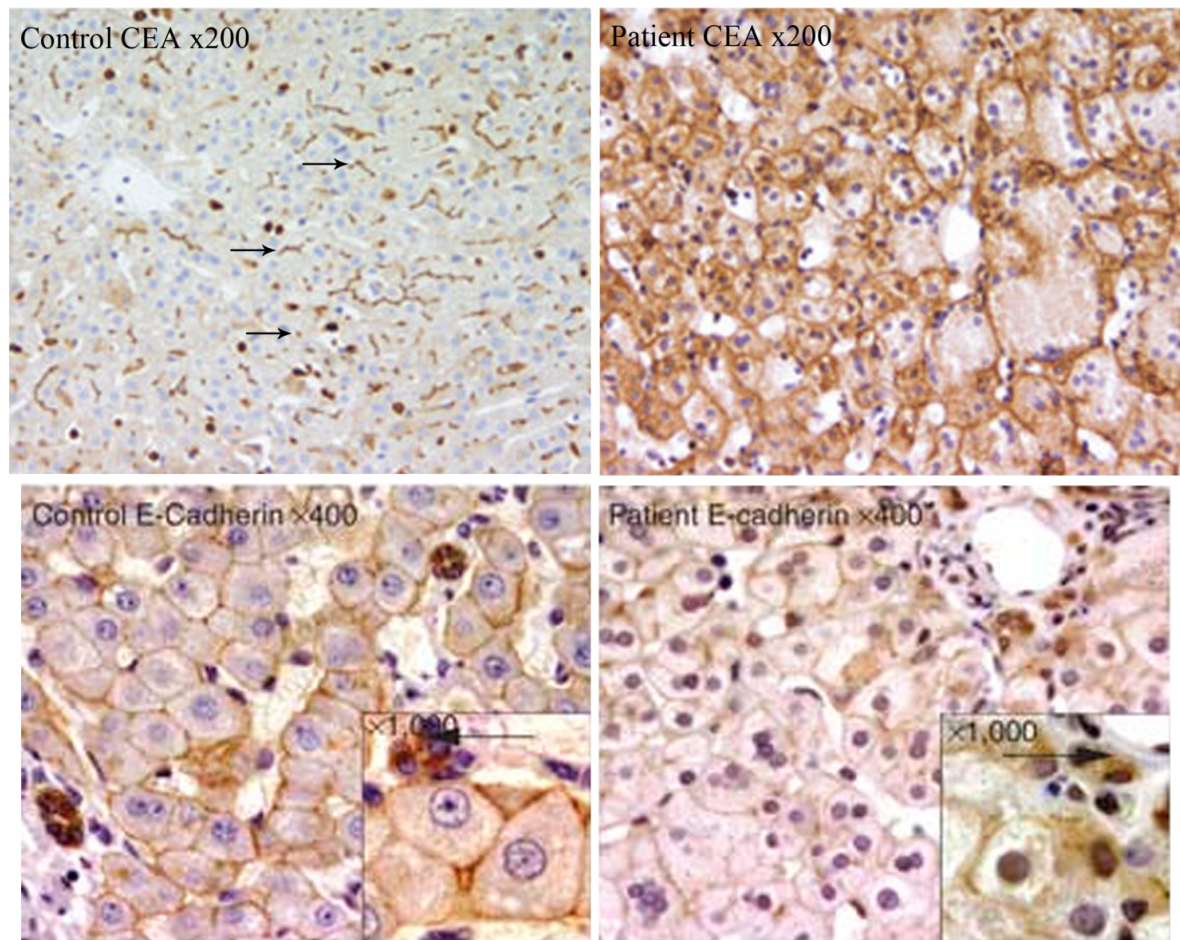
As previously discussed, histological findings in ARC livers are variable. Paucity of the bile ducts (reduction in the number of interlobular bile ducts) was observed in 7 out of 16 ARC patients in one study (Gissen et al. 2006). Lipofuscin deposition (Di Rocco et al. 1990)(Horslen et al. 1994) was observed in 5 of 16 ARC livers (Gissen et al. 2006). Lipofuscin deposits are yellow-brown pigment granules consisting of highly oxidized cross-linked proteins. The deposition of lipofuscin is linked to several cellular processes including the rate of oxidative damage to proteins, the effectiveness of mitochondrial repair systems and the functionality and effectiveness of the lysosomal degradation (Jung et al. 2007). Multinucleate giant cell hepatitis has also been observed (Abu-Sa'da et al. 2005).

Immunohistochemistry analysis of ARC liver biopsies has been conducted for several proteins found within the liver (Figure 1.7). The apical protein BSEP is mislocalised to the basolateral membrane, which may result in impaired bile acid secretion. CEA, also an apical protein was found to be mislocalised to the cytoplasm and basolateral surfaces. MRP2, a

protein which is directly trafficked to the membrane, remains correctly localised to the apical membrane in contrast to BSEP and CEA. The localisation of E-cadherin, a protein found at the AJC's, was also investigated and found to be present in reduced levels (Gissen et al. 2004)(Cullinane et al. 2010).

Eastham et al. first suggested the two pathophysiological mechanisms that may underlie the clinical feature of cholestasis in ARC (Eastham et al. 2001). These include the numerical reduction of intrahepatic bile ducts and reduced bile secretion across the canalicular portion of hepatocyte membrane. Both defects have been seen in other syndromes with cholestasis, and the particular similarity with ARC is seen for the histological findings in PFIC type 2.

Vps33b and Vipar zebrafish morpholinos have been used to model the ARC syndrome, and have been reported as compatible with a partial ARC syndrome phenocopy (Matthews et al. 2005)(Cullinane et al. 2010) as discussed in section 9.1.2. Cholestasis and bile duct paucity were reported. The features of the newly-developed murine model of liver Vps33b deficiency is described in chapter 5.



**Figure 1.7 Staining of apical proteins in control and ARC liver**

CEA is localised to the canalicular membrane in control patients, typical apical staining indicated by arrows. In ARC liver CEA is mislocalised throughout the plasma membrane and is also cytoplasmic. E-cadherin is correctly localised however levels are reduced. Adapted from (Gissen et al 2006) and (Cullinane et al 2010).

### **1.11 Platelets**

Platelets are small anuclear membrane fragments, approximately 2-3 $\mu$ m in size, that circulate in the blood. They originate from their precursor cells, megakaryocytes, and have an average lifespan of 10 days in human and 5 days in mice (Ren et al. 2008)(Grozovsky et al. 2010). Platelets circulate in the bloodstream in a quiescent state and undergo rapid activation when the blood vessel is damaged. In this way they are able to perform their primary function, to aggregate and form a vascular plug in order to prevent further blood loss and occlude the site of damage (Watson & Harrison 2007). There are several stages of platelet activation:

**Tethering** – This phase involves the tethering of platelets to the site of damage, creating a monolayer of activated platelets. Upon damage to the vascular endothelium, extracellular matrix components are exposed including collagen, fibronectin and laminin. In the low shear environment of the venous system, platelet adhesion involves binding to these extracellular matrix components. In the high shear conditions of arteries and arterioles, platelet tethering is dependent on von Willebrand Factor (VWF) which binds to exposed subendothelial collagen fibres (Savage et al 1998)(Jackson et al 2003). The bound VWF undergoes a conformational change (Siedlecki et al. 1996)(Schneider et al. 2007) which permits rapid binding to platelet GPIb-IX-V and therefore platelet capture. This association is however transient due to a fast off-rate thereby allowing platelet translocation along the exposed subendothelial matrix.

**Stabilisation and activation** – The deceleration of the platelets permits binding to the low affinity collagen receptor GPVI which initiates powerful activation of integrins  $\alpha$ IIb $\beta$ 3 and  $\alpha$ 2 $\beta$ 1 and stabilisation through binding to VWF/fibrinogen and collagen, respectively (Watson & Harrison 2007). The signals from GPVI synergise with those from GPIb-IX-V and the

two integrins mediate platelet spreading, secretion of  $\alpha$ - and dense-granules, and de novo production and secretion of TxA<sub>2</sub>. ADP from dense granules and TxA<sub>2</sub> provide a positive feedback mechanism for activation of platelets.

**Further platelet recruitment and aggregation** – Aggregation is mediated through cross-linking of activated platelets via binding of fibrinogen to integrin  $\alpha$ IIb $\beta$ 3. This is mediated through binding of VWF to integrin  $\alpha$ IIb $\beta$ 3 on activated platelets and tethering (or capture) of new platelets through binding of VWF to GPIb-IX-V. VWF is present in the plasma and in platelet  $\alpha$ -granules (Rand et al. 1987), and both sources are required to facilitate platelet aggregation under high shear (Kulkarni et al, 2000). Thus  $\alpha$ -granule secretion is required for thrombus growth.

#### **1.11.1 Platelet storage granules**

Platelets contain 4 types of storage vesicle,  $\alpha$ -, dense, lysosomes and peroxisomes (figure 1.8).

##### **Dense granules**

Dense granules have a mean diameter of 150nm and are present at quantities ranging from 5 to 9 dense granules per platelet. They contain pro-aggregating, non-protein molecules including ADP, ATP, Ca<sup>2+</sup>, polyphosphate and serotonin (Rendu & Brohard-Bohn 2001). Visualisation by EM reveals a characteristic opaque dense core with clear space and single membrane (Figure 1.8).



### **$\alpha$ -granules**

$\alpha$ -granules are 200-500nm in diameter and are the most numerous storage granule in the platelet, with approximately 80 per platelet- a 10-fold greater level than that of dense granules (King & Reed 2002). A proteomics study in 2003 identified 300 proteins released by platelets upon stimulation with thrombin, the contents of  $\alpha$ -granules, dense- granules and lysosomes (Coppinger et al. 2004). Subsequently, a proteomic study of purified  $\alpha$ -granules by mass spectrometry identified 284 non-redundant proteins (Maynard et al. 2007).  $\alpha$ -granules contain a diverse set of proteins that participate in haemostasis and other vascular processes including tissue repair, angiogenesis, inflammation and host defence.

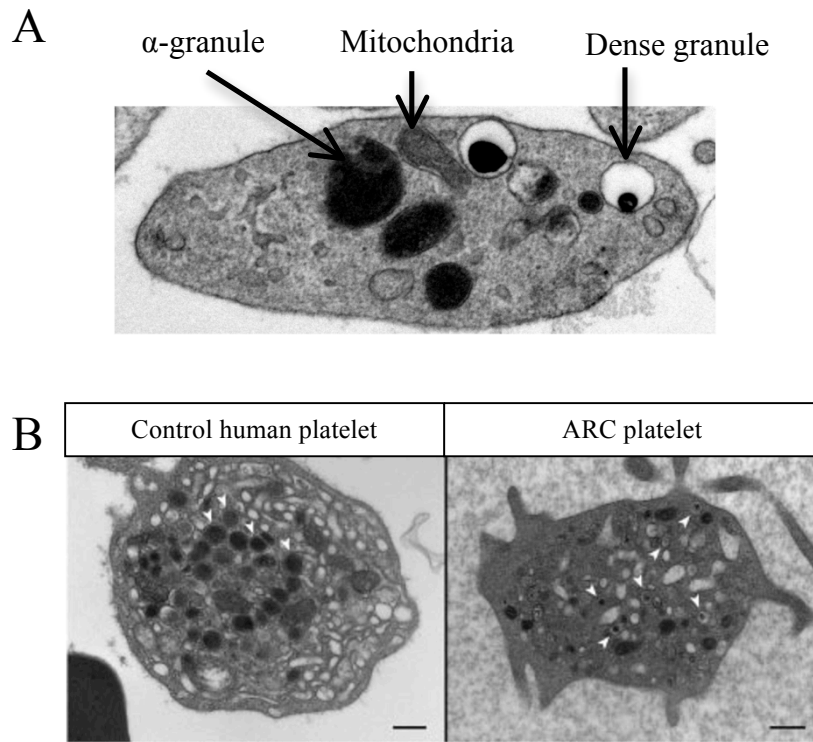
- Fibrinogen, fibronectin and von Willebrands Factor (VWF) participate in haemostasis by supporting platelet-matrix and platelet-platelet interactions leading to adhesion and aggregation (Ruggeri & Mendolicchio 2007)
- Growth factors such as Platelet Derived Growth Factor, Insulin-like Growth Factor-1, Vascular Endothelial Growth Factor and basic Fibroblast Growth Factor are implicated in angiogenesis and wound healing.
- Fibrinolytic agents, such as Plasminogen activator inhibitor-1 and plasminogen, mediate clot remodelling and enhance cell/matrix interactions (Anitua et al. 2004).
- Chemokines attract and activate leukocytes, modulating the production of inflammatory molecules and regulating an immune response (Ren et al. 2008).
- Several transmembrane proteins become exposed on  $\alpha$ -granule fusion with the plasma membrane. These proteins include P-selectin, which promotes chemokine deposition and thus monocyte recruitment (Schober et al. 2002) and integrin  $\alpha$ IIb $\beta$ 3 which supports aggregation.

**Lysosomes**

Lysosomes are intermediate in size, at 175-250nm and their contents are released upon platelet activation (Ciferri et al. 2000). They have a density similar to  $\alpha$ -granules but the density is uniform throughout the granule (Rendu & Brohard-Bohn 2001). They contain a number of digestive enzymes required for elimination of proteins and metabolites not required in the platelet.

**Peroxisomes**

Peroxisomes are single membrane organelles found in most eukaryotic cells (Gabaldón 2010). Peroxisomes are involved in a number of metabolic pathways, with a general feature of peroxisomes being fatty acid catabolism through beta-oxidation (Wanders & Waterham 2006).



**Figure 1.8 Electron microscopy images of platelets**

- A. A representative mouse platelet showing an  $\alpha$ -granule, a dense-granule and mitochondria
- B. A control human patient with  $\alpha$ -granules marked with white arrow heads, and an ARC platelet with no  $\alpha$ -granules. Small abnormal dense bodies are marked with white arrow heads. Adapted from (Lo et al. 2005).

### **1.11.2 $\alpha$ -granules and platelet function**

$\alpha$ -granules contain a diverse set of proteins which must undergo a complex packaging procedure within megakaryocytes and during platelet maturation in order to create mature  $\alpha$ -granules (Rendu & Brohard-Bohn 2001).  $\alpha$ -granules develop from the TGN within the megakaryocyte (Blair & Flaumenhaft 2009) and must mature before they become fully formed granules with distinguishable morphological zones (Rendu & Brohard-Bohn 2001). The maturation process involves the transport of proteins to  $\alpha$ -granules. Most proteins are synthesised early within the maturing megakaryocyte and transported from the rough ER, transported to the golgi and subsequently to the TGN where they are sorted and packaged into vesicles (Harrison & Cramer 1993)(Rendu and Brohard 2001). From here proteins are trafficked directly to the immature  $\alpha$ -granules or indirectly via multivesicular bodies (MVBs). MVBs are intermediate sorting vesicles for granules and contain both dense and  $\alpha$ -granule constituents (Youssefian & Cramer 2000).

Several proteins are also transported to the  $\alpha$ -granules following endocytosis from the plasma (Rendu & Brohard-Bohn 2001). IgG and albumin are taken up passively by fluid-phase endocytosis and are found at low concentrations. Proteins which are found in a higher concentration in platelets than in the plasma are taken up by receptor-mediated endocytosis (Rendu & Brohard-Bohn 2001). For example, plasma fibrinogen is primarily synthesised in hepatocytes and is actively transported into megakaryocytes or circulating platelets from the plasma by endocytosis of integrin  $\alpha$ IIB $\beta$ 3 (Handagama et al. 1993) either via a clathrin-coated vesicle or by a clathrin independent endosome/lysosome route (King & Reed 2002). Endocytosis may occur at the stage of the megakaryocyte or when the platelet is in circulation.

### 1.11.3 Storage pool diseases linked to defective trafficking and vesicle fusion

Patients with platelet storage pool disorders (SPDs) have absent or diminished granules or granule contents and are separated into 3 groups;  $\alpha$ -, dense or  $\alpha\delta$ -SPDs. Dense granule storage is often affected along with other lysosomal related organelles including melanosomes which give rise to characteristic pigment disorders (Huizing et al. 2008).

Hermansky Pudlak Syndrome (HPS) is a dense granule storage pool disease and was first described in 1959. It is an autosomal recessive disorder, rare worldwide but the most common genetic disorder in Puerto Rico with a prevalence of 1 in 1800 (Shotelersuk and Gahl, 1998). 9 causative genes HPS-1 to HPS-9 have been identified to date in man and 15 in mice (Wei 2006)(Cullinane et al. 2011). HPS1-9 are involved in several protein complexes named Biogenesis of Lysosome Related Organelle Complexes -1, -2, and -3 (BLOC-1, -2 and -3) and AP3. BLOCs are a group of proteins which together are involved in the formation and trafficking of lysosome related endosomes (Huizing et al. 2008). BLOC-1 has been implicated as being involved in SNARE mediated membrane fusion by interaction of its protein components with syntaxin 13 and SNAP-25/23 (Falcón-Pérez et al. 2002)(Starcevic & Dell'Angelica 2004). Oculocutaneous albinism and absent platelet dense granules are defining features of HPS and a bleeding tendency is associated with poor platelet aggregation due to the lack of dense granules. The *buff* mouse, with a missense mutation in *Vps33a*, described in section 1.9.1 has been suggested as a HPS model, however no human mutations have been identified in *VPS33A* to date (Suzuki et al. 2003). In total 15 mouse models of HPS have been reported (Wei 2006).

Chediak Higashi Syndrome (CHS) is a severe autosomal recessive syndrome dense granule storage pool disease caused by mutations in LYSosomal Trafficking regulator

(LYST)(Barbosa et al. 1996)(Nagle et al. 1996). When CHS platelets were studied by EM in 1983 a large reduction in dense granules was reported (Rendu et al. 1983). Bleeding diathesis is often mild and includes easy bruising and gum/mucosal bleeding. A prolonged bleeding time with a failure of platelets to aggregate has been observed (Salles et al. 2008). LYST contains a BEACH domain (Domain named after *Beige* mouse, and Chediak Higashi Syndrome), a HEAT (Huntington, Elongation Factor 3, PR65/ATOR) domain and several WD domains in its C-terminal region (Kaplan et al. 2008). Yeast two-hybrids have revealed several LYST interacting proteins which regulate vesicle docking and fusion including Q-SNAREs and R-SNAREs, HRS- a SNARE complex protein, and the signalling protein 14-3-3 $\delta$  (Tchernev et al. 2002)(Ward et al. 2003). A proteomic study comparing the lysosomal contents from the liver of the *beige* mouse, a Chediak-Higashi model, found that the lysosomal contents revealed no major differences but that the membrane had decreased levels of lysosomal membrane proteins such as Lamp1, Lamp2 and Niemann-Pick type C1. There was also an increase in endoplasmic reticulum membrane proteins, for example cytochrome P450. It was suggested that LYST may play a role in preventing the incorporation of inappropriate proteins into the lysosomal membrane, or have a role in membrane recycling/maturation (Zhang et al. 2007). In 2010, Hammel et al. found that secretory granules retained the ability to fuse randomly with other secretory granules no matter the size in the beige mouse. The role of LYST as a negative regulator of granule-granule fusion in mice was suggested (Hammel et al. 2010).

ARC platelets have been described as having a Grey Platelet Syndrome (GPS) appearance (Deal et al. 1990). GPS was first described by Raccuglia in 1971 (Raccuglia 1971). It is a rare congenital syndrome, primarily associated with the grey appearance of platelets when viewed under light microscopy. Diagnosis of GPS is often due to mild symptoms such as easy

bruising or more obvious problems, for example excessive bleeding after operations (Hayward 1997).

GPS platelets have been found to be highly variable in their size and structure (Mori et al. 1984). EM reveals that in Grey platelets  $\alpha$ -granule numbers are significantly reduced (White 1979) whereas the number of dense granules, lysosomes and peroxisomes is within the normal range. GPS platelets often have characteristic large vacuoles, which are made up of  $\alpha$ -granule membranes identified by specific antibodies such as P-selectin, an  $\alpha$ -granule membrane protein. These empty  $\alpha$ -granules redistribute and fuse with the platelet cell surface membrane upon activation reinforcing the idea that GPS is not a secretion problem but a storage deficiency disorder (Rosa et al. 1987).

Protein deficiencies of  $\alpha$ -granule proteins differ from patient to patient. Immunogold labelling has found traces of soluble  $\alpha$ -granule proteins such as VWF and fibrinogen in 'empty'  $\alpha$ -granules and in smaller granules resembling lysosomes (Cramer et al. 1985). Other  $\alpha$ -granule proteins obtained by endocytosis such as albumin and IgG are present and secreted in significant quantities from GPS  $\alpha$ -granules (Rosa et al. 1987). Albumin was localised to the 'small' residual  $\alpha$ -granules by EM (Maynard et al. 2010). Endogenously produced soluble proteins stored in  $\alpha$ -granules are severely deficient in GPS including Platelet Derived Growth Factor, thrombospondin and fibronectin (Hayward et al. 1996). This observation suggests that GPS is caused by a problem in the targeting and packaging of endogenously synthesised proteins and proteins obtained by endocytosis.

GPS patients show great heterogeneity in platelet function. Bleeding times vary, ranging from normal to prolonged (Hayward 1997) and aggregation studies have shown that some patients have normal platelet aggregation (Falik-Zaccai et al. 2001) while others do not.

Morphological studies on control and Grey platelets identify significant differences in appearance during aggregation (Mori et al. 1986). Grey platelets are only loosely cross-linked, resembling the early phase of aggregation that is seen in normal platelets (Nurden & Nurden 2007). This may be explained by the absence of secretion of key adhesive proteins from the  $\alpha$ -granules such that platelets cannot progress to the secretion-dependent phase of platelet aggregation (Nurden & Nurden 2007).

GPS is in most cases assumed to be an autosomal recessive disorder, as familial studies have shown siblings but not parents to be affected (Bolton-Maggs et al. 2006). There has however been one large Japanese family identified with an autosomal dominant form of the disease (Mori et al. 1984). In 2011, mutations in *NBEAL2* (neurobeachin-like 2) were identified in 15/25 GPS patients with the autosomal recessive subtype (Gunay-Aygun et al. 2011)(Kahr et al. 2011)(Albers et al. 2011). Five missense, three nonsense, four frameshift and three splice site mutations were identified in *NBEAL2* (Gunay-Aygun et al. 2011). The heterogeneity in GPS may therefore be partially due to the wide variety of mutations seen in these patients, and the resultant effect on *NBEAL2* structure. The function of this protein in megakaryocytes is not known, but it has been shown to be localised to the dense tubular system in platelets (Gunay-Aygun et al. 2011).

*NBEAL2* contains 3 domains: WD40, ARM-type and a BEACH domain, which are highly conserved and necessary for protein-protein interactions, membrane dynamics and vesicle trafficking (Gunay-Aygun et al. 2011). The BEACH domain and WD40 domains are also found in *LYST*, mutations in which cause CHS. Both diseases involve impaired formation and trafficking of platelet vesicles.



#### 1.11.4 ARC syndrome platelets

A defect in platelet morphology in ARC was first described in 1990 in a patient whose platelets resembled those of GPS (Deal et al. 1990). They lacked  $\alpha$ -granules and had low levels of the  $\alpha$ -granule proteins  $\beta$ -thromboglobulin, Platelet Factor 4 (PF4) and thrombospondin. Furthermore, 7 out of 16 ARC patients who underwent organ biopsy experienced severe life threatening haemorrhaging consistent with a platelet defect (Gissen et al. 2006).

Eastham et al. reported that the blood films of 4 ARC patients had abnormally large platelets with a mean platelet diameter of up to 10 $\mu$ m compared to the average of 3 $\mu$ m (Eastham et al. 2001). Structural abnormalities were observed in Wright-Giemsa blood films and resembled platelets from patients with GPS with the platelets being large, pale and agranular (Deal et al. 1990). Lo et al. performed transmission EM on two ARC patients and reported the complete absence of  $\alpha$ -granules in comparison to control platelets containing an average 5.5 granules per platelet. They also lacked  $\alpha$ -granule membranes in contrast to GPS platelets. On the other hand, small 'densities' were identified in ~50% of the ARC platelets which were absent in controls and could represent primitive granules that are capable of release (Lo et al. 2005). In 2010, a study of 12 ARC patients confirmed the findings of Eastham and Lo, that the majority of the platelets were large and agranular, and all lacked  $\alpha$ -granules (Kim et al. 2010). The grey appearance of platelets is therefore also a cardinal feature of ARC. Quantitation of  $\alpha$ -granule proteins within ARC platelets by immunoblotting revealed deficiencies in the endogenously synthesised and secreted  $\alpha$ -granule proteins, PF4, VWF,  $\beta$ -thromboglobulin and Thrombospondin-1, as well as fibrinogen derived from the plasma and  $\alpha$ -granule membrane protein P-selectin (Lo et al. 2005). Song also reported severe VWF deficiency in

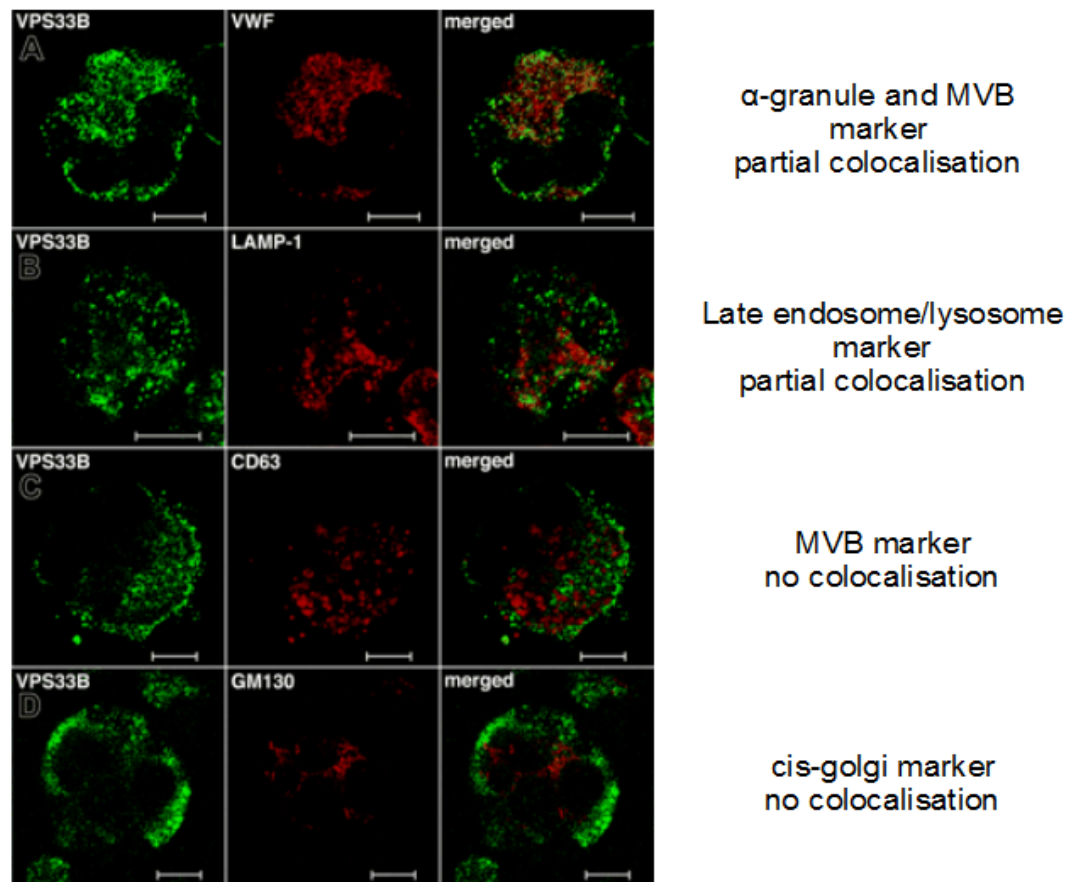
ARC platelets (Song et al. 2003). In megakaryocytes, the level of PF4 was also found to be severely deficient (Lo et al. 2005).

The number of dense granules was increased in ARC platelets with an average of 6.5 per ARC platelet in comparison to 1.4 per control platelet observed by whole mount EM (Lo et al. 2005). Only 2 patients however were analysed, therefore it is difficult to draw any conclusions from this data. In contrast to the findings of Lo et al, Kim et al. did not identify abnormalities in dense granules, although the data was not shown (Kim et al. 2010).

Due to the rarity of ARC syndrome, the young age of patients and the severity of phenotype, blood for functional studies is very limited. As a result, studies on ARC platelet function are incomplete. Reduced aggregation to arachidonic acid and absent secondary aggregation wave to ADP have been reported when using platelet rich plasma (PRP)(Lo et al. 2005). In a separate study, one patient presented without a secondary aggregation wave in response to collagen and ADP but a normal response to epinephrine (Song et al. 2003), however details about experimental procedure were not provided. To draw any conclusions from this work it must be known if PRP or washed platelets were used as fibrinogen is present in plasma as well as  $\alpha$ -granules.

#### **1.11.5 Vps33b in megakaryocytes**

Vps33b is not present in platelets suggesting that it plays a critical role at the level of the megakaryocyte (Lo et al. 2005). In ARC megakaryocytes grown in culture, numerous vacuole-like structures present suggesting a defect in megakaryocyte maturation. The localisation of Vps33b in megakaryocytes has been investigated using antibodies for Vps33b and various vesicle markers (Lo et al. 2005). These experiments revealed that Vps33b



**Figure 1.9 Immunofluorescence localisation of VPS33B with vesicle/organelle markers**

VPS33B partially co-localised with von Willebrand factor (VWF) an MVB and  $\alpha$ -granule marker. It also partially co-localises with LAMP-1, a marker for late endosome/lysosomes, but not with CD63 which is found in MVBs, dense granules and lysosomes. VPS33B is also absent from cis-golgi (GM130) membranes. Adapted from (Lo et al. 2005)

co-localises partially with VWF, a MVB and  $\alpha$ -granule marker. It also partially co-localises with LAMP-1, a marker for late endosome/lysosomes, but not with CD63 which is found in MVBs, dense granules and lysosomes suggesting that Vps33b is absent from lysosomes. Vps33b is also absent from cis-golgi (GM130) membranes (figure 1.9). Vps33b therefore co-localises with  $\alpha$ -granules and late endosomes, but not with lysosomes, cis-golgi or dense granules.

### **1.12 Thesis Aims**

The molecular mechanisms underlying ARC pathogenesis remain unknown. In order to begin to elucidate the proteins and pathways involved in this severe syndrome two different strategies have been adopted in this study.

1. By modelling patient mutations, insights into the effect of the mutation on protein interaction/localisation may be gained. Therefore, the aim of the first approach is to identify novel mutations in VPS33B and VIPAR by screening putative ARC patients. By modelling a variety of mutations, the aim is to learn about how mutations may disturb correct cellular function.
2. Whilst VPS33B and VIPAR function has been studied in knockdown cell lines and model organisms including *Drosophila* and *C. elegans*, study in mammals is limited to what can be learnt from ARC patients. However, due to the severity of ARC syndrome, patient material for study is incredibly limited. Therefore the aim of the work presented is to develop a murine model of ARC syndrome in order to investigate the effect of Vps33b deficiency in specific cell types and organs, such as megakaryocytes/platelets and the liver. It is the hope that a Vps33b deficient mouse will also provide a model for development of treatments for ARC syndrome in the future.

## **CHAPTER 2 – MATERIALS AND METHODS**

All reagents are from Sigma-Aldrich, Poole, UK unless otherwise stated.

## **2.1 ARC-LOVD Database**

An online locus-specific ARC database (<https://grenada.lumc.nl/LOVD2/ARC>) was compiled using the Leiden Open Source Variation Database (LOVD) software system. To establish the database all relevant data from HGMD ([www.hgmd.org](http://www.hgmd.org)) was added and a literature search was performed. The terms ‘VPS33B’, ‘VIPAR’ and ‘ARC syndrome’ were entered into PubMed (<http://www.ncbi.nlm.nih.gov/sites/entrez?db=PubMed>) and abstracts and full-text articles retrieved were screened for descriptions of sequence variants. The database also contains variants taken from dbSNP (<http://www.ncbi.nlm.nih.gov/projects/SNP>) (Sherry et al. 2001). Any mutations found in patients referred for diagnostic analysis also have been included in the database.

## **2.2 Protein structure predictions of VPS33B and VIPAR**

Predictions of protein secondary structure, globularity and disorder were performed using GlobPlot (<http://globplot.embl.de/>), FoldIndex (<http://bip.weizmann.ac.il/fldbin/findex>), IUPred (<http://iupred.enzim.hu/>), RONN (<http://www.oppf.ox.ac.uk/RONN/>), and HHPRED (<http://toolkit.tuebingen.mpg.de/hhpred>).

## **2.3 Patients and controls**

Informed consent was obtained from all participating families; research ethics committees from all participating institutions approved the study. Primary skin fibroblasts from patients were cultured in Dulbecco’s Modified Eagle’s Medium supplemented with 10% fetal calf serum, 2 mM L-glutamine, MEM Non-Essential Amino Acid solution.

## **2.4 Extraction of DNA from cells and tissue**

The Qiagen DNeasy blood and tissue kit (Qiagen, Crawley UK) was used to extract DNA from patient cultured fibroblasts. A water control was always carried out to monitor for contamination. Fibroblasts cultured in 75cm<sup>2</sup> flasks were washed twice with PBS and scraped into 200µl of PBS. 180µl buffer ATL supplemented with 20µl proteinase K was added to the patient cells to allow direct cell lysis overnight at 56°C. 200µl Buffer AL and 200µl ethanol (96%-100%) were added to allow selective binding of DNA to the DNeasy membrane. Next, the sample was placed in a DNeasy spin column and centrifuged at 6000 x g for 1 minute. The supernatant was discarded and subsequent washing steps with 500µl Buffer AW1 and then 500µl Buffer AW2 were carried out to remove contaminants and enzyme inhibitors. The samples were eluted into 30-50µl water by centrifuging at 6000 x g for 1 minute.

## **2.5 Polymerase Chain Reaction (PCR)**

PCR was carried out to amplify patient's 23 VPS33B and 19 VIPAR exons with flanking intronic sequence using previously designed primers (Appendix 1). PCR was also used to genotype the offspring of mouse matings (Appendix 1). The ThermoPrime PCR kit (ThermoScientific, Kent); Taq, dNTPs, reaction buffer and MgCl<sub>2</sub> was used. A standard reaction mixture of 25µl was prepared, the reagents and volumes found below.

Reagent	Volume (per reaction)
DNA	1µl
Primers (10µM)	0.5µl per primer
10x Reaction Buffer	2.5µl
MgCl <sub>2</sub> (25mM)	1.5µl
dNTP mix (10µM)	1.25µl
Taq	0.2µl
Milipore Water	Make up to 25µl
<b>Total</b>	<b>25µl</b>

The following conditions were applied

96°C	96°C	60°C	72°C	72°C
3 minutes	<b>45 seconds</b>	<b>45 seconds</b>	<b>45 seconds</b>	10 minutes
	<b>35 cycles</b>			

The taq used for these reactions works at up to 74°C, incorporating approximately 1000bp per minute. Therefore, the extension time was adjusted depending on how large the expected PCR product was. The annealing temperature was dependent upon the primers, which were designed to have annealing temperatures of 58°C.

## **2.6 Agarose gel electrophoresis**

In order to determine if the PCR reaction had been successful and to determine the size of the products produced, gel electrophoresis was carried out. A 2% agarose gel was made by dissolving 2% w/v agarose (Bioline, London) in 1 x TBE (90mM Tris base, 90mM Boric



acid, 2mM EDTA, pH8) and adding 10ngml<sup>-1</sup> Ethidium Bromide. The buffer used was 1 x TBE, and 10µl of PCR product with 2µl 6x loading buffer (2 mM EDTA, 50% glycerol and 0.1% orange G) was loaded. 100bp ladder (New England Biolabs, Hitchin, UK) was most commonly used with the 1kb plus ladder used for large products. Dependent on the size of the gel and the degree of separation required, gels were run at 90-140V, for 20-50 minutes.

## **2.7 Sequencing of DNA**

### **2.7.1 Exo-SAP reaction**

In order to purify the PCR products for downstream processing the ExoSAP-IT PCR Clean-up Kit (GE healthcare, UK) was used. This contains two enzymes, Exonuclease 1 which removes unwanted primers, and Shrimp Alkaline Phosphatase (SAP) which dephosphorylates any unused dNTPs. The concentration of the PCR product determined the volumes of reagents used.

Reagent	Volume
DNA	8.5µl
ExoSAP	1.5 µl
<b>Total</b>	<b>10 µl</b>

**OR**

Reagent	Volume
DNA	4.25 µl
Milipore water	4.25 µl
ExoSAP	1.5 µl
<b>Total</b>	<b>10µl</b>

The following conditions were applied:

37°C	80°C
45 minute incubation	15 minute enzyme inactivation

### 2.7.2 Sequencing reaction

To sequence patient DNA, the di-deoxy chain termination method was used. The DNA was sequenced bi-directionally therefore a reaction was carried out for both forward and reverse primers independently. The following reaction mixture was used (Applied Biosystem, Life Technologies, California).

Reagent	Volume
5x sequencing buffer	2 $\mu$ l
PCR product	4.4 $\mu$ l
Primer – forward or reverse (10 $\mu$ M)	1.6 $\mu$ l
Big Dye	1 $\mu$ l
Nuclease free water	1 $\mu$ l
<b>Total</b>	<b>10<math>\mu</math>l</b>

The following conditions were applied

96°C	96°C	50°C	60°C	12°C
30 seconds	<b>30 seconds</b>	<b>15 seconds</b>	<b>4 minutes</b>	forever
	<b>Repeat 30 times</b>			

### 2.7.3 Sample precipitation

In order to remove the unincorporated fluorescent ddNTPs and impurities from the DNA for automated sequencing, a precipitation reaction to clean the sample was carried out. 1 $\mu$ l 0.25M EDTA was firstly added to each sample followed by 32 $\mu$ l 95% ethanol. The sample was left to stand for 10 minutes then centrifuged at 4000 rpm, 4°C for 30 minutes. The ethanol was

removed and 125µl 70% ethanol was subsequently added. A further spin at 4000 rpm, 4°C for 30 minutes was carried out and the ethanol was again removed. The samples were then left to stand at room temperature for 10 minutes to allow the remaining ethanol to evaporate and 10µl HiDi Formamide used (Applied Biosystem, Life Technologies, California), a sample resuspension solution was added. The samples were then incubated at 95°C for 5 minutes to denature the DNA, and subsequently placed on ice.

#### **2.7.4 Sequencing analysis**

Denatured DNA was sequenced by ABI 3730 capillary sequencer (Applied Biosystems, California) and subsequently analyzed using BioEdit Sequence Alignment Editor. The sequence traces were firstly analysed by sight to identify any heterozygous changes. The sequence was then compared against control sequence using the ClustalW function to identify any homozygous sequence changes. If any changes were found they were checked against a SNP database (<http://www.ncbi.nlm.nih.gov/projects/SNP>).

#### **2.8 RNA extraction**

To isolate RNA from fibroblasts the reagent RNA-Bee (AMS Biotechnology Europe Ltd, Abingdon UK) was used. Cells were firstly homogenized by scraping confluent fibroblast cells in a 75cm<sup>2</sup> flask into 0.5ml RNA-Bee, and adding a further 0.5ml RNA-Bee. For the separation into aqueous and organic phase, 0.2ml chloroform was added to the homogenate, shaken vigorously to mix, incubated at room temperature for 5 minutes and then centrifuged at 12,000 x g for 15 minutes at 4°C, this spin removes DNA and protein from the aqueous phase. To precipitate the RNA the aqueous layer was isolated and 0.5ml of isopropanol was added. It was left to incubate for 5 minutes at room temperature and the RNA was subsequently pelleted by centrifuging at 12,000 x g for 15 minutes at 4°C. The RNA pellet

was washed with 1ml 75% ethanol and centrifuged at 7,500 x g for 15 minutes at 4°C. Finally the RNA was solubilised by removing the ethanol, air-drying the pellet for 1 hour and dissolving the RNA in water.

## **2.9 DNA and RNA quantification**

In order to quantify and assess the purity of RNA extracted for the reverse transcription reaction, and DNA for real-time applications, quantification was carried out using a Nanodrop ND-1000 Spectrophotometer. 1µl of sample was placed on the detector and a reading was taken.

Absorbance values were taken at 260nm and 280nm and the ratio 260nm:280nm calculated. A ratio of ~1.8 is accepted as “pure” for DNA and a ratio of ~2.0 is accepted as “pure” for RNA.

For RNA

$$[\text{RNA}] (\text{mgml}^{-1}) = \frac{\text{Absorbance at 260 nm} \times \text{Dilution Factor} \times 40}{1000}$$

For DNA

$$[\text{DNA}] (\text{mgml}^{-1}) = \frac{\text{Absorbance at 260 nm} \times \text{Dilution Factor} \times 50}{1000}$$

## **2.10 RNA analysis**

### **2.10.1 Reverse Transcription**

The Promega reverse transcription system (Promega UK, Southampton UK) was used to produce cDNA from the previously extracted RNA. The reaction mix can be found below.

<b>Reagent</b>	<b>Volume</b>
10x Reaction Buffer	2µl
MgCl <sub>2</sub> (25mM)	4µl
dNTP (10mM)	2µl
Random primers or polydT primers	2µl
Reverse transcriptase	0.8µl
RNA	1µg
H <sub>2</sub> O	Make up to 20µl
<b>Total</b>	<b>20µl</b>

The following conditions were applied:

42°C	96°C
<b>1 hour</b>	<b>5 minutes</b>

### 2.10.2 Sequencing of cDNA

Sequencing of cDNA was carried out as in section 2.4 except that the primers were designed for exonic sequence. Primer sequences for both VPS33B cDNA and VIPAR cDNA can be found in Appendix 1.

## 2.11 Techniques for identification of complex mutations

### 2.11.1 Platinum Taq

Platinum Taq (Life technologies, California) is a hot start Taq which is attached to an enzyme which inhibits it until heated to 96°C which increases specificity and yield. It was used when amplification of DNA proved difficult with ThermoPrime Taq.

Reagent	Volume
DNA	1µl
Primers (10µM)	0.5µl (per primer)
10x Reaction Buffer	2.5µl
MgCl <sub>2</sub> (50mM)	0.75µl
dNTP mix (10mM)	1.25µl
Platinum Taq	0.2µl
Milipore water	make up to 25µl
<b>Total</b>	<b>25µl</b>

The following conditions were applied

94°C	94°C	60°C	72°C	12°C
3 minutes	<b>45 Seconds</b>	<b>45 Seconds</b>	<b>1 minute</b>	forever
	<b>Repeat 35 times</b>			

### 2.11.2 Gel extraction

Extraction of DNA from bands separated by agarose gel electrophoresis was carried out using the Qiagen QIAquick Gel Extraction Kit, spin column protocol (Qiagen, Crawley UK).

Firstly, the bands were cut from the gel and 3 volumes of buffer QG were added to one volume of agarose gel. The gel was then melted at 50°C for 10 minutes. 1 volume of isopropanol was then added to increase DNA yield. The solution was then applied to a QIAquick column and centrifuged at 17,900 x g for 1 minute, allowing the DNA to bind and waste to pass through. The supernatant was discarded and an additional 0.5ml QG buffer was added to the column and centrifuged to remove any remaining agarose, and the supernatant discarded. 0.75ml Buffer PE was then added to the column to wash, and centrifuged and supernatant discarded. The column was spun for a further minute to remove any residual ethanol and the DNA was eluted by adding 30µl water and spinning for 1 minute, collecting the DNA in an eppendorf.

### 2.11.3 Long range PCR

Long range PCR using 5-PRIME PCR extender system (5PRIME, Nottingham UK) was required to amplify genomic DNA too large for standard PCR. The reaction mix can be found below.

Reagent	Volume (per reaction)
5 PRIME PCR Extender enzyme mix	0.3µl
5 PRIME Tuning buffer	5µl
dNTP mix (100µM)	0.8µl
DNA	1µl
Primer (100µM)	0.5µl per primer
Milipore water	Make up to 50µl

<b>Total</b>	<b>50µl</b>
--------------	-------------

The following incremental conditions were applied in order to maximize the amount of PCR product produced.

95°C	95°C	68°C	95°C	68°C	68°C	12°C
2 minutes	<b>30s</b>	<b>3 min 30s</b>	<b>30s</b>	<b>3 min 30s – increase 20s every cycle</b>	15 minutes	forever
	<b>Repeat 11 times</b>		<b>Repeat 26 times</b>			

The extension time was adjusted depending on the size of the PCR product, approximately 1000bp per minute as a guide.

#### 2.11.4 Nested primers

In order to sequence across a deletion found in a patient nested primers were designed. This was necessary as the PCR product was too long to sequence with one forward and one reverse primer. As the PCR product was clean due to gel extraction only the sequencing reaction and precipitation was required prior to sequencing.

#### 2.11.5 3'-RACE

To determine the functional implications of a splice site mutation, OligodT primers with adapter sequence attached from the 3'-RACE kit (Roche Diagnostics, West Sussex) in place of the normal OligodT primers were used for reverse transcription of patient RNA. VPS33B cDNA was then amplified using the 3'-RACE adapter primer and 3F VPS33B cDNA primer. Nested PCR was then carried out to further amplify specific product. 0.5µl of the PCR product was used in the reaction and the 4F VPS33B cDNA primer and 3'-RACE adapter primer were used. The PCR products were analysed using agarose gel electrophoresis.



### 2.11.6 Quantitative Real-time PCR using genomic DNA

PCR primers were designed for *VPS33B* and two house-keeping genes, *actin* and *GAPDH*. Using Primer3 the primers were designed to amplify approximately 200bp and have a melting temperature of 60°C. As the purpose of this experiment was to identify exon deletions, the primers were placed in the intronic sequence flanking the exons being studied. The primer sequences generated were put through nBLAST to check for specificity. The primers were then optimised to eliminate primer-dimers that would skew results as SYBR green binds to double stranded DNA. To do this different primer concentrations from 1 to 0.05µM were used in standard PCR reactions at 60°C, the products of which were electrophoresed on a 4% agarose gel for confirmation that only one product was produced and that primer-dimers weren't present. A final concentration of 0.2µM for exon 4 and 0.1µM for actin and GAPDH were used.

25ng of DNA per reaction was used and each reaction was carried out in triplicate, a blank was used to check for background signal and contamination. A master mix was made for each different primer pair, the reagents below and was aliquoted into a 96-well optical plate and sealed. SYBR green (Applied biosystems, California) was used to detect double stranded DNA production.

Reagent	Volume per reaction (µl)
SYBR Green Master Mix (2x)	12.5
Forward Primer	0.25
Reverse Primer	0.25
Nuclease Free Water	9.5
cDNA	2.5
<b>Total</b>	<b>25</b>

The reaction conditions are as follows

50°C	95°C	95°C	60 °C
2 minutes	5 minutes	15 seconds	90 seconds
40 cycles			

Amplimer levels were measured by an iQ5 BioRad instrument and Ct values were calculated.

A dissociation curve analysis was carried out at the end of the assay in order to confirm that only one product was amplified.

Utilising the Ct values, copy number could be calculated by using the 2 reference genes as a comparison. Firstly the value of the gene is transformed to a quantity relative to a calibrator – the calibrator in this case being a control sample.

$$Q = E^{(\text{calibratorCt} - \text{sampleCt})}$$

Q=quantity sample relative to the calibrator sample

E= amplification efficiency

The relative quantities were then divided by the geometric mean of the 2 reference gene copy numbers.

A haploid copy number of 1 is expected for a normal sample and 0.5 for those with a deletion (Hoebeeck et al. 2005).

## **2.12 Cloning of Vps33b cDNA for sequencing**

### **2.12.1 Ligation reaction**

In order to sequence the gel extracted 3'-RACE PCR product, cloning was conducted using pGEM-T Easy Vector system (Promega, Southampton UK). Firstly a ligation reaction, found below, was carried out.

<b>Reagent</b>	<b>Volume</b>
2x reaction buffer	5 µl
PCR product	2 µl
pGEM-T easy cloning vector (50ng/µl)	1 µl
Water, nuclease free	1 µl
T4 DNA ligase	1 µl
<b>Total</b>	<b>10 µl</b>

The reaction mix was vortexed briefly and incubated at room temperature overnight. This reaction mix was then used for bacterial transformation.

### **2.12.2 Bacterial transformation**

The heat shock method was used to transform *E. coli* competent cells. 10µl of the ligation mixture was added to 50µl of competent cells and left on ice for 15 minutes. The cells were then subjected to heat shock, at 42°C for 45 seconds and were then transferred back to ice for 2 minutes. Finally 500µl of SOC was added to the mixture and left to incubate at 37°C shaking at 220 rpm for 1 ½ hours. The mixture was then centrifuged at 3000rpm for 1 minute, the top 360µl of supernatant removed and the cell pellet resuspended in the remaining supernatant and plated onto Xgal and IPTG treated agar plates supplemented with 100µg/ml

ampicillin. 20µl XGal (50mg/ml) and 100µl IPTG (100mM) were added to the agar plate 30 minutes before plating the bacteria. These were left to incubate overnight at 37°C.

### **2.12.3 Colony Selection**

Xgal and IPTG treated agar plates allowed blue/white selection of colonies, white colonies are recombinant colonies containing an insert, blue are non-recombinant and do not contain an insert. White colonies were selected and transferred to 10ml Luria Broth supplemented with 10µg/ml ampicillin and left to culture overnight at 37°C, shaking at 220 rpm.

### **2.12.4 Miniprep**

To extract and purify the plasmids from bacteria the Qiaprep miniprep kit (Qiagen, Crawley UK), microcentrifuge protocol was used. Firstly the bacterial cells were pelleted by centrifuging at 3000 rpm for 1 minute. The supernatant was discarded and the bacteria were resuspended in 250µl Buffer P1. 250µl Buffer P2 was then added to lyse the cells. Next, 350µl of Buffer N3 was added to adjust the conditions to that of high-salt for DNA binding. The cells were then centrifuged for 10 minutes at 17,000 x g in a microcentrifuge. The supernatant containing the plasmid was then removed and added to the spin column provided and centrifuged for 1 minute at 17,000 x g. The column was then washed to remove exonucleases by adding 0.5ml Buffer PB and centrifuging for 1 minute at 17,000 x g. The spin column was washed with 0.75ml Buffer PE to remove salts and centrifuged for a further 1 minute at 17,000 x g. The flow-through was discarded and the column spun for another minute to remove any excess wash buffer. The plasmid was eluted by adding 50µl water to the column, leaving for 1 minute and then centrifuging for 1 minute at 17,000 x g and collecting the flow-through in a 2.5ml eppendorf.

### 2.12.5 Sequencing a plasmid

Sequencing of the insert within the plasmid is carried out in the same way as in 2.4.2, with plasmid specific primers however, the volumes for the sequencing reaction are altered slightly.

Reagent	Volume
DNA	1 $\mu$ l
Primer – forward or reverse (10mM)	0.8 $\mu$ l
Big Dye buffer	2 $\mu$ l
Big Dye	1 $\mu$ l
Milipore water	5.2 $\mu$ l
<b>Total</b>	<b>10<math>\mu</math>l</b>

### 2.12.6 Site Directed Mutagenesis

To introduce base pair changes into the wild type *VPS33B* and *VIPAR* constructs in order to model known mutations, two complementary primers were designed with the nucleotide change and 15 bp of correct sequence either side. The Stratagene site directed mutagenesis XL kit (Agilent Technologies, Germany) was then used to introduce the mutation. The first step was to introduce the mutation by PCR.

Reagent	Volume
10 $\times$ reaction buffer	5 $\mu$ l
dsDNA template	10 ng
oligonucleotide primer #1	125 ng
oligonucleotide primer #2	125 ng
dNTP mix	1 $\mu$ l
QuikSolution	3 $\mu$ l
<i>PfuUltra</i> HF DNA polymerase	1 $\mu$ l
ddH <sub>2</sub> O	final volume of 50 $\mu$ l

The reaction conditions are specified below

95°C	95°C	60°C	68°C	68°C
1 min	50 seconds	50 seconds	5 ½ mins	7 mins

1µl of DpnI was then added to the reaction mix in order to digest any methylated parental DNA, and incubated at 37°C for 1 hour. XL-1 blue cells were then transformed with 4µl of the reaction mix. Colonies were subsequently selected and screened for the inserted mutation by sequencing. Patient AB *VPS33B-c.1225G>C* construction was more complex several approaches were attempted in order to produce a construct with the mutated cDNA running into intron 16-17. Initially, it was attempted to clone the whole length of the cDNA, this however proved unsuccessful. Introducing novel restriction sites by site directed mutagenesis into wild-type *VPS33B* and the cloned patient cDNA, removing exons 16-23, and inserting the mutant cDNA into the cleaved wild-type construct was successful.

## **2.13 Co-overexpression studies**

### **2.13.1 Cell Culture**

HEK293 cells were grown in growth medium consisting of Dulbeccos's Modified Eagle's Medium supplemented with 10% foetal bovine serum, 2mM L-glutamin, 1x MEM non-essential amino acid solution and 1x penicillin-streptomycin. Cells were passaged through 0.25% trypsin for 5 minutes after being washed twice with PBS and cells were diluted as required in growth medium for replating. Cells were grown at 37°C with 5% CO<sub>2</sub>.

### **2.13.2 Transfection**

HEK293 cells were seeded onto coverslips in a 24 well plate and allowed to grow to ~70% confluence. On the day of transfection the medium was removed and 500µl of Opti-MEM I (Life technologies, California) without antibiotics was added. 0.8µg of plasmid DNA was added to 50µl of Opti-MEM I. Next, Lipofectamine 2000 (Life technologies, California) was added to 50µl of Opti-MEM I and left to incubate for 5 minutes. The DNA and lipofectamine solutions were then mixed and left to incubate for 20 minutes at room temperature. The resulting mixture was then added to the cells and incubated at 37°C with 5% CO<sub>2</sub> overnight. The medium was changed 24 hours later to complete growth medium.

### **2.13.3 Fixation and staining**

Cells were fixed in 4% paraformaldehyde in PBS for 4 minutes. The cells were then washed 3 times with PBS and permeabilised with 0.1% Triton X100 in PBS for 4 minutes. Cells were washed 3 times in PBS and blocked for 30 minutes with 1% BSA in PBS. Coverslips were then transferred to parafilm and incubated with primary antibody for 1 hour. The coverslips were washed 3 times with PBS and again transferred to parafilm for incubation with fluorescently labelled secondary antibody for 45 minutes, antibodies listed in Appendix 1. Cells were again placed in the tray, washed 3 times with PBS and then incubated with TO-PRO-3 (1:1000)(Invitrogen, Paisley, UK) for 2 minutes and washed with PBS 3 times. The coverslips were then mounted face down on microscope slides with 2µl Prolong gold antifade reagent (Life Technologies, California).

### **2.13.4 Immunofluorescence confocal Microscopy**

Microscopic images were captured using an inverted Leica TCS SP2 AOBS confocal microscope (Leica, Milton Keynes, UK) with 63x oil immersion objective and the pinhole set

to 1 Airy unit. Optical sections were collected in the xy plane and merged to maximum projection images.

## **2.14 Protein extraction**

Tissues extracted from mice were snap frozen in liquid nitrogen and stored at -80°C until required. Tissue was crushed in a pestle and mortar using dry ice, and liquid nitrogen to maintain the frozen state of the sample. 2x RIPA lysis buffer (50mM Tris-HCl, 150mM NaCl, 1mM EDTA, 1% Igepal CA630, 0.5% Sodium Deoxycholate, 0.1% SDS and complete mini protease inhibitor cocktail (Roche Diagnostics, Burgess Hill, UK)) was added to the crushed sample. Cultured cells were washed twice with ice-cold PBS and then were scraped into 250ul of MRC lysis buffer (50 mM Tris-HCl pH=7.5, 50 mM Sodium Fluoride, 5 mM Sodium Pyrophosphate, 1 mM Sodium Orthovanadate, 1 mM EDTA, 1 mM EGTA, 0.27 M Sucrose, 1% Triton - X - 100 and complete mini protease inhibitor cocktail (Roche Diagnostics, Burgess Hill, UK)). For megakaryocytes, 50µl per mouse of 2x RIPA buffer was added to lyse the cells. The solution was then centrifuged at 18,000 x g for 15minutes at 4°C to remove any cell debris, and the supernatant transferred to a clean tube.

## **2.15 Western Blotting**

### **2.15.1 Protein quantification**

In order to determine the concentration of protein in the lysate, the BioRad Dc Protein Assay kit was used (BioRad, Hertfordshire, UK). A 2-fold serial dilution of 3µg/µl Bovine serum albumin (BSA) with lysis buffer was carried out for each assay, with lysis buffer alone used as blank. 10µl reagent S was added to 500µl reagent A, to make reagent A'. On a 96-well plate, in each well 5µl of standard or sample, 25µl of A' and 200µl of reagent B was added



and left covered at room temperature for 15minutes to develop. The plate was then read at 690nm for 1 second per well, and protein concentration for the samples extrapolated from the standard curve.

### 2.15.2 SDS-PAGE

To separate the proteins according to their mass, Sodium Dodecyl Sulphate PolyAcrylamide Gel Electrophoreses was carried out. The resolving gel was made first, and the percentage used was dependent on the proteins mass – the larger the protein the lower the percentage gel used. The recipe for 2 1mm gels may be found below.

Reagents	Volume		
	10% polyacrylamide gel	12% polyacrylamide gel	15% polyacrylamide gel
30% Acrylamide	3.3ml	4ml	5ml
Water	3.9ml	3.2ml	2.3ml
10% APS	0.2ml	0.2ml	0.1ml
1.5M Tris pH 8.8	2.5ml		
10% SDS	0.1ml		
TEMED – added	8µl		

After the TEMED was added, the solution was applied to a 1mm glass plate up to the level where the comb sits (BioRad, Hertfordshire, UK). The gel was overlayed with isopropanol, left to set for 20minutes and then rinsed twice with water. The stacking gel was then prepared, as below, and applied to the top of the resolving gel and combs were added. This was left to set for 20 minutes.

Reagents	Volume
30% Acrylamide	1.0ml
Water	3.4ml
0.5M Tris pH 6.8	1.5ml
10% SDS	60 $\mu$ l
10% APS	90 $\mu$ l
TEMED – added last	6 $\mu$ l

Meanwhile, protein lysate with lamelli loading buffer was boiled for 10 minutes. 3 $\mu$ l of a known molecular weight ladder (Page Ruler, Fermentas, York) was used to determine the protein mass and 20 $\mu$ g of protein lysate was loaded per well. The SDS-PAGE was run at 30mA for ~1hr in 1x SDS Running Buffer (192 mM Glycine, 250 M Tris-Base and 0.1% SDS) until the dye reached the bottom of the gel.

### 2.15.3 Protein Transfer

In order to carry out immunoblotting, the proteins were transferred from the gel to a PVDF membrane (GE Healthcare, Chalfont St Giles, UK). The membrane was activated by placing in methanol for 1 minute. All equipment required for the transfer was placed in 1 x Transfer Buffer (192 mM Glycine, 250 mM Tris-Base and 20% methanol). The equipment was the constructed as below, making sure there were no air bubbles between the gel and membrane. The transfer of protein from the gel to the membrane was carried out in 1 x Transfer buffer at 100mA for 1 hour, with an icepack and stirring.

Anode	Fibre Pad
	Filter Paper
	PVDF membrane
	Polyacrylamide Gel
	Filter paper
Cathode	Fibre Pad

#### 2.15.4 Immunoblotting

Membranes were left to block overnight in 10% non-fat dried milk powder (Marvel) dissolved in PBS-Tween 0.1% (PBST) at 4°C, they were then left to incubate at room temperature for 1 hour on a roller with the primary antibody in 5% dried milk in PBST, antibodies and concentrations used may be found in the appendix. Membranes were washed by shaking in PBST for 5 minutes, this was repeated 3 times. The membrane was then blocked in 5% dried milk in PBST for 5 minutes before incubating with the secondary antibody in 5% dried milk in PBST for 1 hour on a roller. The membrane was subsequently washed 3 times in PBST.

#### 2.15.5 Detection

For immunoblotting the secondary antibodies used were Horse Radish Peroxidase (HRP) conjugates and therefore the enhanced chemo-luminescence plus (ECL+) western blotting detection system reagents (GE Healthcare, Chalfont St Giles, UK) were used, 1ml of reagent A and 25µl of reagent B were mixed and added to the membrane for 10 minutes in the dark. The bands were detected using X-ray film (Kodak).

### 2.15.6 Stripping and Re-probing

To strip the membrane of antibodies to reprobe to test for equal loading of protein, the membrane was placed face down in a beaker of boiling water for 20 minutes. The membrane was then blocked overnight in 10% dried milk in PBST and blotted as described in 2.12.4 and 2.12.5.

### 2.15.7 Densitometry

Western blot films were scanned, and ImageJ (<http://rsb.info.nih.gov/ij/index.html>) was subsequently used to calculate relative quantities of protein by densitometry. Step by step instructions are described on the ImageJ website <http://rsb.info.nih.gov/ij/docs/menus/analyze.html#gels>. Each band was measured, and then the quantity normalised against  $\beta$ -actin measurements. In this way discrepancies in loading amounts were taken into consideration and allowed the comparison of different samples.

## 2.16 Mouse strains

Embryonic stem cells containing *Vps33a* gene trap were purchased from Bay Genomics. Chimeric mice were produced by injection of the ES cells into blastocysts by Andrea Bacon, The University of Birmingham. Those containing the allele within their germ cells were used to breed heterozygous mice, *Vps33a*<sup>+/-</sup> on a 129P2 background. Conditional *Vps33b* ES cell lines and subsequent mice with LoxP sites flanking *Vps33b* exons 2-3 were created by Artemis Pharmaceuticals, and *Vps33b*<sup>+/*fl*</sup> mice were provided for breeding. These were subsequently crossed in order to produce *Vps33b*<sup>*fl/fl*</sup> mice on a C57BL/6J background. Cre recombinase transgenic lines were selected for temporal or spatial control of *Vps33b* expression. A ubiquitous cre expressing line, *Pgk*-cre, utilising a 3-phosphoglycerate (PGK-1) promoter was used to remove *Vps33b* from all tissue (McBurney et al. 1994). *Pf4*-cre

mice, utilizing the platelet factor 4 promoter were used to create megakaryocyte and platelet specific *Vps33b*<sup>fl/fl</sup> mouse (Tiedt et al. 2007). A liver specific *Alb*-cre line was selected which utilises the albumin cre promoter to create a liver specific *Vps33b* conditional knockout mouse (Postic et al. 1999). A second liver specific cre line was selected, *Alfp*-cre, which makes use of the albumin promoter and alphafetoprotein enhancers to induce cre expression at an earlier time-point in liver development (Kellendonk et al. 2000).

### **2.17 Animal Husbandry**

Mice were fed standard laboratory mouse diet of grain pellets. A 12 hour uninterrupted light-dark cycle was maintained for best breeding performance and litters were weaned at 3 weeks of age. Ear clipping was carried out after weaning for genotyping and individual mouse identification. The DNA was extracted from these ear clippings using 100µl DirectPCR Lysis Reagent (Viagen Biotech, Los Angeles, CA) and 20µl Proteinase K (Qiagen, Crawley, UK). Incubated overnight at 56°C and then inactivated at 86°C for 1hr. 1µl was subsequently used in a PCR reaction- see Appendix 1 for primer sequences.

## **2.18 Timed matings**

Mice were mated overnight and females were inspected for vaginal plugs the following morning. If plugs were identified, noon that day is considered stage E0.5.

### **2.18.1 Embryo extraction and genotyping**

The uterus was extracted from a schedule 1 culled pregnant mouse at the appropriate time-point. This was done by opening the body cavity and cutting across the cervix and 2 utero-tubal junctions, placing the uterus on a clean surface. The uterus was then removed by inserting scissors into the hole created at the cervix and cutting up the length of the uterine horn. Embryos were removed and dissected as described in 2.15.2-2.15.3. For genotyping the ectoplacental cone and Reichert's membrane are maternally contaminated therefore care must be taken when selecting tissue for genotyping, the yolk sac was primarily used. The yolk sac was added to 150µl ATL buffer containing Proteinase K and incubated at 56°C for 1 hour. 140µl 100% isopropanol was then added to precipitate the DNA. The solution was spun at maximum speed in a centrifuge for 30 minutes at 4 °C. The supernatant was then removed and discarded and the DNA pellet washed with 70% ethanol and spun for a further 10 minutes. Again the supernatant was removed and discarded and the pellet left to air dry for 10 minutes before being dissolved in 20µl H<sub>2</sub>O. 5µl of the DNA was used per PCR reaction. If the first PCR did not allow successful genotyping a subsequent PCR from this reaction was carried out. The mice were genotyped using PCR, primer sequences found in Appendix 1.

### **2.18.2 Dissection of E7.5**

Decidua were moved into fresh DMEM and were dissected using watchmaker forceps. The decidua was cut in half with the embryo remaining in one side. The embryo was then teased away from the remaining decidua. The trophoblast cells must be removed with careful use of forceps and subsequently the Reichert's membrane must be removed by tearing it open by grasping it where it stands away from the underlying tissue at the embryonic pole with two pairs of forceps and pulling apart.

### **2.18.3 Dissection of E8.5-9.5**

The decidua were removed into clean PBS and dissected using watchmaker forceps. The embryo can be found at the opposite end to the mesometrial pole. With one pair of forceps the decidua was secured at the mesometrial pole and then the decidual tissue was peeled back from the embryo. The yolk sac was then carefully removed, and images taken.

## **2.19 Establishing ES cell lines from blastocysts**

### **2.19.1 Mouse Embryonic Fibroblast (MEF) feeder cell preparation**

Timed matings were carried out and the embryos were extracted at E14.5. The heart, liver and cerebellum were removed and the remaining tissue was added to 10ml 1x trypsin in PBS, and left to incubate at 37°C for 30 minutes. 5ml of this solution was removed and added to 5ml DMEM (high glucose) and kept on ice. 5ml 1x trypsin was then added to the remaining solution and again incubated at 37°C for 30 minutes. This process was repeated 6 times. The tubes containing cells were spun at 1200g for 4 minutes and the cell pellet plated in two 150cm<sup>2</sup> dishes with 40ml MEF growth media (Dulbeccos's Modified Eagle's Medium supplemented with 10% foetal bovine serum, 2mM L-glutamine, 1x MEM non-essential amino acid solution and 1x penicillin-streptomycin, 0.1mM  $\beta$ -mercaptoethanol) in each. The

cells were expanded. To stop the feeder cells from dividing they were irradiated with 40 Gy and frozen until required.

### **2.19.2 E3.5 blastocyst extraction**

The uterus removed from an E3.5 pregnant female. The ovary from each uterine horn was removed and a needle used to flush the blastocyst from the uterus with DMEM. Using a dissecting microscope, blastocysts were removed from the petri dish by mouth pipette and placed in a 10cm 0.1% gelatin coated plate containing ES cell media (DMEM-KO, 1% L-Glutamine, 0.5% Pen/Strep (10,000 U/ml), 1% Non-essential amino acid, 15% Serum replacement, 0.1mM  $\beta$ -mercaptoethanol, 0.01% LIF  $10^7$  units, ESGRO LIF Millipore). The blastocysts were incubated at 37°C for 2-3 days until the blastocyst had attached then the media was changed.

### **2.19.3 ES cell culture**

When a defined inner cell mass (ICM) outgrowth could be seen from 2.16.2, after approximately 5-6 days the outgrowth was manually picked using a pipette under 20x magnification on a light microscope. The cells were separated by pipetting the mixture and these were plated on gamma-MEFs in ES cell media. Media was changed daily and approximately 3-4 days after plating when ES cell colonies could be seen the cells were trypsinised (0.25 trypsin-EDTA) for 5 minutes. ES cell medium was then added to inhibit the trypsin and the cells plated on new gamma-MEFs plated a day previous. The cells were expanded as required and frozen down in freezing medium (20% DMSO, 30% ES cell media, 30% serum replacement). For genotyping cells were grown in a MEF free environment to prevent DNA contamination, and genotyped using the protocol used for genotyping the mice.



#### 2.19.4 ES cell transfection with Cre-containing plasmid

ES cells were expanded on MEFs until  $3\text{--}4 \times 10^6$  ES cells (2x 6cm plate) were obtained. On day 1 the ES cell media was changed 2hr before transfection, and the media on the MEFs also changed to ES cell media. After 2 hours the ES cells were trypsinised as described in 2.16.3. The cells were counted and  $3\text{--}4 \times 10^6$  cells were centrifuged at 1200RPM for 3 minutes and the cell pellet washed twice with PBS. The cells were electroporated using Amaxa Nucleofector Technology (Lonza, Basel, Switzerland). The pellet was resuspended in 100 $\mu$ l Nucleofector solution and added to a cuvette containing 10ug of plasmid (5ul of Cre-IRES-EGFP plasmid) making sure there were no airbubbles. The cells were electroporated using Amaxa A-024 Nucleofector programme and then the sample was transferred into 500 $\mu$ l of pre-heated RPMI (37°C) and incubated at 37°C for 1 hour. The ES cells were then plated on MEFs by dropping solution over plate. New gamma-MEFs were plated on day 1. On day 3 the media was changed to ES cell media on the gamma-MEFs. The ES cells were trypsinised as described in 2.16.3, and were centrifuged at 1200RPM and resuspended in 400 $\mu$ l ES media. The cells were filtered through a 50 $\mu$ m filter (Millipore, Billerica, MA) to get a single cell suspension. Cells were sorted using MoFlow High Speed Cell Sorter (Beckman Coulter, High Wycombe, UK), using a high purification threshold for GFP positive cells. These were then plated on gamma-MEFs and single colonies expanded as described in 2.16.3. Cells were grown in a MEF-free environment for genotyping, and were genotyped using the same PCR primers as for *Vps33b*<sup>fl/fl</sup> mice.

## **2.20 Analysis of Liver function**

### **2.20.1 Blood extraction for plasma protein analysis**

Blood samples were taken from the mice at ages specified. 100-150µl of blood was extracted from a mouse into a heparinised tube by nicking the tail with a needle and teasing the blood out. These blood samples were immediately taken to Birmingham Womens Hospital where their bilirubin and ALT levels were measured.

### **2.20.2 Electrospray mass spectrometry of bile acids**

A terminal blood sample was required for bile acid analysis, see section 2.18.5 for method.

Plasma was isolated by centrifuging whole blood at 1000g for 5 minutes, and plasma removed from the top of the eppendorf into a clean tube. The samples were sent to Clinical Chemistry, Sheffield Children's Hospital for electrospray analysis.

### **2.20.3 Fixation and processing of liver samples**

Livers were immediately excised from schedule 1 culled mice. Small sections were taken and fixed in 4% formalin or snap frozen in liquid nitrogen for protein extraction. Subsequent, processing, paraffin embedding and sectioning was carried out by the histology service, Birmingham Women's Hospital.

### **2.20.4 Immunohistochemistry**

All immunohistochemistry specific reagents were obtained from Vector Laboratories, CA, unless otherwise stated. Liver paraffin sections were cleared with two 5 minute washes in histoclear (National Diagnostics, Atlanta, USA). Rehydration of tissue was carried out by progressive 5 minute washes through 100% ethanol (two times), 90% ethanol, 70% ethanol and 50% ethanol. The sections were then washed in water and antigen retrieval undertaken by

boiling for 5 minutes in 10mM Citrate buffer (citric acid monohydrate 2.1g in 1L water, pH6 with 2M NaOH) two times. Samples were then cooled to room temperature and endogenous peroxidase blocked with 6% hydrogen peroxide for 15 minutes. The sections were marked around with a DAKO pen and then blocked with 2% BSA-PBS-0.5% tween (PBST-BSA) for 30 minutes. The sections were then incubated in 150µl of primary antibody diluted in PBST-BSA tween for 1 hour. The slides were then washed 3 times for 5 minutes in PBST and incubated with 150µl of the secondary antibody (biotinylated) for 45 minutes. The sections were again washed 3 times in PBST and then incubated with ABC prepared 30 minutes previous, for half an hour. Slides were washed 3 times in PBST and then incubated with DAB for 2-10 minutes until colour developed. Slides were washed 3 times then counterstained with hematoxylin. The tissue was then dehydrated by passing through 90% ethanol, 100% ethanol and then histoclear before a 1,5 coverslip was placed over the sample using VectaMount. Slides were viewed using a Zeiss Axiovert zoom brightfield microscope, and imaged using AxoCam ICc1 at 40x magnification, na 1,3.

#### **2.20.5 Immunofluorescent staining**

Sections were treated as in 2.17.4 up-to and including antigen retrieval in citrate buffer. Blocking of endogenous peroxidase was not required therefore this step was skipped, primary antibody incubation with chicken  $\alpha$ -BSEP (1/300 dilution) and washing occurred as in 2.17.4. The secondary antibody, Goat  $\alpha$ -chicken Alexa 488 (1/200) was used. Finally the sections were washed 3 times for 5 minutes in PBS and mounted using 1,5 coverslips with Prolong gold antifade reagent (Life Technologies, California) and imaged as described in 2.10.4.

## **2.21 Analysis of platelets and megakaryocytes**

### **2.21.1 Megakaryocyte culture**

To extract megakaryocytes, the rear legs of a schedule 1 culled mouse which had been kept on ice were removed, taking care not to break the head of the femur and placed in a Petri dish containing 70% ethanol. The femur and tibia were separated and cleaned to remove any tissue from the bones. Under a tissue culture hood the ends of the bones were cut and a 25g needle and syringe filled with complete DMEM media (DMEM media supplemented with 10% FBS, 2mM Glutamine and 1% Pen/Strep) were used to flush out the bone marrow (~10ml per mouse). The cells were pelleted by centrifuging at 1200 rpm, 4°C for 5 min, and then resuspended in ACK buffer (0.15M NH<sub>4</sub>Cl; 1mM KHCO<sub>3</sub>; 0.1mM Na<sub>2</sub>EDTA pH7.3), 6ml per mouse and left for 5 minutes. Cells were filtered through a Millex-GP 70µm nylon mesh filter (Millipore, Watford, UK) then spun 1200 rpm, 4°C for 5 min to pellet. Cells were resuspended in 1ml complete DMEM media per mouse. Cells not required were depleted by incubating on ice with Anti-Gr-1, Anti-cd 11b, Anti B220, anti CD16/32 (3µl of each per mouse) (all from eBioscience, San Diego). 1ml of complete DMEM per mouse was added to the cells and spun at 1200 rpm, 4°C for 5 min to pellet and resuspended in 1ml complete DMEM per mouse. 50µl sheep anti-rat Dynabeads (Invitrogen, Paisley, UK) per mouse were prepared by washing 3 times in complete DMEM, and resuspended in 50µl complete DMEM per mouse. 50µl Anti-rat Dynabeads per mouse were added to the cells, spun at 1200 rpm, 4°C for 5 min, and subsequently resuspended in their supernatant. Resuspension and spin was repeated and then a magnet was used to pull down the beads. The supernatant was removed to a separate tube, and 500µl of complete DMEM was added to the remaining beads and the beads were resuspended and pulled down, the supernatant pooled with that obtained previously. The cells were spun at 1200 rpm, 22°C for 5 minutes. The pellet was resuspended

in 1.5ml complete Stempro media (Stempro media, 2mM L-Glutamine, Stempro Nutrient Supplement) per mouse supplemented with 20ng/ml stem cell factor (SCF)(Peprotech, NJ, USA) placed in a 6 well plate and incubated for 48 hours at 37°C, 5% CO<sub>2</sub>. Next the cells were resuspended in 1.5ml complete Stempro media per mouse supplemented with 20ng/ml SCF and 50ng/ml murine TPO (Peprotech, NJ, USA) and left to incubate for a further 3-4 days. In order to separate the megakaryocytes from the undifferentiated stem cells a BSA gradient was prepared for each mouse (4ml of 3% BSA on bottom, 4ml of 1.5% BSA on top), cells were resuspended in their medium and layered on top of the gradient and left for 45 minutes. The top 8ml was removed for a second round of culture, and the bottom 2ml was centrifuged at 1200 rpm, 22°C for 5 minutes. The supernatant was removed and the pellet resuspended in 1ml PBS, centrifuged at 1200 rpm, 22°C for 5 minutes and then lysed with 50µl RIPA buffer (50mM Tris-HCl, 150mM NaCl, 1mM EDTA, 1% Igepal CA630, 0.5% Sodium Deoxycholate, 0.1% SDS and complete mini protease inhibitor cocktail (Roche Diagnostics, Burgess Hill, UK)).

#### **2.21.2 Bleeding time tests**

Mice were anaesthetised with the inhalation anaesthetic isoflurane (Abbott, Maidenhead) and transferred to mask. They were then given 0.05ml buprenorphine by intraperitoneal injection. 2mm was removed from the tail tip using a razor blade, and the drops of blood were counted and collected. Bleeding was measured for a maximum of 10% blood loss, 20 minutes or was stopped if no blood had fallen for 5 minutes. Blood droplets were assumed to be 30µl from previous normalisation. The tail was then cauterised in order to prevent further bleeding, and animals were left to recover.

### **2.21.3 Platelet count and Mean Platelet Volume**

Platelet count and mean platelet volumes were measured in whole blood by ABX Pentra 60 whole blood counter.

### **2.21.4 Spleen measurement**

Mice were weighed before the procedure and their spleens were removed after the terminal bleed. The spleen length was measured and the weight recorded. These values were then normalized to body weight.

### **2.21.5 Mouse platelet preparation**

Mice were culled by anaesthetising deeply with isoflurane (Abbott, Maidenhead) and then CO<sub>2</sub> for cessation of breathing. Blood was drawn by performing a laparotomy and blood was drawn from the inferior vena cava into 200µl acid citrate dextrose (ACD)(Sodium Citrate 25g/L, Glucose 20g/L, citric acid 15g/L). Cervical dislocation was then performed. The needle was then removed to prevent platelet shearing and the blood was added to 200ul Modified Tyrodes Hepes buffer (134mM NaCl, 2.9mM KCl, 0.34mM Na<sub>2</sub>HPO<sub>4</sub>.12H<sub>2</sub>O, 12mM NaHCO<sub>3</sub>, 20mM HEPES, 1mM MgCl<sub>2</sub>, 5mM glucose) pH 7.3 in a 1.5ml eppendorf. Blood was spun at 2000 rpm for 5 minutes using a microfuge. The top 70% of blood was removed into a new 1.5ml eppendorf and centrifuged at 200g for 6 minutes at room temperature. Platelet Rich Plasma (PRP) was removed and 200µl Modified Tyrodes Hepes buffer was added to the remaining cells to extract more PRP and centrifuged again at 200g for a further 6 minutes. For washed platelets further steps were carried out. 10µg PGI<sub>2</sub> was added to the PRP and then centrifuged at 1000g for 6 minutes room temperature to pellet the platelets. Platelets were resuspended in 200µl Modified Tyrodes Hepes buffer pH 7.3. Cells

were counted using a Coulter Particle Counter and size analyser and were adjusted to the required concentration with Modified Tyrodes Hepes buffer.

#### **2.21.6 $\alpha$ -granule secretion analysis by Flow Cytometry**

One-colour analysis of  $\alpha$ -granule secretion was conducted using 5 $\mu$ l rat anti-mouse CD62P-FITC conjugated antibody (Emfret analytics). Platelets were diluted to  $2 \times 10^7$  and 50 $\mu$ l of this platelet sample was subsequently stimulated with 1U/ml thrombin 10 minutes at 37°C. 5 $\mu$ l of rat anti-mouse CD62P-FITC conjugated antibody was added and incubated in darkness at room temperature for 20 minutes. 200 $\mu$ l of MTH buffer was added and samples were analysed within 30 minutes. Flow cytometry analysis (using Becton Dickinson FACsCalibur) was performed on each sample, a total of 10,000 events per sample were collected and the platelet population was identified by forward and side scatter profile. Data were analysed using CellQuest software.

#### **2.21.7 Aggregometry and dense granule secretion**

0.3ml of  $2 \times 10^8$  mouse platelets were analysed using a lumiaggregometer, Chrono-log Corporation Lumi-dual aggregometer. Aggregation was measured using light transmission under stirring (1200 rpm) conditions at 37°C. Platelets were preincubated for 3 minutes at 37°C before stimulation with agonist. Each sample was allowed to aggregate for at least 2.5 minutes. Dense granule release was monitored using the Chrono-Lume luciferin/luciferase reagent (Chrono-log corporation) to detect adenosine triphosphate (ATP) release. 10 $\mu$ l of luciferin/luciferase was added 2 minutes prior to addition of agonist. Following 2.5minutes of secretion/activation an ATP standard was added in order to calculate secretion. Aggregation and ATP release were monitored simultaneously.

### 2.21.8 *In vitro* flow assay

Thrombi formation under shear conditions was observed by conducting an *in vitro* flow assay through collagen coated capillaries. The glass capillaries (1x0.1mm Camlab, Cambridge) were filled with 100µg/ml collagen by capillary action and left to rotate in an upright rotator at room temperature for 1 hour. A rubber tube was then attached to the end of the capillary, the collagen flushed out, and 5mg/ml FAF (fatty acid free) BSA was drawn up into the capillary and rotated again for 1 hour at room temperature in order to block the capillary. The capillary was then attached to a glass slide with superglue and tape to secure. Blood from the mouse was drawn by cardiac puncture under terminal anaesthesia into 100µl Modified Tyrodes Hepes buffer (recipe in 2.18.5) pH 7.3 supplemented with 40µmol P-PAC and 5U/ml heparin. The needle was then removed to prevent platelet shearing and the blood was added to a further 200µl Modified Tyrodes Hepes buffer pH 7.3 supplemented with 40µmol P-PAC and 5U/ml heparin in a 1.5ml eppendorf and incubated at 37°C for 10 minutes before the flow experiment. The microscope slide-mounted capillary was then attached to the flow apparatus and washed with Modified Tyrodes Hepes buffer at the required flow rate of 1000/s (0.1ml/min) allowing it to normalize. 400µl of whole blood was then flowed through the capillary for 4 minutes, and a subsequent wash for ~5 minutes with Modified Tyrodes Hepes buffer was carried out.

The capillary for imaging was flushed with 100µl 3.7% paraformaldehyde, left for 30 minutes and then rinsed 3 times with PBS, and left at 4°C until it was required. Imaging was carried out using a Zeiss Axiovert zoom DIC microscope, with AxioCan ICc1 and Slidebook software. 3 images were captured at x20 magnification (na 0,4) and 5 images at x63 oil emersion magnification (na 1,4) at different sections of each capillary for visual analysis.



The capillary for quantification of platelet adhesion was washed 3 times with 50µl Modified Tyrodes Hepes buffer. The capillary was then washed with 50µl NP-40 lysis buffer (150mM NaCl, 10mM Tris, 1mM EGTA, 1mM EDTA, 1% NP-40, 2.5mM Na<sub>3</sub>VO<sub>4</sub>, 1mM AEBSA, 5µg/ml leupeptin, 5µg/ml aprotinin, 1.25µg/ml pepstatin) and the lysate was collected in an eppendorf for further analysis.

#### **2.22.9 Platelet preparation for EM**

The platelets were prepared as described in 2.18.5 up to and including the pelleting stage. The platelets were then resuspended in 1ml 2.5% EM grade glutaraldehyde in PBS.

# **CHAPTER 3 – ASSOCIATIONS AMONG GENOTYPE, CLINICAL PHENOTYPE AND INTRACELLULAR LOCALISATION OF TRAFFICKING PROTEINS IN ARC SYNDROME**

### **3.1 Introduction**

Arthrogryposis, Renal dysfunction and Cholestasis syndrome (ARC; MIM 208085) is an autosomal recessive multisystem disorder caused by mutations in *VPS33B* and *VIPAR* (Gissen et al. 2004)(Cullinane et al. 2010). Characteristic presentation of ARC syndrome includes neonatal cholestatic jaundice, renal tubular acidosis, arthrogryposis and severe failure to thrive. Most patients fail to survive past the first year of life (Gissen et al. 2006).

VPS33B is a member of the Sec1/Munc18 family proteins, which directly interact with SNAREs and aid SNARE complex formation, thus facilitating membrane tethering and fusion (Hata et al. 1993)(Yamaguchi et al. 2002)(Dulubova et al. 2003). VPS33B and VIPAR are homologues of yeast Vps33p and Vps16 respectively. In yeast these proteins along with 2 other class C vps proteins (Vps11 and Vps18) make up the core of HOPS and CORVET complexes responsible for the maturation and control of vesicular trafficking from early to late endosomes and vacuoles (Peplowska et al. 2007). Study of the subunit organisation of HOPS and CORVET showed that Vps16 is required for Vps33p association with Vps11 and Vps18 (Reider and Emr, 1997), more specifically residues 451-595 at the C-terminal domain in yeast Vps16 mediates binding to Vps33 (Pulipparacharuvil et al. 2005). Vps18 has a crucial role in the assembly of HOPS and the removal of Vps18 prevents the co-immunoprecipitation of all other subunits with Vps11 (Plemel et al. 2011). Mammalian equivalents of HOPS have been studied by several groups (Kim et al. 2001)(Nickerson et al. 2009)(Zhu et al. 2009). In metazoans there are 2 homologues of yeast Vps33p, VPS33A and VPS33B. It is probable that VPS33A in metazoans is a part of the HOPS complex (Sriram et al. 2003), but the conditions in which the VPS33B-VIPAR complex may be involved in HOPS are unknown (Cullinane et

al. 2010)(Zlatic et al. 2011). At present it is unclear whether there is a mammalian equivalent of the yeast CORVET complex (Zlatic et al. 2011).

It has been reported that VPS33B forms a complex with VIPAR and that together they partially co-localise and co-immunoprecipitate with Rab11a. Rab11a is a small GTPase associated with apical recycling endosomes, thus implicating a role for the VPS33B-VIPAR complex in the apical recycling pathway (Cullinane et al. 2010). Furthermore, mislocalisation of apical membrane proteins in the liver and kidneys of ARC patients (Gissen et al. 2004)(Cullinane et al. 2010) and structural and functional abnormalities in the apical junction complex (AJC) in mIMCD3 cells with VPS33B and VIPAR stable knockdown support a role for VPS33B-VIPAR complex in the maintenance of apical-basolateral polarity (Cullinane et al. 2010).

### **3.2 Aims and methodology**

The role of the VPS33B-VIPAR complex in apical-basolateral polarity has not been delineated. Identification of disease-causing mutations which modify the structure of wild-type protein can advance understanding of protein interactions and ultimately of their roles in intracellular processes. Therefore, in order to learn more about VPS33B and VIPAR, patient mutations identified by genetic screening- both published and novel, have been compiled in a LOVD database for ARC. Additionally, cell-based assays have been used with the aim to determine the effect of various mutations that occur in ARC patients on VPS33B-VIPAR complex formation. The interactions of wild-type VPS33B and VIPAR with the HOPS complex protein, VPS18, were studied to detect any possible functional evidence of the interaction of VPS33B-VIPAR with the HOPS complex.

### **3.3 Results**

#### **3.3.1 ARC-LOVD Database Construction**

In collaboration with Ekaterina Gogolina, an online locus-specific ARC database (<https://grenada.lumc.nl/LOVD2/ARC>) was compiled using the Leiden Open Source Variation Database (LOVD) software system (Fokkema et al. 2011).

To establish the database, relevant data from the Human Gene Mutations Database ([www.hgmd.org](http://www.hgmd.org)) was added, and any mutations identified by literature search were included. The database also contains 188 unique variants taken from dbSNP (<http://www.ncbi.nlm.nih.gov/projects/SNP>) (Sherry et al. 2001) and the most up to date information from the 1000 Genomes Project (<http://www.1000genomes.org/>), including information on frequency.

20 previously unpublished pathogenic variants were identified when patients with classical ARC phenotype were referred for molecular diagnosis and all coding exons and intron-exon boundaries were screened for mutations in *VPS33B* and *VIPAR*. One patient was screened for mutations in *VPS33B* by Prevention Genetics (<http://www.preventiongenetics.com>). These 20 mutations were included in the database.

Variants were named according to HGVS nomenclature guidelines (<http://www.HGVS.org>) and numbered using the *VPS33B* reference sequence (NG\_012162.1, NM\_018668.3) and the *VIPAR* reference sequence (NG\_023421.1, NM\_022067.3). Previously published mutations were renamed accordingly and all annotations were checked using Web-based Mutalyzer software linked to LOVD (Wildeman et al. 2008).

*VPS33B* and *VIPAR* each have a gene homepage which provides general information about

the gene. In the “variants” section are variant-specific fields for each gene (exon, pathogenicity, template/technique used for detection, DNA/RNA/protein change, frequency, number of times reported, database ID, phenotype, and reference). Records describing variants per individual patient can be accessed, along with information on patient phenotype and ethnic/geographic origin.

### **3.3.2 New Variants**

The database includes 15 novel variants in *VPS33B* that have been classed as ‘pathogenic’ (Table 3.1). Of the disease-causing variant types, most common are substitutions (n=11: 9 splice-site and 2 nonsense). The effect of the splicing mutations was predicted by bioinformatic analysis using the BDGP Splice Site Prediction software NNSPLICE ([http://www.fruitfly.org/seq\\_tools/splice.html](http://www.fruitfly.org/seq_tools/splice.html)). 3 deletions which are predicted to result in frameshift and premature termination of transcription are included, as well as one whole-gene deletion. A variant of particular interest is the splicing mutation c.1225+5G>C, as it is associated with an attenuated ARC phenotype (see section 3.3.4 and 3.3.7).

In the database 5 novel mutations in *VIPAR* are included (Table 3.1), including substitutions (n=3: 2 missense and 1 nonsense), a deletion which is predicted to result in frameshift and premature termination of transcription, and a splicing mutation. All are classed as ‘pathogenic’ or ‘probably pathogenic’.

Database ID	Gene	Exon	DNA Change	Protein Change
VPS33B_00221	<i>VPS33B</i>	1	c.67C>T	p.(Arg23*)
VPS33B_00223	<i>VPS33B</i>	1i	c.97-2A>C	p.(?) <sup>a</sup>
VPS33B_00231	<i>VPS33B</i>	2i	c.178-2A>C	p.(?)
VPS33B_00224	<i>VPS33B</i>	2i	c.178-1G>C	p.(?)
VPS33B_00225	<i>VPS33B</i>	10	c.711del	p.(Phe237Leufs*2)
VPS33B_00226	<i>VPS33B</i>	11i	c.853-3C>G	p.(?)
VPS33B_00227	<i>VPS33B</i>	13i	c.1030+5G>T	p.(?)
VPS33B_00230	<i>VPS33B</i>	16i	c.1225+5G>C	p.(?)
VPS33B_00229	<i>VPS33B</i>	17	c.1261_1262del	p.(Gln421Valfs*8)
VPS33B_00228	<i>VPS33B</i>	20	c.1498G>T	p.(Glu500*)
VPS33B_00232	<i>VPS33B</i>	Δ4	c.240-577_290-156del	p.(Leu81Serfs*5)
VPS33B_00233	<i>VPS33B</i>	3i	c.240-1G>C	p.(?)
VPS33B_00234	<i>VPS33B</i>	21i	c.1657+1G>A	p.(?)
VPS33B_00226	<i>VPS33B</i>	11i	c.853-3C>G	p.(?)
VPS33B_00235	<i>VPS33B</i>	1-23	c.(?-354)_(*431+d127_?)del	p.(0?) <sup>b</sup>
VIPAR_00023	<i>VIPAR</i>	9	c.638T>C	p.(Leu213Pro)
VIPAR_00021	<i>VIPAR</i>	6	c.463_464del	p.(Trp155Glufs*4)
VIPAR_00022	<i>VIPAR</i>	6	c.484C>T	p.(Arg162*)
VIPAR_00019	<i>VIPAR</i>	13	c.1021T>C	p.(Cys341Arg)
VIPAR_00020	<i>VIPAR</i>	11i	c.837-1G>T	p.(?)

**Table 3.1 Novel Pathogenic *VPS33B* and *VIPAR* variants listed in ARC database**

Nucleotides are numbered from the A of the ATG initiation codon. Del, deletion; Fs, frameshift; i, intron; \*, stop; Δ, whole exon deletion; <sup>a</sup>p.(?) effect of the variant upon the protein is unknown. <sup>b</sup>p.(0?) no protein product is predicted

### 3.3.3 Database Analysis

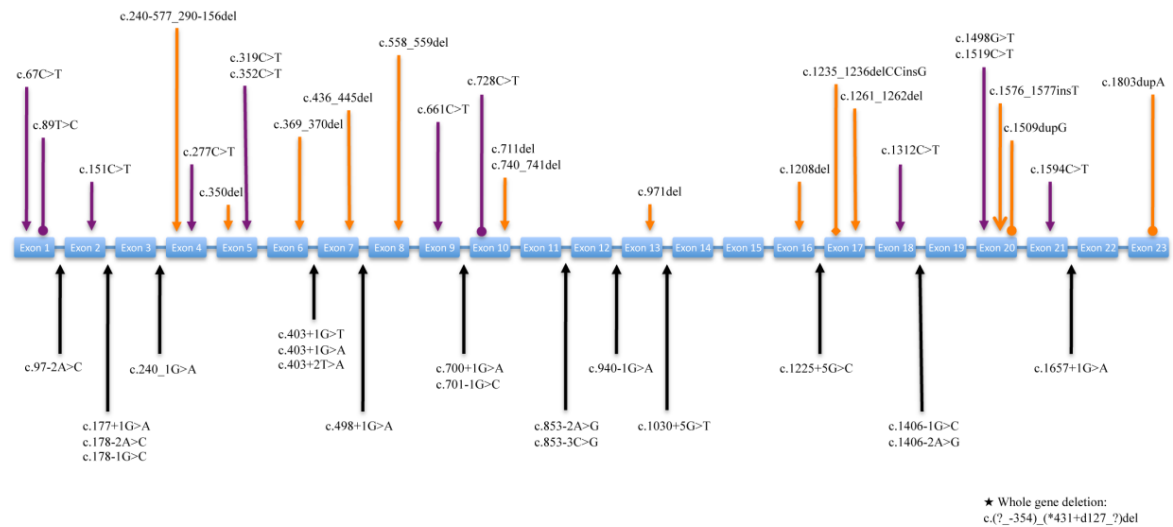
As of January 2012, the ARC database contained 235 unique variants in *VPS33B* and 23 in *VIPAR*. Forty-six variants in *VPS33B* have been classed as ‘pathogenic’ or ‘probably pathogenic’ due to their predicted effect on the protein and the clinical presentation of the patients in whom they were found. Most of these are substitutions (n=32; 20 splice-site, 10 nonsense, and 2 missense). There are also deletions (n=9; including 1 whole gene deletion), duplications (n=2), insertions (n=1), and indels (n=1), all of which are predicted to result in frameshift and premature termination of transcription. There are 9 recurrent variants, of which 3 are more prevalent; a splice site mutation, c.403+2T>A (reported in 11 individual patients, all of Korean origin), a nonsense mutation, c.1312C>T (reported in 9 patients; 8 of Pakistani origin and one Arabic), and a nonsense mutation c.1519C>T (reported in 7 patients; 3 Portuguese, 1 Korean, 1 Hispanic, 2 unknown ethnicity) (references are provided within the database).

There are 11 ‘pathogenic’ variants in the *VIPAR* gene, most of which are substitutions (n=8; 6 nonsense and 2 missense). There also are 2 deletions (resulting in frameshift) and one splice-site mutation. There are two recurrent variants; a nonsense mutation, c.658C>T (reported in 2 patients; of Italian and Turkish ethnic origins) and nonsense mutation, c.808C>T (reported in 2 patients; Pakistani and Arab-Israeli).

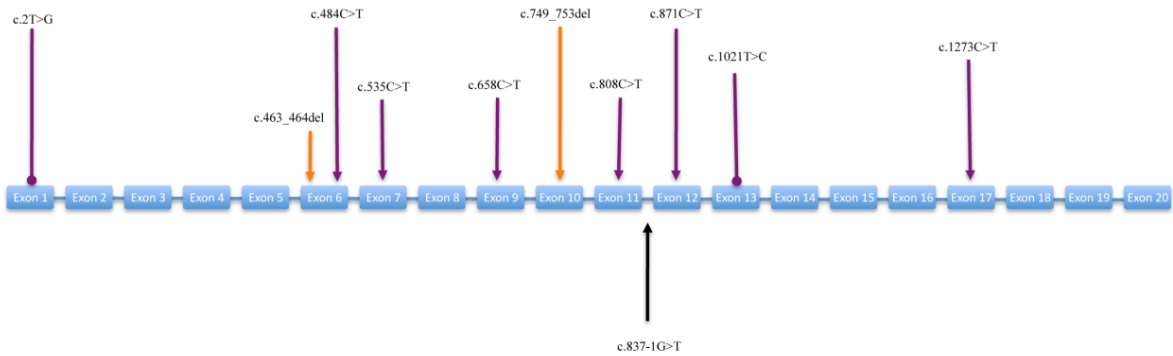
The distribution of variants is relatively uniform within *VPS33B*; no obvious mutational hotspots were identified (Figure 3.1). Protein structure predictions for *VPS33B* and *VIPAR* suggest that both proteins contain globular regions with well-defined secondary structure elements. *VPS33B* contains a Sec1 domain spanning almost the entire protein, amino acids 31-611. A large disordered protein segment has been consistently identified by multiple structure prediction software at the N-terminus of *VIPAR* (Figure 3.1). At present, with the



### *VPS33B*



### *VIPAR*



**Figure 3.1 ARC-LOVD database content analysis.**

***VPS33B*** Gene map of distribution of ‘pathogenic’ and ‘probably pathogenic’ variants in *VPS33B*. The boxes represent the exons (not to scale). All variants are described at the DNA level. Variants below the genogram represent intronic mutations, affecting splice-sites. Variants above the genogram represent mutations in exons. Purple pointers indicate substitutions; → indicates a nonsense mutation, —• indicates a missense mutation. Orange pointers indicate deletions/duplications/indels; → indicates a deletion, —• indicates a duplication, and —♦ indicates an indel.

***VIPAR*** Gene map of distribution of ‘pathogenic’ and ‘probably pathogenic’ variants in *VIPAR*. The boxes represent the exons (not to scale). All variants are described at the DNA level. Variants above the genogram represent mutations in the exons. Purple pointers indicate substitutions; → indicates a nonsense mutation, —• indicates a missense mutation. The orange pointer → indicates a deletion.

exception of a single pathogenic mutation in the start codon, the N-terminal part of VIPAR is devoid of mutations. This might suggest that this region of VIPAR is dispensable for VPS33B-VIPAR interaction.

### **3.3.4 Identification of patients with an attenuated ARC phenotype**

Patients with the suspected diagnosis of ARC were referred for molecular diagnosis. Patient AB was referred for mutation screening at 2 ½ years with what appeared to be an attenuated phenotype of ARC. AB is a son of non-consanguineous Peruvian and Puerto Rican descent. His clinical features included failure to thrive, developmental delay with sensorineural hearing loss, renal loss of protein and amino acids, bilateral talipes with osteopenia and mild cholestasis. The MRI scan of the brain showed dysmorphic ventricles with coaptation of the occipital horns and irregular contour along the margins of the lateral ventricles. There was also mild confluent hyperintense T2 signal in the periventricular white matter consistent with early in utero ischaemic injury. He had very troublesome ichthyosis, which was associated with increased serum concentrations of bile acids and was not responsive to conventional therapy. Clinical management with supplemental feeds via gastric-tube achieved steady growth along 0.3 percentile for his weight and height. Pruritus responded to cutaneous biliary diversion performed at age 3 years (Figure 3.2A-D).

At the age of 5.5 AB is attending kindergarten and a special school for children with hearing impairment. He is making slow progress in his development, such as learning to say two-syllable words. AB has difficulties with using sign language due to severe hyperkeratosis and lichenification of the skin on his hands. He is able to walk on his own. He likes to play with other children particularly basketball, when he likes to dribble and shoot baskets. He is able to ride his bicycle with training wheels. Although thick, calloused hand skin (Figure 3.2C)

interferes with fine motor tasks, this problem seems to be responding to dermatological management.

AB continues to have osteopenia with shortening of the proximal fibula, generalised amino-aciduria and nephrotic range proteinuria, and recurrent episodes of epistaxis associated with the absence of platelet  $\alpha$ -granules (personal communication, Dr R Romero).

Patient CD was referred for a clinical opinion at the age of 12 months with the features of possible ARC. She was found to have arthrogryposis and failure to thrive at two weeks of age. Further investigations identified renal tubular defect, mild cholestasis, hyperpigmented lichenified skin, bilateral hip dislocations, decreased muscle bulk and sensorineural hearing loss (Figure 3.2E-I). She was not jaundiced but had hypercholanaemia. Magnetic resonance imaging at 14 months showed a thin corpus callosum and diffuse paucity of white matter. However, she continued to progress in her development with appropriate socialisation. Speech improved after a hearing aid was fitted. Pruritus improved with rifampicin, phenobarbitone and ursodeoxycholic acid treatment. CD continues to fail to thrive despite supplementary feeds. At age 3 years she underwent corrective surgery for hip dysplasia; she is starting to walk. Additional clinical problems include abnormal dental composition with weak enamel and easily chipped teeth (Figure 3.2E) (personal communication, Dr R Chang).



**Figure 3.2 Patients with attenuated ARC syndrome.**

A-D Patient AB. Aged (A) 3 years and (B) 5 years. Hyperkeratosis and lichenification of palm of right hand (C) and sole of left foot (D).

E-I, Patient CD. Facies aged 3 (E); in plaster after corrective hip surgery (F). Hyperkeratosis, dorsum of right foot (G). Radiographs of right foot showing vertical talus (H) and of pelvis showing hip dislocation (I).

### 3.3.5 Mutation identification in Patient AB

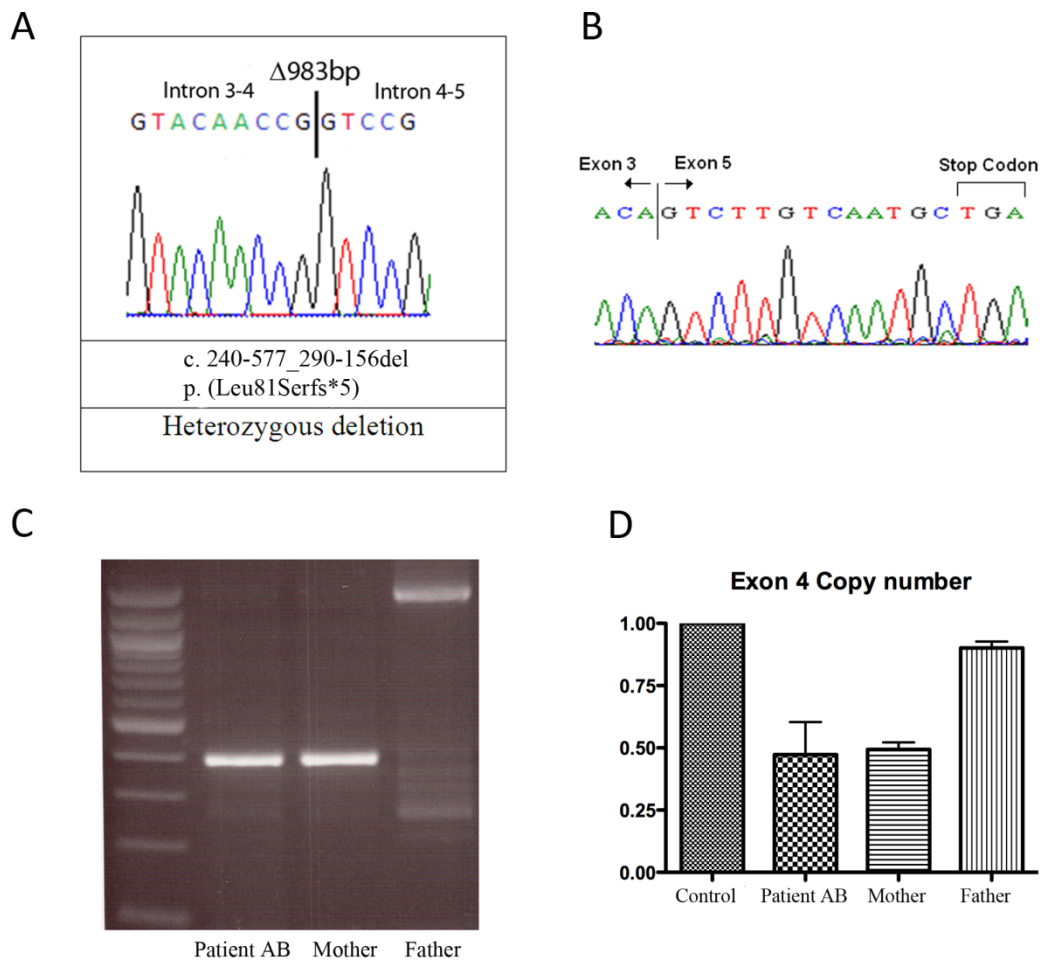
Sequencing of *VPS33B* identified a heterozygous splice donor mutation *c.1225+5 G>C* in intron 6, also identified in the father (figure 3.4A). A single heterozygous mutation however is insufficient for diagnosis of ARC syndrome. Amplification of the first 5 exons of cDNA by PCR identified wild type length cDNA and cDNA approximately 50bp shorter. Sequencing of this fragment found that exon 4 was absent from the cDNA (figure 3.3B), resulting in a frameshift and premature stop codon, *p.Ser81Valfs\*5*. Subsequent long-range PCR and nested sequencing allowed characterisation of the second heterozygous mutation identified in patient AB, a 983bp deletion, *g.8164\_9176del983* also present in the mother (figure 3.3A). The patient therefore was compound heterozygous for mutations in *VPS33B*.

In the case of Patient AB, an exon deletion could be identified due to the availability of patient fibroblasts for RNA and protein analysis. However, when patient fibroblasts are not available, a heterozygous deletion of an exon is not detected by standard sequencing. An alternative method to using RNA analysis to detect exon deletions would therefore be useful. Quantitative real time PCR on genomic DNA was used in order to calculate exon 4 copy numbers in patient AB and family members. A haploid sample would give the value 1 once normalised against reference genes and 0.5 for those with a heterozygous deletion (Hoebeeck et al. 2005). Patient AB and the mother were found to have the deletion, the control and father not. There are patients referred for ARC syndrome screening found to have a single heterozygous mutation by standard sequencing. ARC syndrome diagnosis cannot be confirmed with a single heterozygous hit therefore these patients may benefit from the analysis of exon copy number within *VPS33B* and *VIPAR*. Subsequent to this work, whole exon deletions in further ARC patients have been identified by Birmingham Women's

Hospital by alternative methods including microarray confirming the need to look for whole exon deletions in suspected ARC patients.

### **3.3.6 Mutation identification in Patient CD**

*VPS33B* sequencing, carried out by Prevention Genetics, found the patient to be compound heterozygous for c.1261-1262delCA, predicted to result in a frame-shift and premature protein termination (p.Gln421Valfs\*8), and c.1225+5G>C, the splice donor site mutation identified in patient AB.



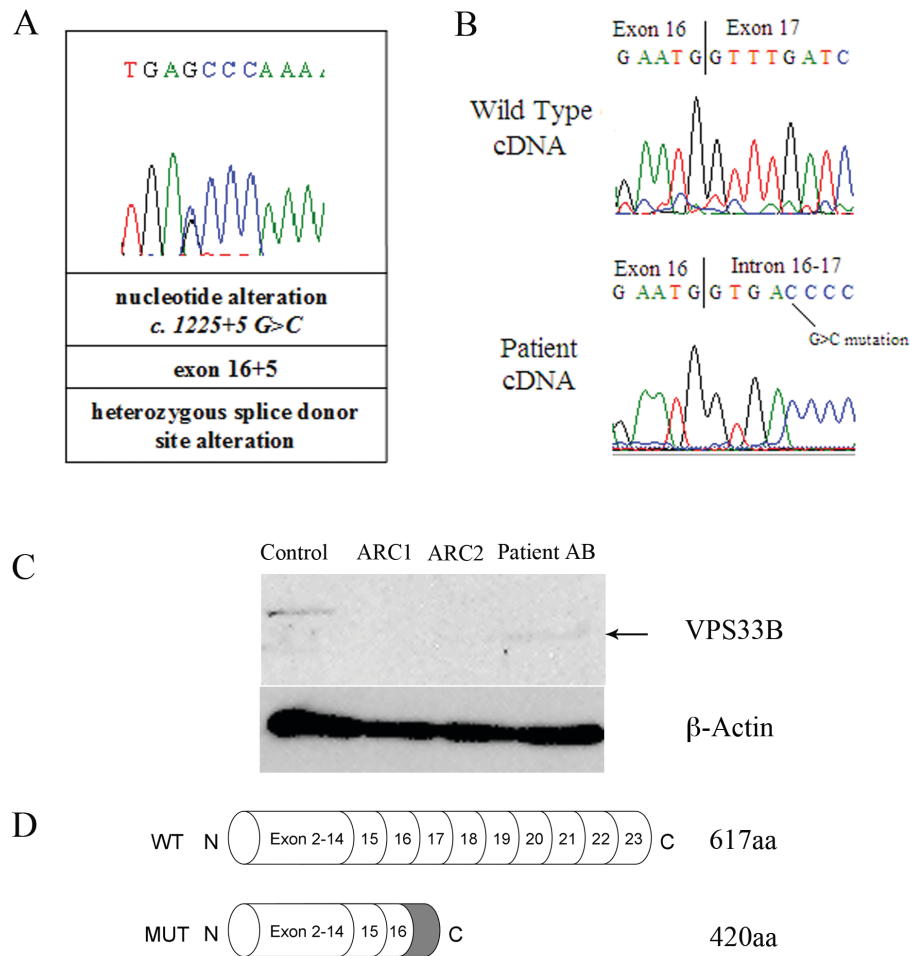
**Figure 3.3 Characterisation of the heterozygous deletion mutation in Patient AB**

(A) Electropherogram identifying the location of the 983bp deletion c.240-277\_290-156del in *VPS33B* and an electropherogram (B) of the resultant cDNA lacking exon 4. The deletion results in a frameshift and premature stop codon in *VPS33B*. (C) PCR products using primers flanking the deletion indicate that maternal DNA contains the deletion but DNA from father does not. qRT-PCR results using genomic DNA (D) confirm this finding. Exon 4 is normalized against GAPDH and actin. Samples containing 2 copies of the exon will give the result 1, and those containing one copy due to a heterozygous deletion will give the result 0.5. Samples from the mother and Patient AB contain only one copy of exon 4.

### **3.3.7 Characterisation of the donor splice site mutation in Patient AB and Patient CD**

Although the mutations present were predicted to yield a severe phenotype, both AB and CD had an attenuated form of ARC. This finding merited further investigation. Immunoblotting of protein obtained from AB's fibroblasts indicated the presence of VPS33B protein product shorter than control (figure 3.4C). When 3'-RACE was used to amplify the *VPS33B* transcript of unknown composition resulting from the splice site mutation, 114bp of intron 16 were found integrated into the *VPS33B* transcript before termination with a polyA tail (figure 3.4B). The predicted protein composition therefore includes 12 additional amino-acid residues, encoded by this intronic sequence, before a stop codon. Exons 17-23 are absent from the cDNA thus resulting in a predicted protein length of 420aa in comparison to the wild-type 617aa (figure 3.4D).





**Figure 3.4 Characterisation of the heterozygous splice site mutation in Patient AB**

Electropherograms showing (A) the c.1225+5G>C mutation and (B) the difference in *VPS33B* cDNA composition between wild-type and patient; 114bp of intronic sequence after exon 16 was integrated into the *VPS33B* transcript before termination with a polyA tail. (C) *VPS33B* immunoblot using protein obtained from control fibroblasts (lane 1), patients with c.1312C>T (lane 2), c.1594C>T and c.1225+5G>C (lane 4) identifies a smaller protein product in lane 4. (D) A diagram showing the predicted protein composition of mutant (MUT) *VPS33B* in comparison to wild type (WT) including 12 additional aminoacid residues encoded by the intronic sequence before a putative stop codon. Exons 17-23 are absent.

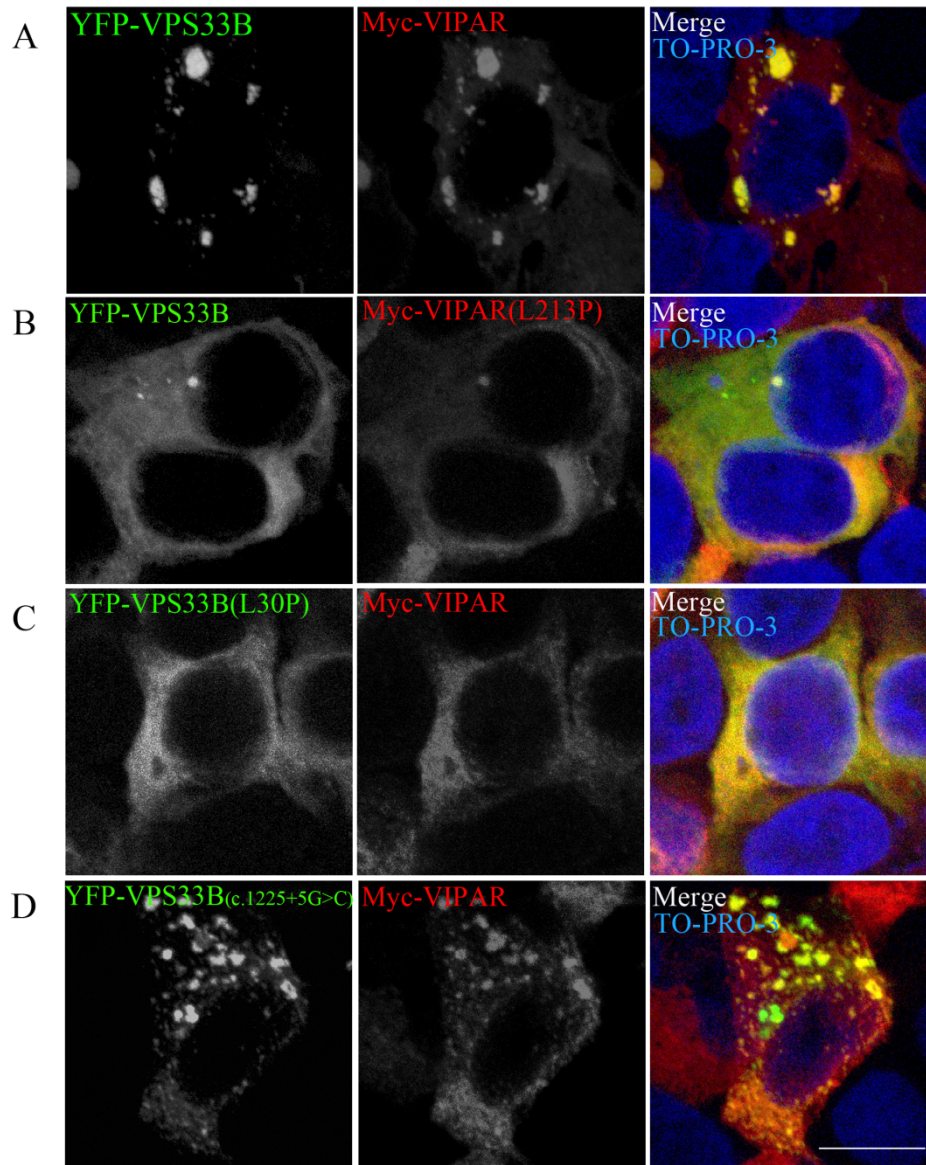
### 3.3.8 Genotype-phenotype correlation, VPS33B-VIPAR complex formation

Most known *VPS33B* and *VIPAR* mutations result in complete absence of the protein product (Cullinane et al. 2009). Mutations predicted to result in an expressed protein from patients with phenotypes assessed as severe (*VPS33B* p.Leu30Pro and *VIPAR* p.Leu213Pro) and moderate (*VPS33B* c.1225+5G>C) phenotypes were selected for modelling to gain further insight into VPS33B and VIPAR function.

Overexpression of VPS33B and VIPAR within HEK293 cells has found that these 2 proteins strongly co-localise to defined spots, and that these partially co-localise with RAB11A, a marker for recycling endosomes (Cullinane et al. 2010).

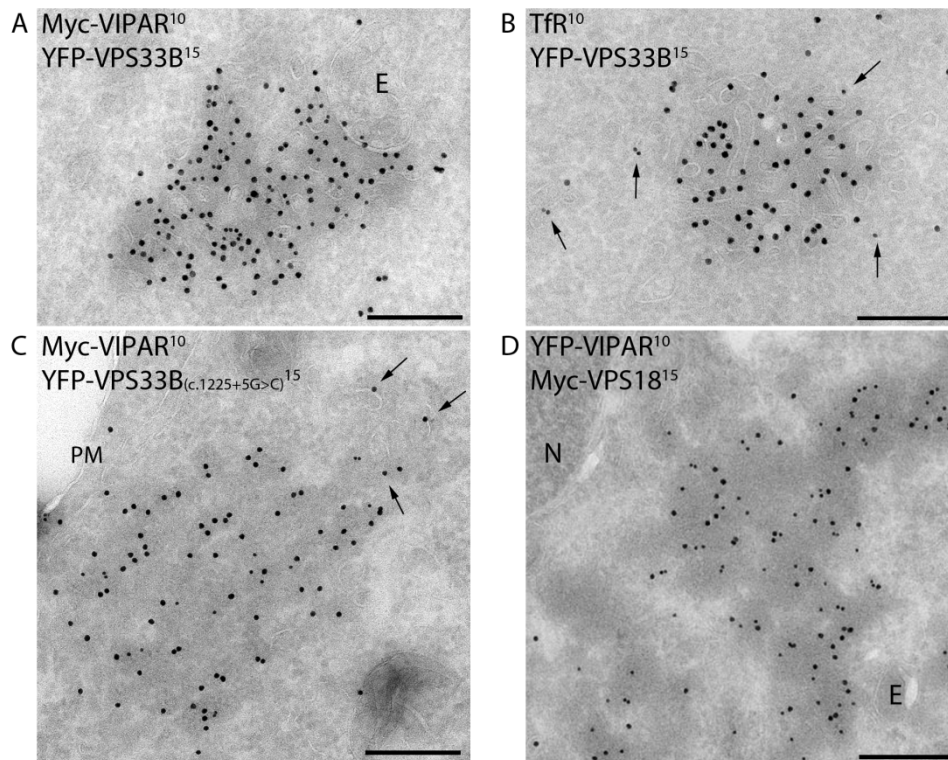
Transfections of epitope-tagged constructs were used to investigate whether patient mutations in VPS33B or VIPAR disrupt the interaction between these proteins when overexpressed in HEK293 cells using co-localisation studies. Whilst wild-type VPS33B and VIPAR co-localised (Figure 3.5A), co-overexpression of VPS33B and VIPAR(L213P) mutant did not result in co-localisation; a cytoplasmic distribution for both proteins was observed (figure 3.5B). Similarly, co-overexpression of VPS33B(L30P) mutant with VIPAR (figure 3.5C) also resulted in cytoplasmic distribution for both proteins. The severe clinical phenotype associated with these mutations confirms the importance of VPS33B-VIPAR complex formation for the function of these proteins. Finally, when VPS33B(c.1225+5G>C) mutant (known to be associated with an attenuated clinical phenotype, see sections 3.3.4 and 3.3.7) was co-overexpressed with wild type VIPAR (figure 3.5D), specific fluorescent spots containing both proteins were observed. In addition aggregates containing only VPS33B could be seen. Thus it appears that the c.1225+5G>C VPS33B mutant retains partial ability to interact with VIPAR.

To investigate the sites of co-localisation of VPS33B and VIPAR in ultrastructural detail cryo-immunogold electron microscopy (EM) of HEK293 cells overexpressing different combinations of constructs was performed in collaboration with Romain Galmes, Utrecht. This showed that the wild-type proteins co-localised on endosome-associated tubular-vesicular membranes also positive for transferrin receptor (figure 3.6A and 3.6B). The morphological and molecular characteristics of these membranes, including the presence of RAB11A as seen by immunofluorescence, identifies them as recycling endosomes (Sachse et al. 2002). When VPS33B(c.1225+5G>C) mutant was co-transfected with VIPAR, the 2 proteins co-localised mainly in electrondense cytoplasmic clusters that contained no membranes (Figure 3.6C). Interestingly however, some staining for VPS33B(c.1225+5G>C) could be detected on vesicles found at the rims of these cytoplasmic aggregates. Thus, the VPS33B(c.1225+5G>C) mutation seems to affect the ability of the complexes to co-localise properly on tubular-vesicular recycling membranes, which is likely to abrogate at least partially its cellular functioning.



**Figure 3.5 VPS33B and VIPAR interaction**

Confocal fluorescence photomicrographs of HEK293 cells co-transfected with wild-type and mutant constructs of YFP-tagged VPS33B and Myc-tagged VIPAR. Wild-type YFP-VPS33B and Myc-VIPAR co-localised (A). However, constructs modelled on severe-phenotype mutant proteins (B) Myc-VIPAR(L213P) and (C) YFP-VPS33B(L30P) resulted in a disruption of VPS33B-VIPAR interaction. (D) Transfection for YFP-VPS33B(c.1225G>C), modeling an attenuated phenotype, resulted in partial co-localisation. Myc-VIPAR was immunostained with mouse monoclonal antibody anti-myc (Sigma) at a 1:400 concentration and anti-mouse ALEXA-568 conjugate secondary antibody (Invitrogen) at a concentration of 1:400. Nuclei are stained with TO-PRO-3. Scale bars, 10µm, n=3.



**Figure 3.6 Ultrastructural localisation of VPS33B, VPS33B(c.1225+5G>C), VIPAR and VPS18 constructs.**

Transmission electron micrographs of ultrathin cryosections of HEK293 cells. (A and B), Cells co-transfected with YFP-tagged VPS33B and Myc-tagged VIPAR were immunogold-stained with anti-GFP/YFP (15 nanometer gold) and anti-Myc (10 nanometer gold) (A), or anti-GFP/YFP (15 nanometer gold) and anti-TfR (10 nanometer gold) (B). Co-localisation was observed on endosome (E)-associated tubular-vesicular membranes typical of recycling endosomes, which was confirmed by the presence of TfR (arrows in B). (C) Cells co-overexpressing YFP-VPS33B(c.1225G>C) and Myc-VIPAR were immunogold-labelled for anti-GFP/YFP (15 nanometer gold) and Myc (10 nanometer gold). The two proteins co-localised in cytosolic aggregates with partial staining of VPS33B(c.1225G>C) on nearby vesicles (arrows). (D) Cells co-overexpressing YFP-tagged VIPAR (labelled with antiGFP; 10 nanometer gold) and Myc-tagged VPS18 (labelled with anti-Myc, 15 nanometer gold) showed co-localisation in cytosolic aggregates. E: endosome, N: Nucleus, PM: Plasma Membrane. Scale bars, 200nm.

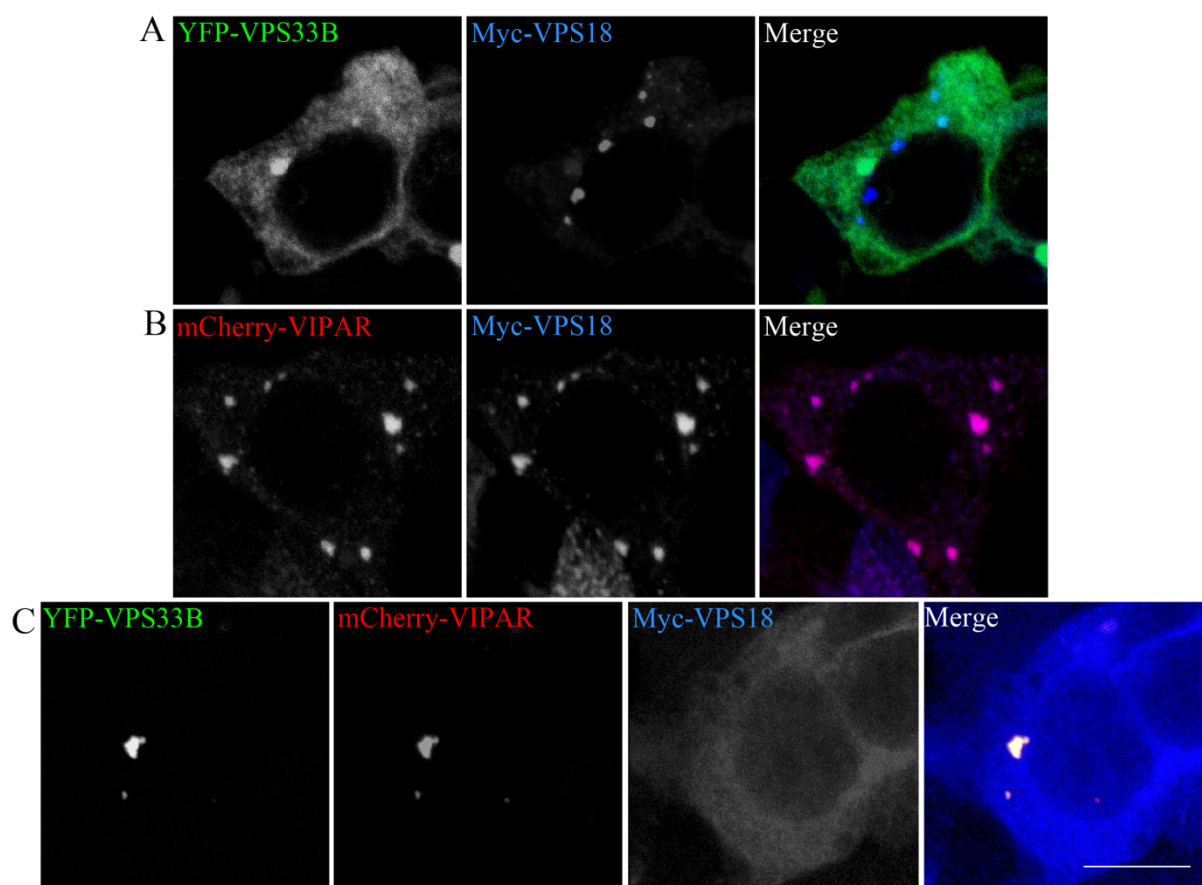
Performed in collaboration with Romain Galmes, University Medical Centre, Utrecht

### **3.3.9 Interaction of VPS33B and VIPAR with the core HOPS complex protein VPS18**

To identify whether VPS33B and/or VIPAR may interact with the mammalian HOPS, their co-localisation with human VPS18 protein, which has a central role in HOPS subunit interactions was studied (Ostrowicz et al. 2010)(Plemel et al. 2011).

When VPS18 was co-overexpressed with VPS33B, the 2 proteins did not co-localise (Figure 3.7A): VPS33B was cytoplasmic and VPS18 formed small spots. When transfected independently, VPS18 has a small punctate distribution (data not shown), however, when co-transfected with VPS33B it forms larger spots. This maybe an induction of VPS18 aggregate formation secondary to VPS33B overexpression, however the reason for this is unknown. When VPS18 was co-overexpressed with VIPAR there was co-localisation in large fluorescent spots (Figure 3.7B). However, by immuno-EM these spots were identified as cytoplasmic aggregates, without any membranes associated (figure 3.6D).

Interestingly, when all 3 constructs were co-transfected into HEK293 cells (figure 3.7C), VIPAR co-localised and formed clusters with VPS33B, whilst VPS18 was cytoplasmic. These interactions were confirmed by co-immunoprecipitation experiments: HA-VIPAR could pull down members of the HOPS complex, especially VPS18 where a strong interaction was seen (Appendix 2). However, when this experiment was repeated in the presence of overexpressed YFP-VPS33B this strong interaction diminished considerably, confirming the immunofluorescence findings (Appendix 2).



**Figure 3.7 VPS33B and VIPAR interaction with VPS18.**

Confocal fluorescence photomicrographs of HEK293 cells co-transfected with (A) YFP-VPS33B and Myc-VPS18 found these proteins do not co-localise. However, (B) mCherry-VIPAR and Myc-VPS18 do co-localise in clusters in the absence of YFP-VPS33B. If all three proteins were co-transfected, then YFP-VPS33B and mCherry-VIPAR formed clusters and Myc-VPS18 assumed independent cytoplasmic distribution (C). Myc-VPS18 was immunostained with mouse monoclonal antibody anti-myc (Sigma) and anti-mouse ALEXA-568 conjugate secondary antibody (Invitrogen), both at a concentration of 1:400. Scale bar, 10µm, n=3



### **3.4 Conclusions**

Mutations in *VPS33B* and *VIPAR* have typically resulted in a severe ARC phenotype causing death within the first year (Gissen et al. 2004)(Cullinane et al. 2010). Previously reported mutations plus 20 novel mutations were collated to form an online database (<https://grenada.lumc.nl/LOVD2/ARC>). Mutations are distributed throughout the length of *VPS33B*, consistent with the Sec1 domain spanning the length of the protein (Carim et al. 2000), whereas mutations in *VIPAR* are only present at the C-terminal globular region of the protein.

#### **3.4.1 VPS33B and VIPAR co-localisation is disrupted when severe ARC phenotype mutations are modelled**

The mutated proteins *VPS33B*(L30P) and *VIPAR*(L213P), which are associated with a severe ARC phenotype, did not co-localise with their respective wild type partners. The mutation L30P, modelled using bioinformatics analysis (Gissen et al. 2005), is predicted to disrupt an alpha-helix in *VPS33B*. Predicted secondary structure of wild type *VIPAR* includes an extended disordered region at the N-terminus (residues 1-150) followed by a 100% alpha-helical domain that extends to the C-terminus (residues 105-491). A Leu213Pro substitution in *VIPAR* is predicted to result in the disruption of an alpha helix in the core of a folded region of *VIPAR* structure. Both *VPS33B*(L30P) and *VIPAR*(L213P) mutations might affect the overall folding of the protein and thus their interaction with wild-type *VIPAR* or *VPS33B* respectively and/or other potential binding partners.

#### **3.4.2 Identification of an attenuated phenotype, and partial VPS33B-VIPAR co-localisation**

Two patients with an attenuated ARC phenotype were identified. They have a c.1225+5G>C splice site mutation in *VPS33B* in common. This mutation generates a truncated form of *VPS33B* (residues 1-420) that still partially co-localises with *VIPAR* (Figure 3.5D). From this



evidence and also the electron microscopy experiments it can be affirmed that truncation of the C-terminal region of VPS33B, as seen with the c.1225+5G>C splice mutation, may alter the overall interaction between VPS33B and VIPAR and the localisation of the complex. However, the attenuated clinical phenotype and the presence in cell culture of VPS33B- and VIPAR-containing clusters suggest that some of the function of the VPS33B-VIPAR complex may be retained. The finding that clusters containing VPS33B(c1225+5G>C) and VIPAR are mainly cytoplasmic suggests that the expected interaction of SM protein VPS33B with transmembrane SNAREs might be important for the proper localisation and function of the complex. In addition, interaction with SNARE proteins might be possible only after VIPAR binding to VPS33B, since overexpression of VPS33B alone is not sufficient to localise VPS33B on recycling endosomes.

#### **3.4.3 VPS33B and VIPAR interaction with the HOPS complex protein, VPS18**

Co-overexpression studies in HEK293 cells suggest that VIPAR may interact with VPS18 only in the absence of VPS33B. Therefore, the VPS33B-VIPAR complex is unlikely to be involved in HOPS interaction. However, VIPAR may interact with VPS18 in cells with mutant VPS33B, implying that this interaction might be involved in ARC pathogenesis.

This work highlights the importance of VPS33B-VIPAR co-localisation at membranous organelles, typical of recycling endosomes, for the correct cellular functioning of this complex. It also suggests that this complex may not be involved in HOPS complex interaction.

## **CHAPTER 4 - Vps33a AND Vps33b MOUSE MODELS**

#### **4.1 Introduction**

Multiple model organisms have been used to investigate the function of the two homologues of yeast Vps33p, Vps33a and Vps33b, and the homologue of yeast vps16, Vpar, described in section 1.9. Vps33a models include, a *carnation* mutant in *Drosophila* and the *buff* mouse, with missense mutation in *Vps33a* (Sevrioukov et al. 1999)(Suzuki et al. 2003)(Akbar et al. 2009). *C. elegans* Vps33b knockdown using RNAi, and Zebrafish morpholino (Matthews et al. 2005)(Zhu et al. 2009)(Matthews et al. 2005) have been developed to study Vps33b. Finally, Vpar models include *C. elegans spe-39* mutant, a *fob* *Drosophila* homozygous null allele and a zebrafish morpholino (Zhu et al. 2009)(Cullinane et al. 2010)(Akbar et al. 2011).

When creating a disease model the choice of organism should be considered carefully as each has its own advantages and disadvantages, a good summary found in Model Organisms- A historical perspective (Müller & Grossniklaus 2010). The mouse was selected to create knockout models of Vps33a and Vps33b deficiency, as 1) no mammalian models of ARC syndrome have yet been reported and 2) the *buff* mouse may not represent the true deficiency of a constituent HOPS complex component protein.

Mice have been widely used to model human disease due to the striking homology between the two genomes (Chinwalla et al. 2002) with the percentage of mouse genes without a human homologue and vice versa at less than 1%. As a result of this homology, mice are similar to humans in many ways ranging from anatomy and physiology to cell biology. The blood for example can be analysed in the same way as human blood to characterise defects in organ, immune or platelet function. They have an advantage over other mammals as they are small and therefore cheaper to maintain, and have quick gestation period of 19-21 days. Another advantage is that they are available as inbred strains, where littermates have been crossed for

at least 20 generations, in this way on average 96.8% of the loci are homozygous. Some strains have been bred for 150 generations and are essentially entirely homozygous and genetically identical, therefore a genetic profile of the strain can be carried out by looking at an individual mouse (Beck et al. 2000). This has the advantage that transplantation such as bone marrow and liver transplantation may be carried out without rejection due to their MHC antigens being identical (Coico & Sunshine 2009). In addition, different strains are more suitable for different applications, for example senescence-accelerated mice display accelerated ageing (Takeda et al. 1997).

One of the major benefits of using mice as a model for genetic disorders is our ability to perform gene knockouts in laboratory mice via ES cells, a tool that has been successfully used for the past 2 decades (Collins et al. 2007) making it a widely used model for human disease.

Targeted gene disruption, utilises the process of homologous recombination which occurs during cell division. It requires individual vectors for each gene to be produced and thus is low throughput (Thomas & Capecchi 1987). A construct is made containing flanking sequences homologous to the gene of interest, and a central deleterious mutation such as a truncating mutation which is inserted into the construct (Bockamp et al. 2002). By introducing this construct into ES cells the deleterious construct can be introduced into the gene of interest by homologous recombination thus creating a null allele or 'knockout'. Reporter genes, such as GFP or *neo* (neomycin resistance) may also be inserted allowing enrichment of successful recombination events – a low frequency event (Kent 2007). As targeted homologous recombination is a low throughput process, random insertion of 'genetrapping' vectors into the genome, and subsequent identification of the disrupted gene by sequencing the cDNA by use of an identifying marker has allowed the production of a large volume of commercially available ES cells available for research (Stryke et al. 2003).

The ES cells produced by both of these approaches are injected into the blastocoel (open cavity) of an E3.5 wild-type blastocyst and implanted into a surrogate mother. Chimeric offspring are subsequently produced and mice containing the mutated allele in their germ cells are bred to create mice heterozygous and eventually homozygous for the genetrapped.

Since 15% of gene knockouts result in embryonic lethality (<http://www.genome.gov/12514551>) a method for selective removal of the gene of interest temporally or spatially is required. Two major systems have been utilised in transgenic mice, the phage based system using Cre/loxP (Sauer 1998), and a prokaryotic-based system using the tet operon (Furth et al. 1994).

The Phage based system utilises targeted gene targeting and requires 2 elements. A vector containing loxP elements flanking an area of the gene of interest (termed floxed DNA) is constructed. This is inserted into ES cells by homologous recombination which are then used to produce chimeric mice by injection of the ES cells into blastocysts, and subsequent heterozygous and homozygous mice by breeding. LoxP elements are 34bp elements, consisting of two 13bp inverted repeats separated by a central 8bp spacer, the consensus sequence for cre-recombinase binding (Yamamoto et al. 2001). Once mice homozygous for this vector are created, they can be crossed with mouse lines containing specific promoter driven cre-recombinase lines. Cre-recombinase is a site specific DNA recombinase of the integrase family isolated from the P1 bacteriophage (Sternberg & Hamilton 1981). In the cells where the cre-recombinase is produced, two cre-recombinase molecules bind to each LoxP site, these then form a tetramer to bring the two sites together excising the floxed DNA and allowing the genomic DNA to recombine (Yamamoto et al. 2001). This process may be temporally or spatially controlled by controlling the expression of cre-recombinase and thus DNA excision. Various cre-recombinase lines have been engineered with promoters active in

select cells to allow the expression of cre in various tissues at different timepoints. This allows the gene to be turned on or off in a controlled manner (Jaisser 2000). For example, use of the albumin promoter allows expression of cre-recombinase in the liver. Cre-recombinase expression may also be controlled temporally by using cre- recombinase fused to the ligand binding domain of nuclear receptors, preventing cre from accessing the floxed DNA. The ligand binding domains are mutated in order to recognise only exogenous ligands, e.g. tamoxifen. When the ligand is added, the fusion protein is able to translocate into the nucleus, where the cre-recombinase can carry out its excision (Sauer 1998)(Metzger & Feil 1999).

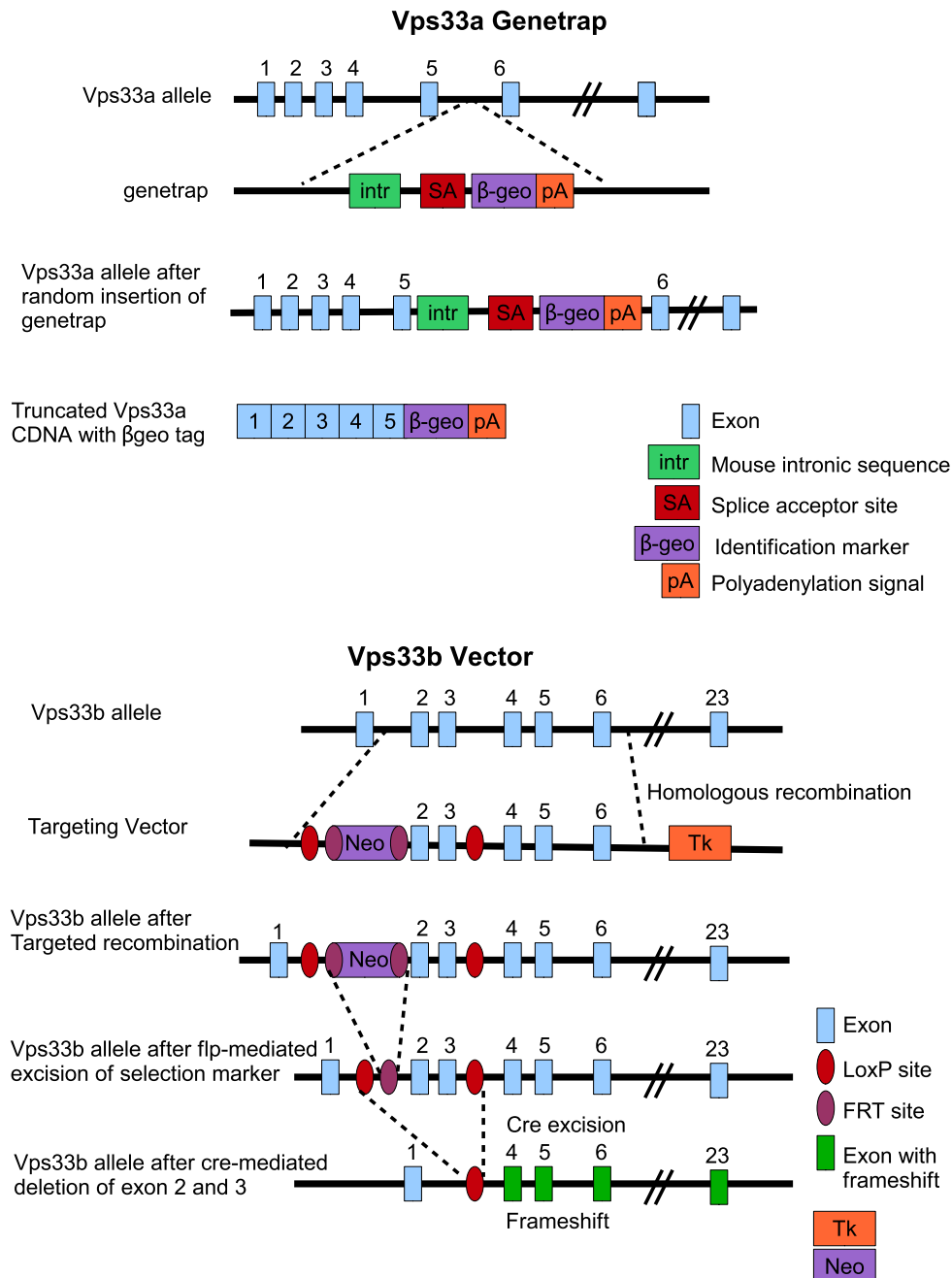
A prokaryotic based system was developed by the Herman Bujard laboratory (Furth et al. 1994). It utilises the transposon-10 specified tetracycline-resistance (tet) operon of *E.coli* (Yamamoto et al. 2001), and relies on 2 components, a tetracycline-controlled transactivator (tTA), and a tTA dependent promoter that controls expression of the gene of interest. In the absence of tetracycline or its derivative doxycycline, tTA is constitutively active and able to bind to the tTA dependent promoter allowing the gene of interest to be expressed. In the presence of tetracycline or doxycycline however, tTA is no longer able to bind to its DNA and the gene is downregulated. This is known as a ‘Tet-OFF’ system (Gossen & Bujard 1992)(Furth et al. 1994). A ‘Tet-ON’ system is also available (Kistner et al. 1996), this is where a mutant tTA termed rtTA is used. rtTA is not active until doxycycline is administered, the opposite function of tTA. The tet system has been widely used for the induced expression of transgenes in order to study subjects such as prion disease and memory (Tremblay et al. 1998)(Mansuy et al. 1998). One of the advantages of the tet system is that the effects are reversible by stopping treatment with doxycycline, therefore the reversibility of the effects of knockdown or overexpression may be studied.

Although a Vps33a mouse mutant, the *buff* mouse has been reported, the creation of a Vps33b or Vipar deficient mouse model has not. Therefore the aim of this work was to create and phenotype a ubiquitous Vps33b deficient mouse and its homologue, a Vps33a deficient mouse. In this way the roles of Vps33b and its homologue Vps33a can be investigated in a model system closely resembling human physiology.

#### **4.2 Methodology - Developing Vps33a and Vps33b deficient mice**

The Vps33a knockout mouse was created using a genetrap method, with stem cells purchased from BayGenomics. The stem cells were originally created by BayGenomics using random insertion of a genetrap vector into intronic DNA (Stryke et al. 2003). The gene into which the genetrap was inserted was identified by cDNA sequencing, in this case *Vps33a*. Chimeric mice and subsequent heterozygous mice were created at the University of Birmingham, (figure 4.1).

Since 1/3 of 'knockout' mice have been reported to be embryonically lethal, a cre/loxP vector for *Vps33b* was created by Taconic Artemis. In this way if the ubiquitous Vps33b knockout mouse was embryonically lethal, tissue specific Vps33b conditional knockout mouse could be created. Using tissue specific Vps33b conditional knockout mice is also a good way to determine the contribution of each tissue to the ARC phenotype. The vector used allowed the insertion of loxP sites before exon 2 and after exon 3 of *Vps33b*. This mouse was then crossed with a ubiquitous cre- recombinase line with Phosphoglycerate kinase (*Pgk*) promoter in order to produce a mouse with *Vps33b* excision in all tissues. When cre-recombinase is introduced, exons 2 and 3 are spliced out resulting in a frameshift and premature termination of protein production, figure 4.1. Additional methods for development of a genetically modified mouse strain are found in sections 2.13-2.16.



**Figure 4.1 Murine *Vps33a* and murine *Vps33b* inactivation in the mouse germline.**

*Vps33a* Genetrap. Genomic organisation of *Vps33a* and gene inactivation strategy: the genetrap vector was constructed such that a splice acceptor site and  $\beta$ -geo identification marker were inserted into intron 5 of the *Vps33a* allele subsequently truncating the cDNA and protein.

*Vps33b* Vector. Genomic organisation of *Vps33b* and gene inactivation strategy: the targeting vector was constructed such that homologous recombination resulted in exons 2 and 3 being flanked by LoxP sites allowing subsequent removal of these exons by Cre recombinase, resulting in frameshift preventing production of functional Vps33b.



## 4.3 Results

### 4.3.1 Ubiquitous *Vps33a*<sup>-/-</sup> and *Vps33b*<sup>fl/fl</sup>-*PgkCre* mice are embryonically lethal

The crossing of *Vps33a*<sup>+/-</sup> mice resulted in 28 litters consisting of 33 *Vps33a*<sup>+/+</sup> mice and 59 *Vps33a*<sup>+/-</sup> mice, no *Vps33a*<sup>-/-</sup> mice were found. Similarly, if only the offspring positive for the *Pgk*-cre recombinase are considered, the genotypes from *Vps33b*<sup>+fl</sup> x *Vps33b*<sup>+fl</sup> -*PgkCre* matings resulted in 29 *Vps33b*<sup>+/+</sup> mice and 41 *Vps33b*<sup>+fl</sup> mice from 23 litters, no *Vps33b*<sup>fl/fl</sup> mice were identified (Table 4.1).

Targeted Gene	Number of litters	Wild-type	Heterozygous
<i>Vps33a</i>	28	33	59
<i>Vps33b</i>	23	29	41

**Table 4.1 Genotypes of offspring from *Vps33a*<sup>+/-</sup> x *Vps33a*<sup>+/-</sup> matings and offspring positive for *Pgk*-Cre from *Vps33b*<sup>+fl</sup> x *Vps33b*<sup>+fl</sup>-*PgkCre* matings. Genotyping of offspring from heterozygous intercrosses reveals no homozygous mice**

From the number genotyped it can be deduced that removing *Vps33a* or *Vps33b* in the mouse results in embryonic lethality. *Vps33a* litters conformed to the mendelian mode of inheritance if removal of the gene is embryonically lethal. Confirmation that *Vps33a*<sup>-/-</sup> morulae were created was carried out by Ania Straatman-Iwanowska, Birmingham University. It was found at E3.5 that 2 of 7 morulae were *Vps33a*<sup>-/-</sup>.

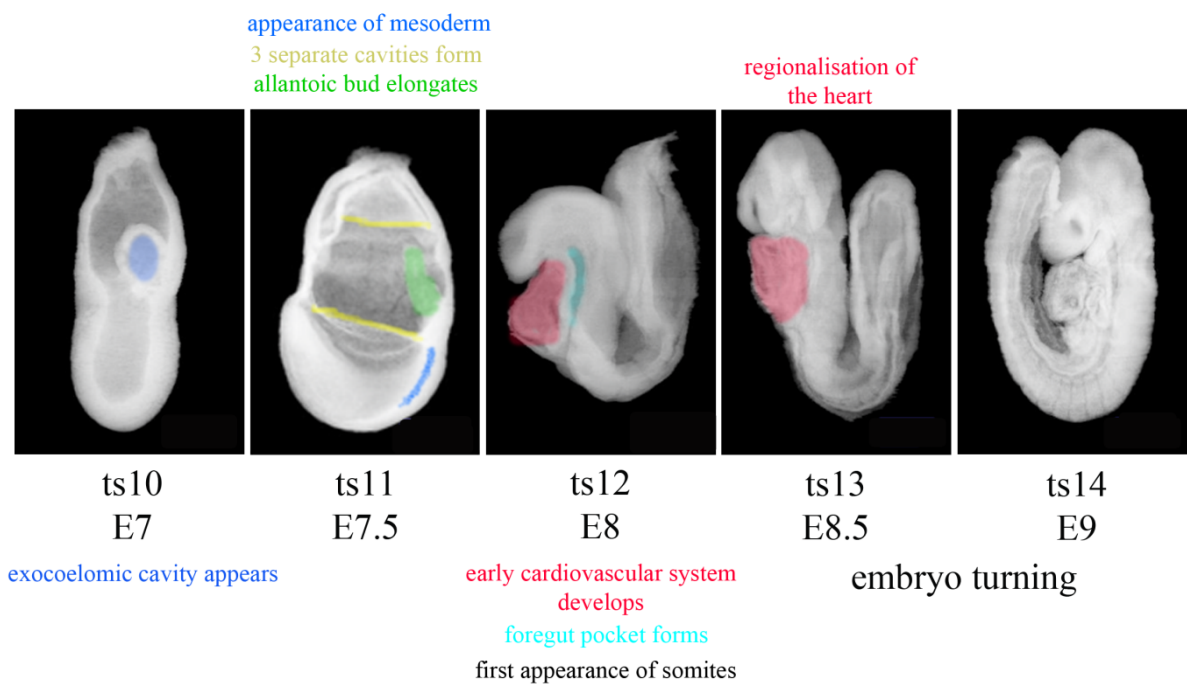
*Vps33b* litters suggest a close to mendelian mode of inheritance if removal of *Vps33b* is embryonically lethal. Heterozygous mice appear healthy, live as long as the wild-type counterparts and are fertile, therefore it is unlikely that viability is affected in *Vps33b*<sup>+fl</sup>-*PgkCre* embryos.

### 4.3.2 Determining time-point of lethality

The average gestation period for a C57BL/6 mouse is 19-21 days. In order to determine the time-point of lethality, timed matings were carried out. The time-point E12.5 was selected as a start point and then earlier or later time-points in gestation were selected as necessary.

Resorption sites were observed at E12.5 in both *Vps33a* and *Vps33b* pregnancies (Table 4.2 and Table 4.3). No *Vps33a*<sup>-/-</sup> or *Vps33b*<sup>fl/fl</sup>-*PgkCre* embryos were present at this stage and no embryonic remains could be identified. As resorption sites were observed it was assumed that the blastocysts implant into the uterus, a process which occurs at E4.5. Resorption sites were also observed at E10.5 in both mice, however at E9.5 digested remains of embryos could be genotyped without maternal contamination (Figure 4.3 and Figure 4.4). These were confirmed to be *Vps33a*<sup>-/-</sup> and *Vps33b*<sup>fl/fl</sup>-*PgkCre* embryos.

Due to the level of degradation it could be determined that lethality in both cases most likely occurred between E7.5 and E8.5, a timepoint at which many developmental processes occur (Figure 4.2). Timed matings were carried out at E7.5 and no resorption sites were observed. All embryos were intact and not digested, however maternal contamination prevented accurate genotyping as all embryos appeared heterozygous for the wild type and transgenic alleles.



### **Figure 4.2 Murine development between E7-E9**

Many complex processes occur between E7 and E9. Highlighted areas on the embryo correspond to text above or below the image. ts – Theiler stage

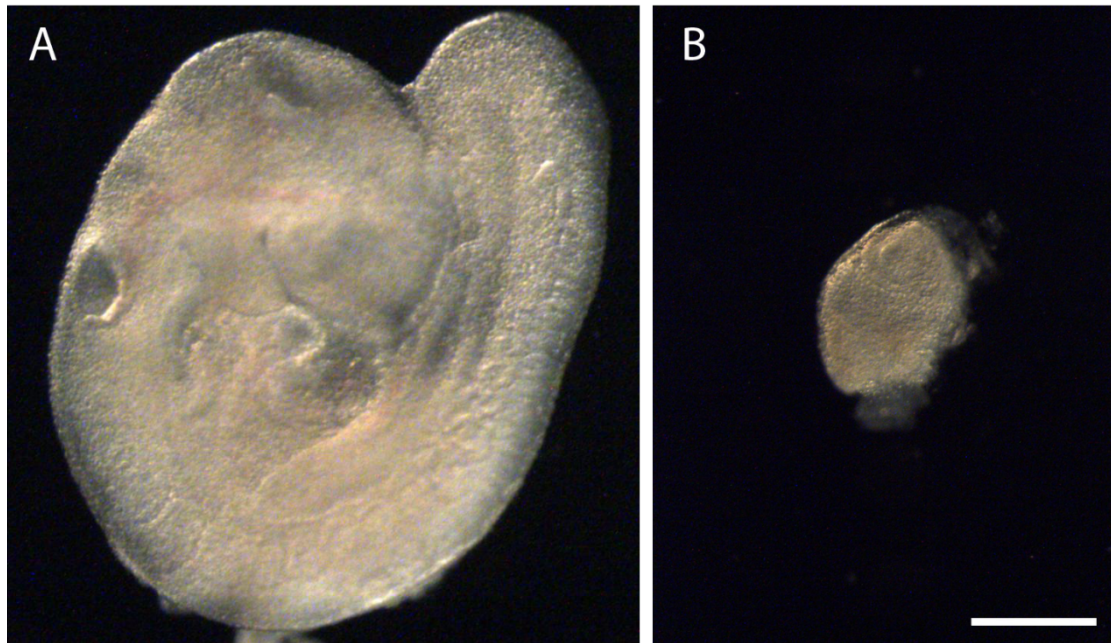
Figures adapted from the Edinburgh Mouse Atlas

(<http://www.emouseatlas.org/emap/home.html>)

Gestation day (number in litter)	<i>Vps33a</i> <sup>+/+</sup>	<i>Vps33a</i> <sup>+/-</sup>	<i>Vps33a</i> <sup>-/-</sup>	unable to genotype (resorptions)
E12.5 (13)	3	10	0	(3)
E10.5 (10)	1	2	0	5 (2)
E9.5 (10)	4	4	1	(1)
E9.5 (8)	2	3	2	1
E9.5 (7)	3	2	0	(1)
E8.5 (4)	1	1	1	1
E8.5 (4)	2	2	0	0
E8.5 (6)	1	3	0	2
E3.5 (8)	2	4	2	0

**Table 4.2 Genotypes of offspring from *Vps33a*<sup>+/-</sup> x *Vps33a*<sup>+/-</sup> timed matings.**

**Genotyping of offspring from *Vps33a* heterozygous intercrosses reveals embryonic lethality at approximately E8.5 when there was homozygous *Vps33a* inactivation.**



**Figure 4.3 E9.5 Morphology of *Vps33a* Embryos.**

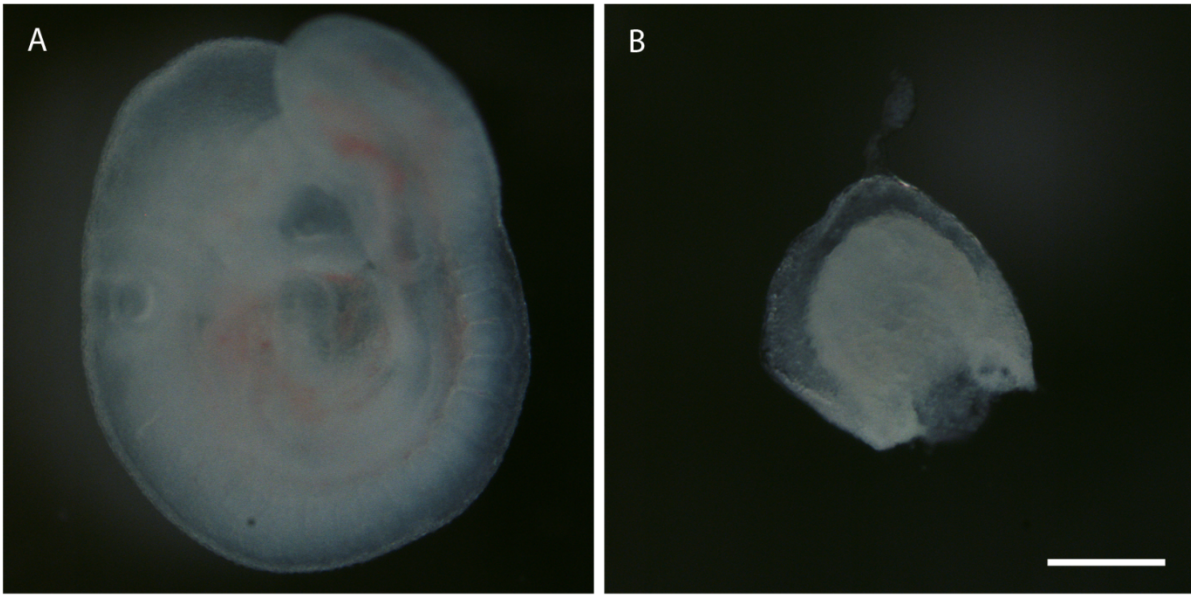
A. Representative *Vps33a*<sup>+/+</sup> wild-type littermate and B. *Vps33a*<sup>-/-</sup> digested remains,

Scale bar = 100μm. At this time-point the decidua containing *Vps33a*<sup>-/-</sup> remains were smaller than *Vps33a*<sup>+/+</sup> and *Vps33a*<sup>+/-</sup>. *n*=1

<b>Gestation day (number in litter)</b>	<b><i>Vps33b</i><sup>+/+</sup></b>	<b><i>Vps33b</i><sup>+/<i>fl</i></sup></b>	<b><i>Vps33b</i><sup><i>fl/fl</i></sup></b>	<b>Unable to genotype (resorptions)</b>
E16.5 (8)	1	3	0	(4)
E12.5 (8)	1	5	1 (cre negative)	(2)
E10.5 (9)	4	3	0	1 (1)
E9.5 (3)	1	1	0	(1)
E9.5 (8)	0	5	1 (cre positive)	2

**Table 4.3 Genotypes of offspring from *Vps33b*<sup>+/fl</sup> x *Vps33b*<sup>+/fl</sup>-*PgkCre* timed matings.**

**Genotyping of offspring from *Vps33b* heterozygous intercrosses reveals embryonic lethality at approximately E8.5 when there was homozygous *Vps33b* inactivation.**



**Figure 4.4 E9.5 Morphology of *Vps33b* Embryos.**

A. Representative *Vps33b*<sup>+/+</sup> wild-type littermate and B. *Vps33b*<sup>fl/fl</sup>-*PgkCre* digested remains. Scale bar = 100μm. At this time-point the decidual containing *Vps33b*<sup>fl/fl</sup>-*PgkCre* remains were smaller than *Vps33b*<sup>+/+</sup> and *Vps33b*<sup>+/fl</sup> littermates. n=1

### 4.3.3 Isolation of embryonic stem cells from knockout blastocysts

It has been determined that both animal models are embryonically lethal at an early stage. To make use of these model systems, it was decided to establish embryonic stem (ES) cell lines from the blastocysts of  $Vps33a^{+/-}$  x  $Vps33a^{+/-}$  matings, and  $Vps33b^{fl/fl}$  matings, see section 2.16 for materials and methods.

Figure 4.5 shows an example of an attached blastocyst 3 days after extraction. The brighter mass is the inner cell mass which was selected and expanded to create ES cell lines.

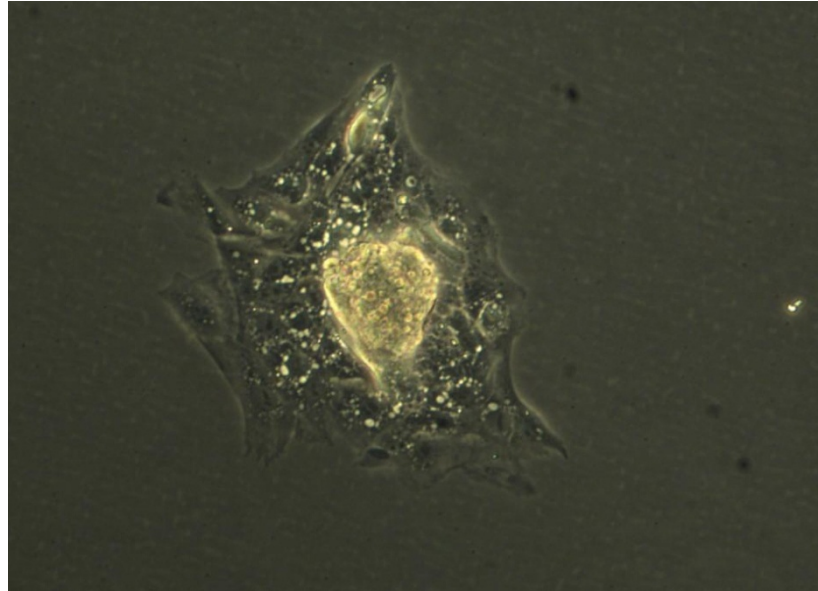
## 4.4 Discussion

$Vps33a^{-/-}$  embryonic lethality suggests that this protein plays an important role in development. This may explain why no human mutations in this gene have ever been identified. The *buff* mouse with missense mutation in  $Vps33a$ , has been suggested as a model for Hermansky Pudlak syndrome (HPS) (Suzuki et al. 2003). Therefore, *VPS33A* has been screened in many HPS-like patients with unknown mutations but no mutation has been identified to date. The missense mutation in the *buff* mouse may allow the protein to retain partial functionality thus allowing embryo development and explain survival of this mouse. Lethality during development has been observed in *Drosophila* (Akbar et al. 2009).

Embryonic lethality in the  $Vps33b^{fl/fl}$ -*PgkCre* mouse was unexpected due to the survival of ARC syndrome patients born with mutations in this gene. The reason for ARC patient survival may only be postulated. It may be that patients are able to express alternative transcripts of *VPS33B*, which allows them to bypass embryonic lethality. The finding of an



alternative transcript in the patient with attenuated phenotype may support this hypothesis. It is also possible that the incidence of miscarriage is increased in families with ARC, however



**Figure 4.5 Blastocyst outgrowth 3 days after isolation.**

A representative *Vps33b*<sup>fl/fl</sup> blastocyst outgrowth isolated at E3.5 and grown for 3 days. The inner cell mass appears as a bright mass in the centre, which was isolated and trypsinised in order to establish embryonic stem cells. The outer cells are trophectoderm. In the case of *Vps33b*<sup>fl/fl</sup> ES cells, a Cre-recombinase containing plasmid was introduced to create *Vps33b*<sup>-/-</sup> ES cells.

it is difficult to ascertain if this is the case. It may also be that VPS33A may be able to compensate for VPS33B during human embryo development.

It can be concluded from this work that the removal of Vps33a or Vps33b results in embryonic lethality in the mouse at E7.5-E8.5. Between these time-points many different processes occur. Major landmark processes include: the formation of the amnion to create 3 cavity egg cylinder, formation of the allantois which grows out towards the ectoplacental cone and fuses with the developing chorion, formation of the mesodermal layer and the beginnings of development of the heart, and finally turning, where the embryo rotates on its body axis (figure 4.5)(Theiler 1989). These processes involve many different signalling pathways and molecules; the appropriate location of which guides correct development.

At present the possible reasons for embryonic lethality can only postulated. It has been suggested from work in other model organisms that Vps33a plays a role in the biogenesis of lysosome related organelles and the fusion of autophagosomes with lysosomes in *Drosophila* (Akbar et al. 2009), as well as the fusion of uroplakin-degrading MVBs with lysosomes in mouse urothelium (Guo et al. 2009), resulting in defective degradation of proteins. Vps33b has been implicated in apical recycling of receptors, with apical proteins in the ARC liver being mislocalised to the basolateral membrane. In Vps33b knockdown mIMCD cells a similar observation was made with the P75 neurotrophin receptor protein which is normally restricted to the apical membrane (Cullinane et al. 2010). If receptors and signalling molecules are incorrectly trafficked or degraded, developmental cues including those dependent on correct orientation may not be properly interpreted, thus leading to a halt or defect in development. This may be the case in the *Vps33a*<sup>-/-</sup> or *Vps33b*<sup>*fl/fl*</sup>-*PgkCre* mice.

Supporting this hypothesis is the finding that disruption of the HOPS complex component, Vps39, has been found to cause embryonic lethality between E3.5-6.5 (Messler et al. 2011). It was originally identified as a protein that may be involved in TGF- $\beta$  signalling due to 25% homology to TGF- $\beta$  receptor associated protein-1 (TRAP-1), and subsequently found to bind to TGF- $\beta$  receptors and Smad4 (Felici et al. 2003).

TGF- $\beta$  and the cytokines belonging to the TGF- $\beta$  superfamily are important during embryogenesis for many processes including establishment of body axis and tissue differentiation (Harland 1994)(Neumann & Cohen 1997). TGF- $\beta$  elicits intracellular signalling pathways through activation of the TGF- $\beta$  receptors type I and type II, serine/threonine kinases which subsequently signal through phosphorylation of downstream effectors including those in Smad-dependent and Smad-independent pathways such as the Ras-MAPK Erk1/2 pathway (Moustakas & Heldin 2008). In the Smad dependent pathway Smads are phosphorylated by TGF- $\beta$  RI, associate with Smad4 and subsequently translocate to the nucleus where they act as transcriptional regulators.

For TGF- $\beta$  signalling in many cell types, internalisation of the type I receptors to early endosomal antigen (EEA) 1-positive endosomes is required (Di Guglielmo et al. 2003). TGF- $\beta$  receptors also constitutively recycle in a Rab11 dependent manner (Mitchell et al. 2004). It was proposed by Felici et al. that Vps39 may direct activated TGF- $\beta$  receptors from the plasma membrane to Smad3-containing endocytic subdomains to facilitate formation of Smad3/4 complexes (Felici et al. 2003). This is consistent the requirement of Vps39 for vesicular trafficking in yeast for biogenesis of the vacuole (Nakamura et al. 1997) and it has been hypothesised that the phenotype observed in Vps39 deficient mice is a result of defective trafficking (Messler et al. 2011).

Further investigation of embryonic lethality and protein function of Vps33a and Vps33b may use a similar approach to that used in the study of CHMP5 (Shim et al. 2006). CHMP5 is homologous to Endosomal Sorting Complex Required for Transport-III (ESCRT-III) complex proteins, and when absent causes embryonic lethality at approximately E10. It was suspected that CHMP5 may play a role in regulation of endocytosis or lysosomal transport of receptors involved in signal transduction. Primary embryonic cells from E8.5 embryos were cultured and ES cell lines were established. These were used along with stable knockdown cells to establish that it was endocytosis of receptors such as NF- $\kappa$ B that was disrupted. As a result, processes involved in embryonic development were disrupted. This was found to be due to incorrect regulation of receptors important in embryogenesis at this stage, such as Transforming Growth Factor- $\beta$  (TGF- $\beta$ ) receptors.

With the establishment of *Vps33b*<sup>-/-</sup> ES cell lines this work is now possible. In addition, full morphological analysis of embryos at E7.5 and E8.5 should be undertaken. This could indicate the exact stage at which lethality occurs and may include whole mount staining or paraffin embedding and sectioning.

As a cre-lox system was used in order to create the ubiquitous *Vps33b*<sup>fl/fl</sup> mouse, selection of a different cre recombinase line will allow production of a tissue specific *Vps33b*<sup>fl/fl</sup> conditional mouse in order to avoid embryonic lethality. In chapter 5 and 6 the development of tissue specific Vps33b deficient mice is described. These models are particularly valuable for investigation of the role of Vps33b in specific cell types.

## **CHAPTER 5 - A LIVER-SPECIFIC V<sub>ps33b</sub> CONDITIONAL KNOCKOUT MOUSE**

## **5.1 Introduction and overview**

Intrahepatic cholestasis is a cardinal feature of ARC syndrome. In PFIC types 1, 2 and 3 it has been shown to be caused by mutations in genes located at the apical membrane involved in transport across the apical membrane. Mutations in tight junction proteins have also been shown to cause intrahepatic cholestasis thought due to loss of cell polarity and paracellular leakage between the hepatocytes. At present the molecular mechanisms that result in cholestasis in ARC syndrome are unknown. Staining of patient livers has however found the apical proteins CEA and BSEP are mislocalised, and E-cadherin and claudin-1 levels are reduced. Further investigation is required to understand the pathways involved.

Technical problems have slowed progress in the understanding of hepatocyte polarity and cholestasis. Loss of structural polarity in primary hepatocyte culture and the mixing of membranes made poor models for the study of apical-basolateral polarity. Difficulties prompted the use of secondary hepatocyte cell lines such as HepG2 cells, however these too have disadvantages. They express many liver specific genes but have a low polarity index making them unsuitable for morphologic study (Arias et al. 2009). Development of models of liver disease is therefore very important to help understand these processes and thus improve the clinical outcome of liver diseases such as intrahepatic cholestasis.

## **5.2 Aims**

As ubiquitous removal of Vps33b in the mouse results in embryonic lethality, the aim is to develop a suitable mammalian model of the ARC syndrome liver for future use in experimental work to understand the molecular mechanisms of ARC and help aid future patient treatment.

## **5.3 Results**

### **5.3.1 Developing a liver-specific Vps33b conditional knockout mouse**

In order to create a liver specific knockout mouse, a cre-recombinase with albumin promoter was selected as albumin expression is restricted to hepatocytes (Pinkert et al. 1987). The number of births from  $Vps33b^{fl/fl}$  x  $Vps33b^{fl/fl}$ -AlbCre matings was 26  $Vps33b^{fl/fl}$  and 24  $Vps33b^{fl/fl}$ -AlbCre mice, conforming to the mendelian mode of inheritance.  $Vps33b^{fl/fl}$ -AlbCre mice thrived with no obvious ill effects. They were aged and removal of Vps33b in the liver had no obvious adverse effect on livelihood at 1 year of age. No signs of jaundice were observed.

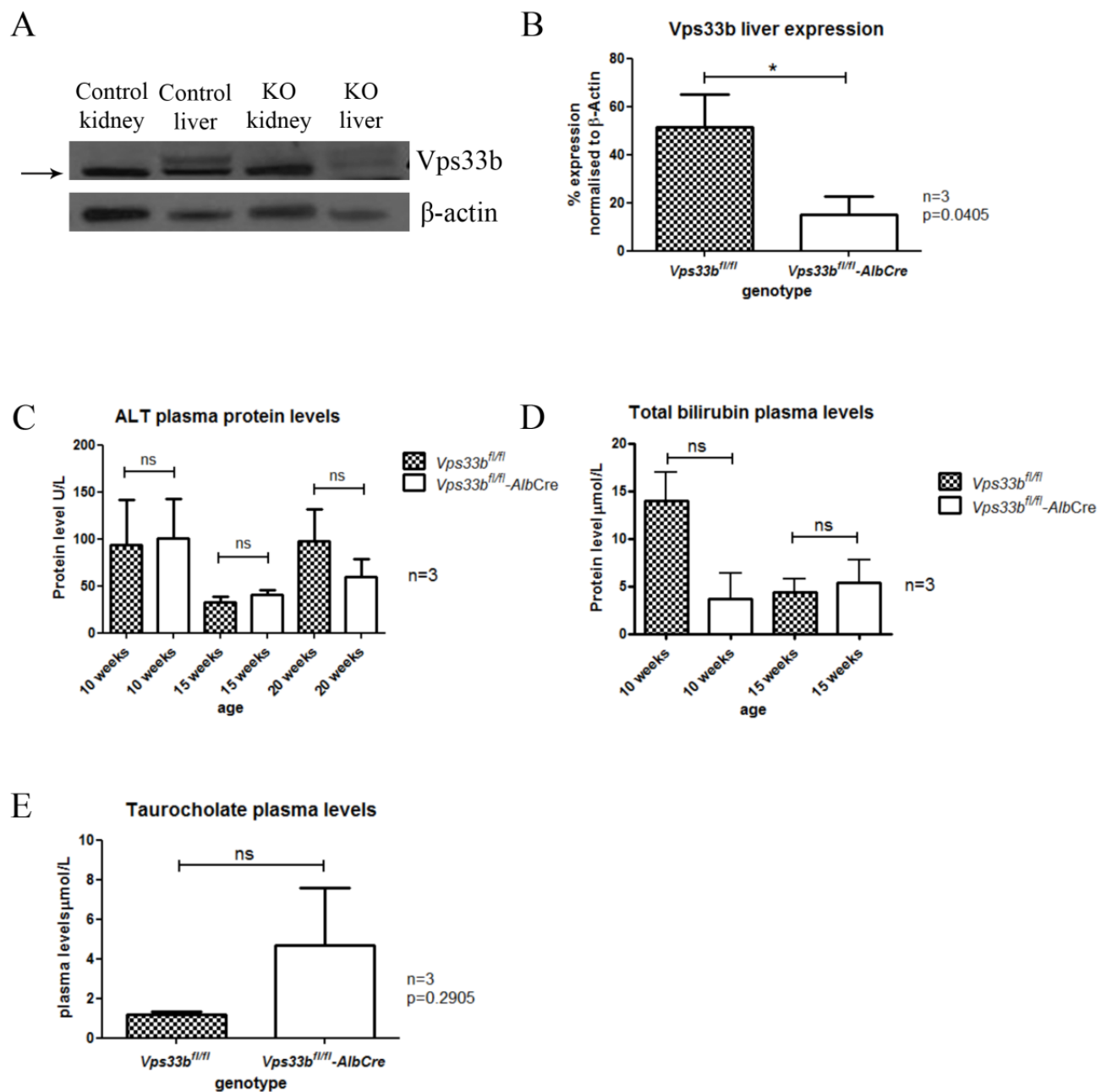
Protein lysates obtained from crushed livers extracted at 15 weeks from control  $Vps33b^{fl/fl}$  mice and  $Vps33b^{fl/fl}$ -AlbCre mice were immunoblotted for Vps33b (figure 5.1A). The percentage expression of Vps33b when normalised again  $\beta$ -Actin in  $Vps33b^{fl/fl}$ -Albcre was reduced by approximately 71% when compared to  $Vps33b^{fl/fl}$  controls (figure 5.1B). Total removal of Vps33b was not expected due to the presence of a mixed population of cells in the liver (Pinkert et al. 1987). Hepatocytes make up approximately 70% of the liver mass, and 60% of the cellular number, therefore when using crushed liver the protein from other cell types are included in the lysate produced. For example, the liver is highly vascularised, and the endothelium of these blood vessels do not produce albumin, therefore Vps33b expression in these cells would not be affected as cre-recombinase is not produced.

### 5.3.2 *Vps33b<sup>fl/fl</sup>*-*Alb*Cre liver function tests

In order to fully characterise the liver, tests for liver damage were carried out (figure 5.1C and D). In the clinic, ALT and bilirubin levels are tested for initial assessment of liver damage/dysfunction. Due to blood sampling restrictions, 10% of the total mouse blood volume every month is permitted to be taken, therefore ALT and bilirubin levels were checked once every 5 weeks, from 10 weeks of age. ALT levels were not elevated in *Vps33b<sup>fl/fl</sup>*-*Alb*Cre mice, indicating there is no significant liver damage.

One knockout mouse was observed to be very itchy from 10 weeks onwards, and as a result of scratching had patchy fur and broken skin. Therefore bile acid levels within the blood were checked (figure 5.1D). Results were very variable, with the 'itchy' mouse having 10 times the level of tauro-trihydroxycholeanoate than the control animals. The other knockout mice had levels equivalent to control or up to 3 times that of control, the difference was not statistically significant due to the variation between animals.





**Figure 5.1 *Vps33b<sup>fl/fl</sup>-AlbCre* Liver characterisation**

(A) Immunoblot of kidney and liver protein lysates using primary rabbit anti-VPS33B, 1:500 dilution and secondary HRP-conjugated goat anti-rabbit 1:500 dilution. β-Actin used as a loading control. Kidney immunoblot was carried out to check for *Alb*-cre liver specificity. n=3. (B) Densitometry of Vps33b immunoblot, Vps33b is normalised against β-actin. Vps33b is reduced by 72% in comparison to control. n=3 (C) ALT plasma protein levels measured at 10-20 weeks, no significant difference was observed. n=3. (D) Bilirubin plasma levels at 10 and 15 weeks, no significant difference was observed. n=3. (E) Plasma levels of taurocholate by electrospray mass spectrometry identified no significant difference, n=3. Data from graphs

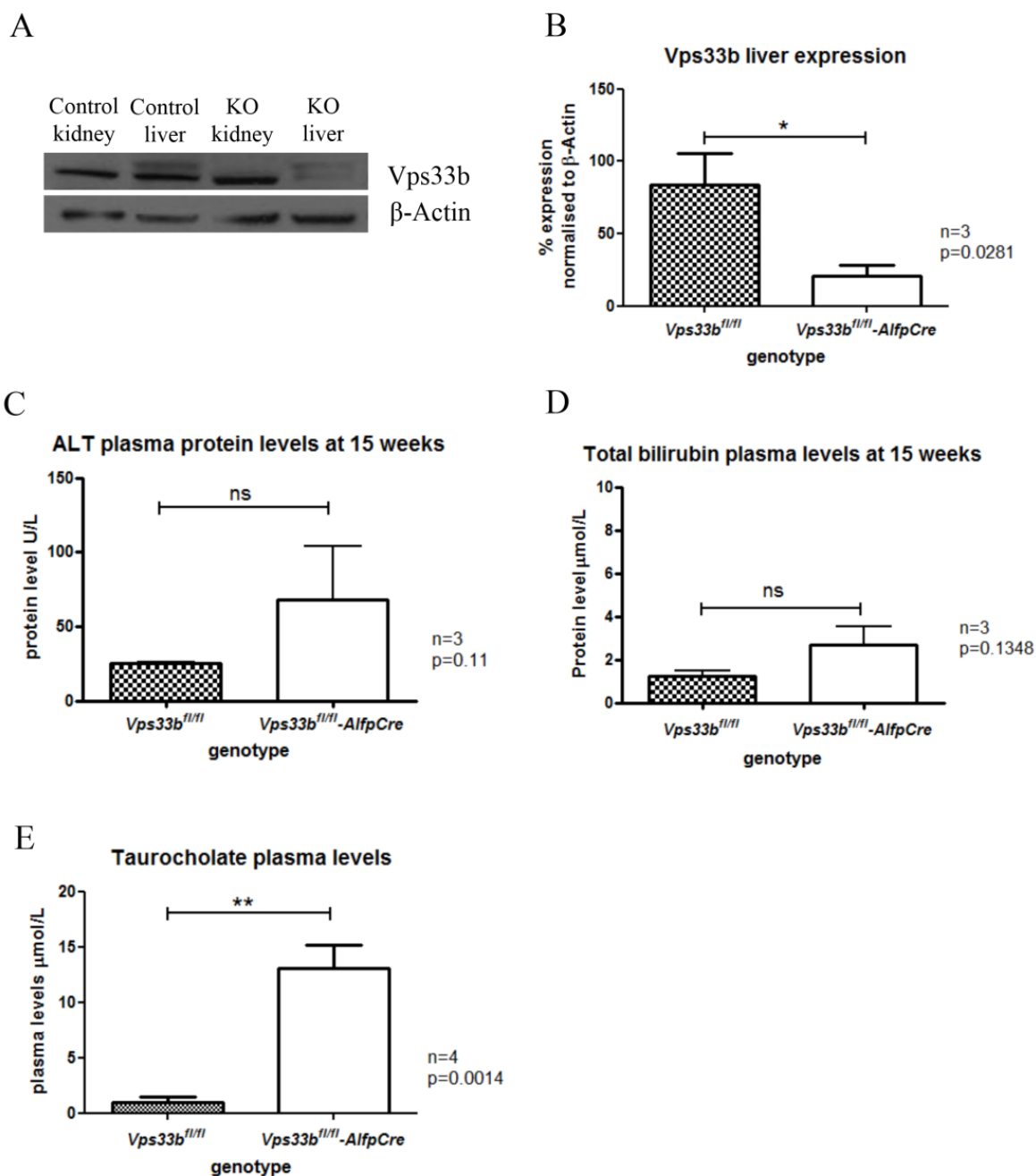
B-E were analysed using a two-tailed Student t test and the mean data points and standard error of mean error bars are presented.

### 5.3.3 Developing a second liver specific Vps33b conditional knockout mouse

Since the *Vps33b<sup>fl/fl</sup>-AlbCre* mouse produced variable results and it was reported that the expression of *Alb*-Cre was low prenatally (Postic & Magnuson 2000), it was decided to try a variation of the *Alb*-Cre line, AFP-albumin cre. This line contains the albumin promoter but also additional alpha-fetoprotein (AFP) enhancers, and is referred to as the *Alfp*-Cre line. *Alfp*-Cre has been shown to be expressed at much higher levels prenatally than *Alb*-Cre (Kellendonk et al. 2000) and therefore was expected to produce a more consistent phenotype in ARC model. This is because at least some of the liver defect is likely to be due to abnormal prenatal liver development. Vps33b levels were again assessed at 15 weeks in *Vps33b<sup>fl/fl</sup>-AlfpCre* mice by immunoblot. The percentage expression of Vps33b when normalised against  $\beta$ -Actin was reduced by approximately 76% when compared to *Vps33b<sup>fl/fl</sup>* controls (figure 5.2A-B).

### 5.3.4 *Vps33b<sup>fl/fl</sup>-AlfpCre* liver function tests

Identical tests were performed for ALT, bilirubin and bile acid levels as for the *Vps33b<sup>fl/fl</sup>-AlbCre* mice. These tests were performed at 15 weeks of age. There was no significant difference observed between control *Vps33b<sup>fl/fl</sup>* and *Vps33b<sup>fl/fl</sup>-AlfpCre* mice in ALT and bilirubin levels (figure 5.2C-D), as found in the *Vps33b<sup>fl/fl</sup>-AlbCre* mice. Bile acid tests however show a consistently significant increase in the levels of tauro-trihydroxycholeanoate (figure 5.2E), in contrast to the *Vps33b<sup>fl/fl</sup>-AlbCre* mice. Levels were elevated by at least 8 times and up to 18 times that of the mean level of control.

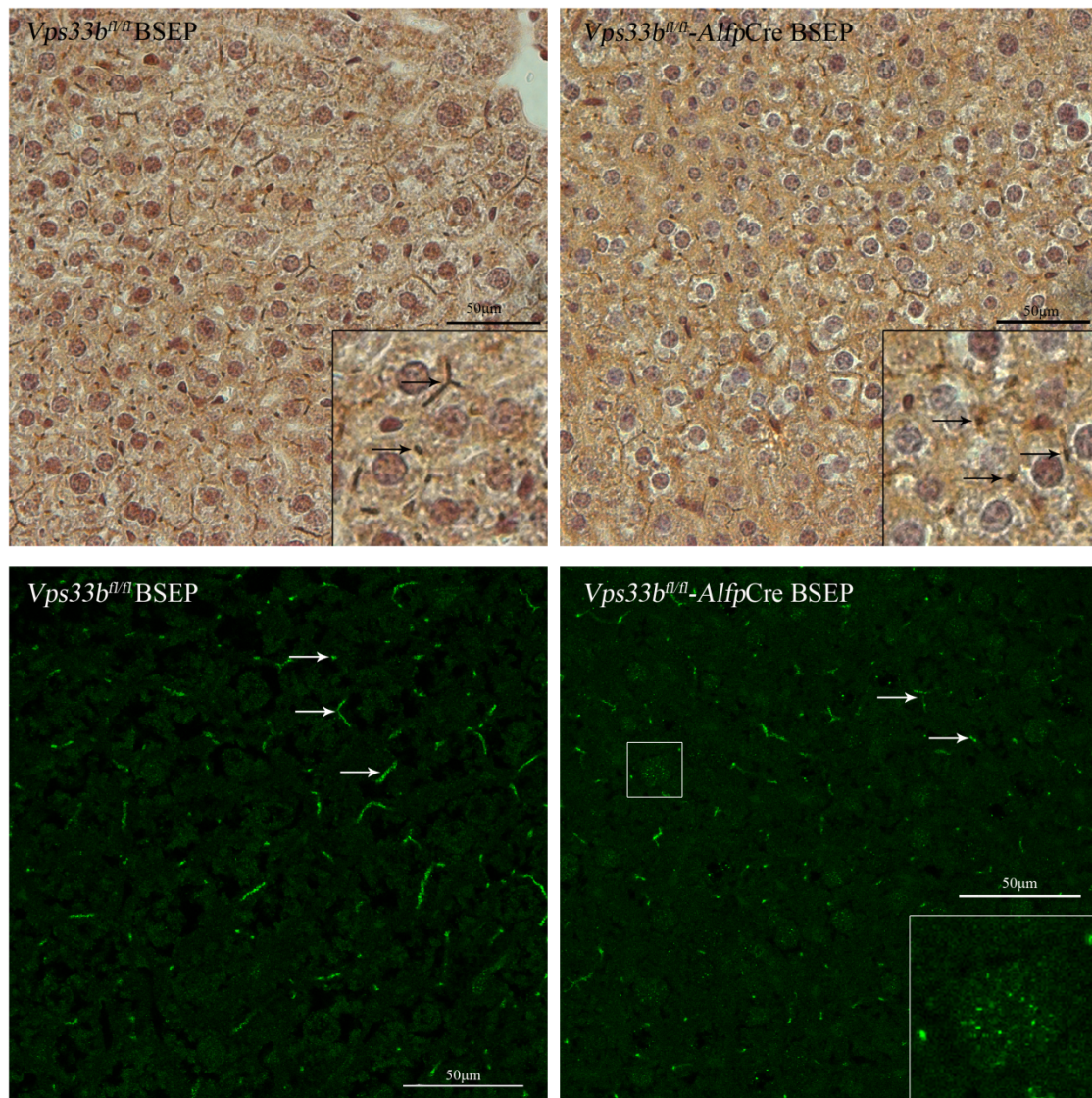


**Figure 5.2 *Vps33b<sup>fl/fl</sup>-AlfpCre* Liver characterisation**

(A) Immunoblot of kidney and liver protein lysates using primary rabbit anti-VPS33B, 1:500 dilution and secondary HRP-conjugated goat anti-rabbit 1:500 dilution. β-Actin used as a loading control. Kidney immunoblot was carried out to check for *Alfp*-cre liver specificity. n=3. (B) Densitometry of Vps33b immunoblot, Vps33b is normalised against β-actin. Vps33b is reduced by 76% in comparison to control. n=3 (C) ALT plasma protein levels measured at 15 weeks, no significant difference was observed. n=3. (D) Bilirubin plasma levels at 15 weeks, no significant difference was observed. n=3. (E) Plasma levels of taurocholate by electrospray mass spectrometry identified a significant increase, n=3. Data from graphs B-E were analysed using a two-tailed Student t test and the mean data points and standard error of mean error bars are presented.

### 5.3.5 Localisation of liver proteins in *Vps33b<sup>fl/fl</sup>-Alfp*Cre mice

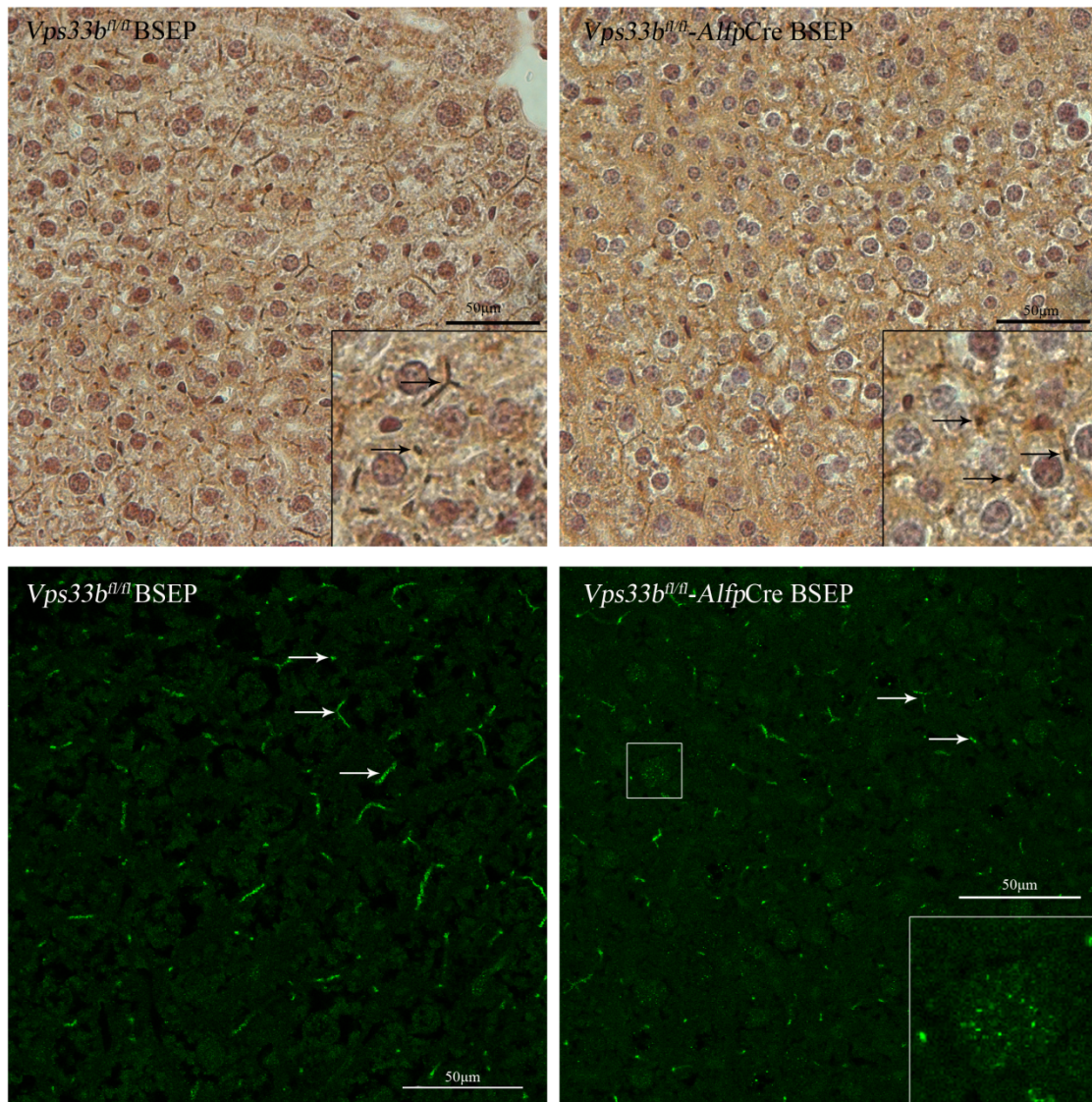
Histological analysis of hemotoxylin and eosin stained liver sections identified no abnormalities such as bile duct paucity or lipofuscin granules. Immunostaining of *Vps33b<sup>fl/fl</sup>-Alfp*Cre liver sections found CEA to be mislocalised to the cytoplasm and both apical and basolateral membrane (figure 5.3). The localisation of E-cadherin, an adherens junction protein, and ZO-1, a tight-junction associated protein were not disrupted by *Vps33b* deficiency. Immunostaining for BSEP, the primary bile acid transporter on the canalicular membrane identified apical staining; however it appeared reduced with fewer ‘branched’ stainings visible (figure 5.4). Immunofluorescent staining again showed reduced apical staining in the *Vps33b<sup>fl/fl</sup>-Alfp*Cre mice, but also revealed an increased number of hepatocytes with punctate cytoplasmic staining when compared to control. This suggests there may be a defect in the trafficking of BSEP to its correct canalicular location.



**Figure 5.3 Immunohistochemical analysis of protein localisation in mouse liver**

5 micron sections of paraffin embedded liver were immunostained for CEA, E-cadherin and ZO-1, antibody information in Appendix 1, sections were counterstained with hematoxylin, scale bar- 25µm. Apical staining is indicated with an arrow in control CEA staining. CEA was found mislocalised throughout the cytoplasm and plasma membrane in *Vps33b<sup>fl/fl</sup>-AlfpCre* livers. E-cadherin and ZO-1 were correctly localised. n=3





**Figure 5.4 Immunohistochemical and immunofluorescent analysis of BSEP localisation in mouse liver**

Top row: 5 micron sections of paraffin embedded liver were immunostained for BSEP, antibody information in Appendix 1, sections were counterstained with hematoxylin. Typical canalicular staining is indicated with an arrow in control *Vps33b<sup>fl/fl</sup>* livers. *Vps33b<sup>fl/fl</sup>-AlfpCre* livers also show canalicular staining indicated with an arrow, however staining appeared reduced.

Bottom row: Immunofluorescent staining for BSEP, antibody information in Appendix 1, found the same canalicular staining as by immunohistochemistry, but also revealed an increased number of hepatocytes in the *Vps33b<sup>fl/fl</sup>-AlfpCre* liver containing punctate intracellular staining, magnified 4 times in bottom right image. Scale bar - 50µm, n=3

## **5.4 Discussion**

An *Alb*-cre line was selected as albumin expression is exclusively restricted to hepatocytes (Meehan et al. 1984). Albumin is expressed early during mouse development at 7-8 somites (Gualdi et al. 1996) therefore the use of an albumin promoter to drive cre recombinase expression was deemed suitable for our use. It is a widely used cre-promoter and has proven useful in cre-dependent excision in adult hepatocytes (Postic et al. 1999). Only a mild phenotype was found in the liver specific *Vps33b* knockout developed this way. One mouse was identified as being itchy and high blood bile acid levels were observed, with bile acid results ranging from equivalent to control mice levels to the level 10 times higher than control mouse levels (the itchy mouse). It has been reported that recombination due to cre excision with *Alb*-Cre transgene is progressive over time, with recombination being 40% at birth progressing to full recombination at 6 weeks shown by southern blotting (Postic & Magnuson 2000). In the same publication use of a ROSA26 reporter mouse showed 99% of hepatocytes had undergone recombination at 12 days. It was hypothesised that expression of cre is below the threshold level necessary to cause rapid recombination in hepatocytes. Subsequently however, this finding was disputed, with the hypothesis that the alteration in recombination is due to a change in the ratio of hepatocytes:non-hepatocytes within the liver during juvenile development (Weisend et al. 2009). Since no further work was published on this topic and due to the varied results given by *Alb*-Cre in the *Vps33b*<sup>fl/fl</sup> mice, it was decided to develop a second liver specific line. The *Alfp*-Cre line contains albumin regulatory elements but also AFP enhancers. AFP is a fetal protein secreted in the liver during embryonic life. AFP enhancers are thought to influence albumin expression therefore this was done to mimic the organisation of the albumin gene (Kellendonk et al. 2000). The *Alfp*-Cre line was shown to produce cre-recombinase as early as E10.5. The *Vps33b* knockout mouse that resulted from

crosses with *Alfp*-Cre also produced a mild liver phenotype, but had less variable results during bile acid level analysis and therefore was used for further investigation.

#### **5.4.1 Is the *Vps33b<sup>fl/fl</sup>*-*Alfp*Cre mouse a phenocopy of the ARC liver?**

ALT, a marker for liver damage was not increased in the *Vps33b<sup>fl/fl</sup>*-*Alfp*Cre mice. In ARC patients it has been reported that ALT levels range from normal levels to just slightly raised. This test was carried out in order to confirm that the removal of *Vps33b* in the mouse liver did not result in a more severe phenotype or different presentation than the patient.

Conjugated hyperbilirubinaemia is seen at some point in time in all severely affected ARC patients, although the levels may fluctuate (Gissen et al. 2006). Diseases that reduce the flow of bile or transport of bilirubin into the bile produce an increased level of conjugated bilirubin in the blood due to its reflux out of hepatocytes into blood (Iyanagi et al. 1998). Non-excreting biliary isotope tests in ARC patients indicate reduced bile flow out along the bile duct and into the intestine. Total bilirubin was not increased in the *Vps33b<sup>fl/fl</sup>*-*Alfp*Cre mouse, indicating a milder phenotype. Discoveries made in previous cholestatic mouse models identifying differences between human and mouse may help explain our findings.

A BSEP knockout mouse (*spgp*) was created to model PFIC type 2. These mice developed intrahepatic cholestasis, but phenotype was less severe than PFIC type 2 (Wang et al. 2001). There was a dramatic decrease in the export of hydrophobic bile acids such as cholate into the bile (6% of wild-type) due to the lack of BSEP, however total bile acid output remained 30% of wild-type. Within the liver trihydroxylated bile acids were reduced (66% in males and 42% in females), and the atypical tetrahydroxy bile acid was present. The polarity of bile acids (hydrophobic or hydrophilic) is assumed to depend on the number of hydroxyl groups, therefore it was suggested that tetrahydroxy bile acids are more hydrophilic than the



trihydroxylated bile acids, resulting in reduced toxicity in the mouse liver (Perwaiz et al. 2003). The bile acids secreted into the bile were normal hydrophilic bile acids and tetrahydroxy bile acids are not normally detected (Perwaiz et al. 2003). Biliary secretion of these bile acids suggested an alternative transport mechanism for hydrophilic bile acids in mice. The P-glycoprotein genes *Mdr1a* and *Mdr1b* were found to be upregulated in these mice (Lam et al. 2005). Mdr1 was shown to have the ability to transport bile acids but at a lower affinity than BSEP (Lam et al. 2005). Triple knockouts were therefore produced (BSEP, *Mdr1a* and *Mdr1b*) (Wang et al. 2009). The knockout of these 3 genes led to a much more severe phenotype with impaired bile formation, jaundice and increased mortality. The conclusion was that mice have a compensatory mechanism which reduces the severity of cholestasis. This compensatory mechanism however was not enough to protect the BSEP knockout mouse (*spgp*) against cholestasis when fed a cholic acid diet, and severe intrahepatic cholestasis with jaundice, liver necrosis and high mortality was observed (Wang et al. 2003).

Bile acid levels, specifically tauro-trihydroxycholanoate, were increased ranging from 8 to 18 times that of control in the *Vps33b<sup>fl/fl</sup>-Alfp*Cre mice. Increased plasma bile acids is a sign of a liver secretion defect and is suspected to be a causative factor of the itching (pruritis) experienced by ARC patients. Only one ‘itchy’ mouse, a *Vps33b<sup>fl/fl</sup>-Alb*Cre mouse was identified. Tauro-trihydroxycholanoate has been found to be the best indicator along with total bile acid concentrations of cholestatic hepatobiliary disease in newborns (Mushtaq et al. 1999). The increased level of tauro-trihydroxycholanoate in the blood of the knockout mice indicates a defect in secretion of bile acids.

A mislocalisation of apical proteins was observed in the mouse. CEA is a glycoprotein involved in cell adhesion. It is a GPI-anchored cell surface glycoprotein that undergoes both N- and O- glycosylation, and is found on the apical surface of healthy hepatocytes (Ordenez

et al. 2007). CEA is mislocalised in the *Vps33b<sup>fl/fl</sup>-AlbCre* mice, found throughout the plasma membrane and in the cytoplasm, phenocopying the distribution seen in ARC livers. BSEP is trafficked via a Rab11-positive endosome pathway. The localisation also resembled that of patients, with reduced apical staining and increased intracellular protein.

In conclusion, it appears that in respect to protein localisation and plasma bile acid accumulation, the *Vps33b<sup>fl/fl</sup>-AlfpCre* mice are a good phenocopy of the ARC liver. The milder phenotype with regards to liver morphology may be induced by feeding a cholic acid diet. As a result these mice may be used in the future for further experiments to aid understanding of the ARC liver.

**CHAPTER 6 - A MEGAKARYOCTYE AND  
PLATELET-SPECIFIC V<sub>ps33b</sub>  
CONDITIONAL KNOCKOUT MOUSE**

## **6.1 Introduction and overview**

An  $\alpha$ -granule defect in ARC platelets was first reported by Deal et al. in 1990 when it was identified that patient platelets resembled those of Grey platelet syndrome (Deal et al. 1990). Subsequently a bleeding diathesis was reported when >50% of patient liver biopsies resulted in severe life threatening haemorrhaging (Gissen et al. 2006). Deficiencies in both  $\alpha$ -granule membranes and contents distinguish ARC platelets from the  $\alpha$ -granule storage pool disease Grey platelet syndrome in which  $\alpha$ -granule membranes appear intact.

$\alpha$ -granules are predicted to play multiple functions, a result of the diverse and numerous proteins contained within these granules (Maynard et al. 2007). These roles include angiogenesis, wound healing and immune response activation (Ren et al. 2008). It would therefore be of great interest to create a mouse severely deficient or completely lacking  $\alpha$ -granules and their contents in order to study their suspected wide reaching functions. Consequently, the aim is to create and characterise a megakaryocyte and platelet specific Vps33b conditional knockout mouse. This is because most of the platelets in ARC patients completely lack  $\alpha$ -granules, and have greatly reduced or absent levels of  $\alpha$ -granule proteins. Creating a mouse with reduced Vps33b within its megakaryocytes may allow us to create a mouse severely lacking platelet  $\alpha$ -granules. In addition to the exploration of different roles of  $\alpha$ -granules, it would also allow us to investigate further the role of Vps33b in platelet formation, helping us to learn more about the proteins function.

## **6.2 Methodology**

A transgenic *Pf4*-Cre recombinase strain (Tiedt et al. 2007) was used in a conditional knockout strategy to target megakaryocyte lineage and therefore platelets. The *Pf4*-Cre transgene has been shown to partially excise floxed alleles in hematopoietic progenitors, however shows full excision in megakaryocytes (Coppinger et al. 2004). Therefore, this cre-recombinase line was deemed suitable for our use.

## **6.3 Results**

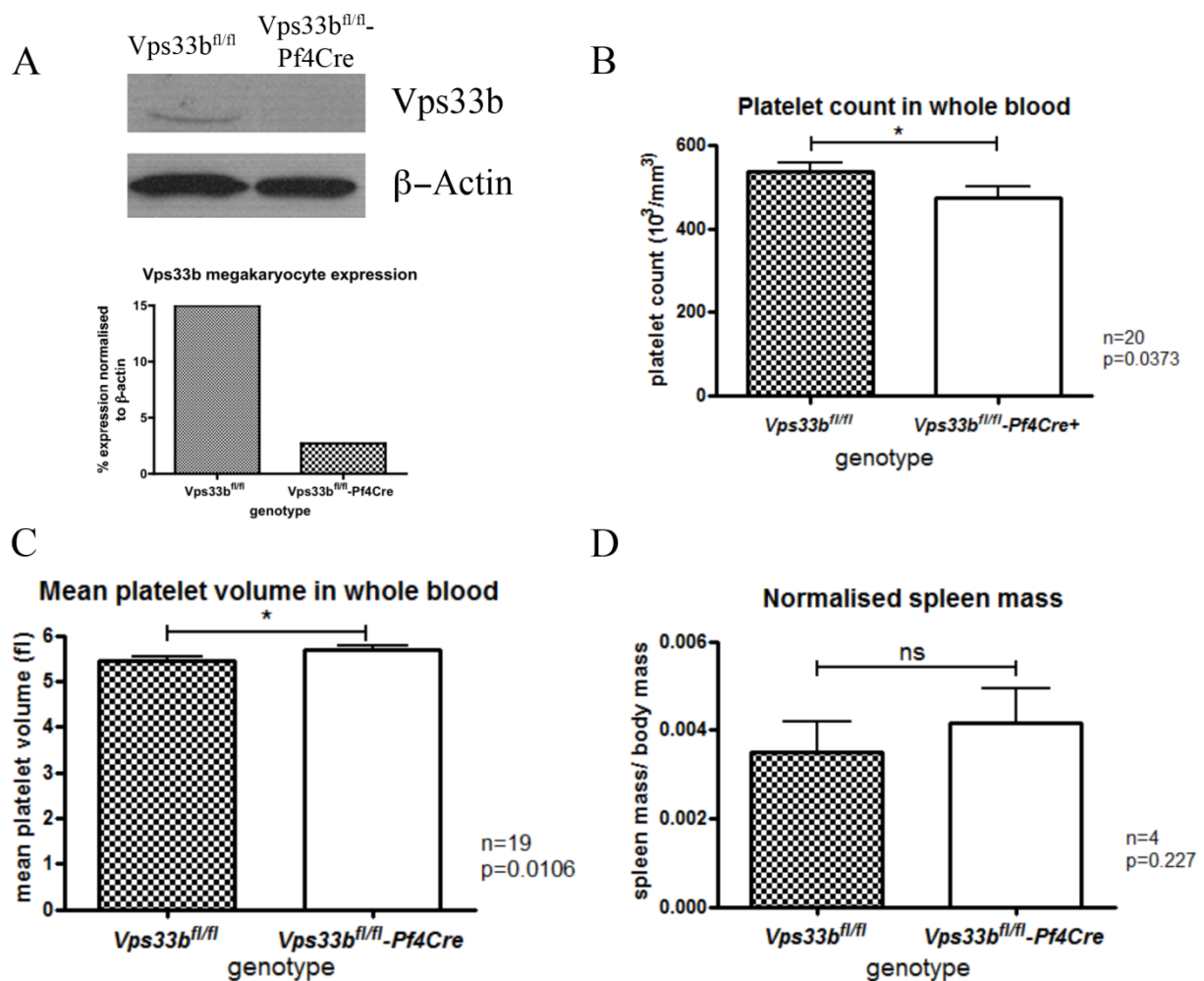
### **6.3.1 Megakaryocyte *Vps33b*<sup>fl/fl</sup>-*Pf4*Cre mice**

The offspring resulting from *Vps33b*<sup>fl/fl</sup> x *Vps33b*<sup>fl/fl</sup>-*Pf4*Cre matings resulted in a 1:1 ratio of *Vps33b*<sup>fl/fl</sup> and *Vps33b*<sup>fl/fl</sup>-*Pf4*Cre live births, thus indicating that the excision of *Vps33b* by *Pf4*-Cre recombinase does not affect embryo viability.

As *Vps33b* is not present in platelets (Lo et al. 2005) it must function in the megakaryocyte. Analysis of *Vps33b* levels in megakaryocytes was undertaken using megakaryocytes differentiated from haemopoietic stem cells of the control *Vps33b*<sup>fl/fl</sup> and *Vps33b*<sup>fl/fl</sup>-*Pf4*Cre mice. Immunoblotting of *Vps33b* and found that *Vps33b* levels were reduced by approximately 82% in the *Vps33b*<sup>fl/fl</sup>-*Pf4*Cre megakaryocytes in comparison to control *Vps33b*<sup>fl/fl</sup> megakaryocytes (figure 6.1A). A reduction and not complete loss of *Vps33b* may be observed due to the nature of the *Pf4*-Cre recombinase transgene discussed in section 6.4.3 (Tiedt et al. 2007). The Cre-recombinase may not act early enough in megakaryocyte maturation to prevent production of *Vps33b*, thus explaining the low levels seen.

### 6.3.2 Analysis of platelet count, volume and spleen size

Platelet count in the  $Vps33b^{fl/fl}-Pf4Cre$  mouse whole blood was analysed using an ABX Diagnostics Pentra 60. There was no significant difference in platelet count observed (figure 6.1B). There was an increase of in mean platelet volume by approximately 4.4% in the  $Vps33b^{fl/fl}-Pf4Cre$  mouse platelets (figure 6.1C). In mice with platelet defects often an enlargement of the spleen can be observed, therefore the spleen was measured in 9 week old mice, with the spleen mass being normalised to body mass. No significant difference was observed (figure 6.1D).



**Figure 6.1 Immunoblot for Vps33b, platelet count, mean platelet volume and spleen mass**

A. Immunoblot for Vps33b in megakaryocytes, mouse anti-Vps33b primary antibody (Proteintech) at a concentration of 1:500, and rabbit anti-mouse HRP-conjugated secondary antibody (Invitrogen) at a concentration of 1:500 was used. Loading was confirmed by immunoblotting for β-Actin, n=3. A graph displaying the densitometry of the Vps33b immunoblot, Vps33b is normalised against β-actin. Vps33b is reduced by 82% in comparison to control. n=3

B. Platelet count in whole blood using the ABX Pentra 60 whole blood counter, no significant difference was observed, n=20.

C. Mean platelet volume measured using the ABX Pentra 60 whole blood counter, a slight increase was in MPV was observed, n=19.

D. Spleen mass normalised to body mass, aged 9 weeks, n=4. No significant difference was observed.

Data in B-D was analysed using a two-tailed Student t-test with mean and standard error of mean error bars presented.

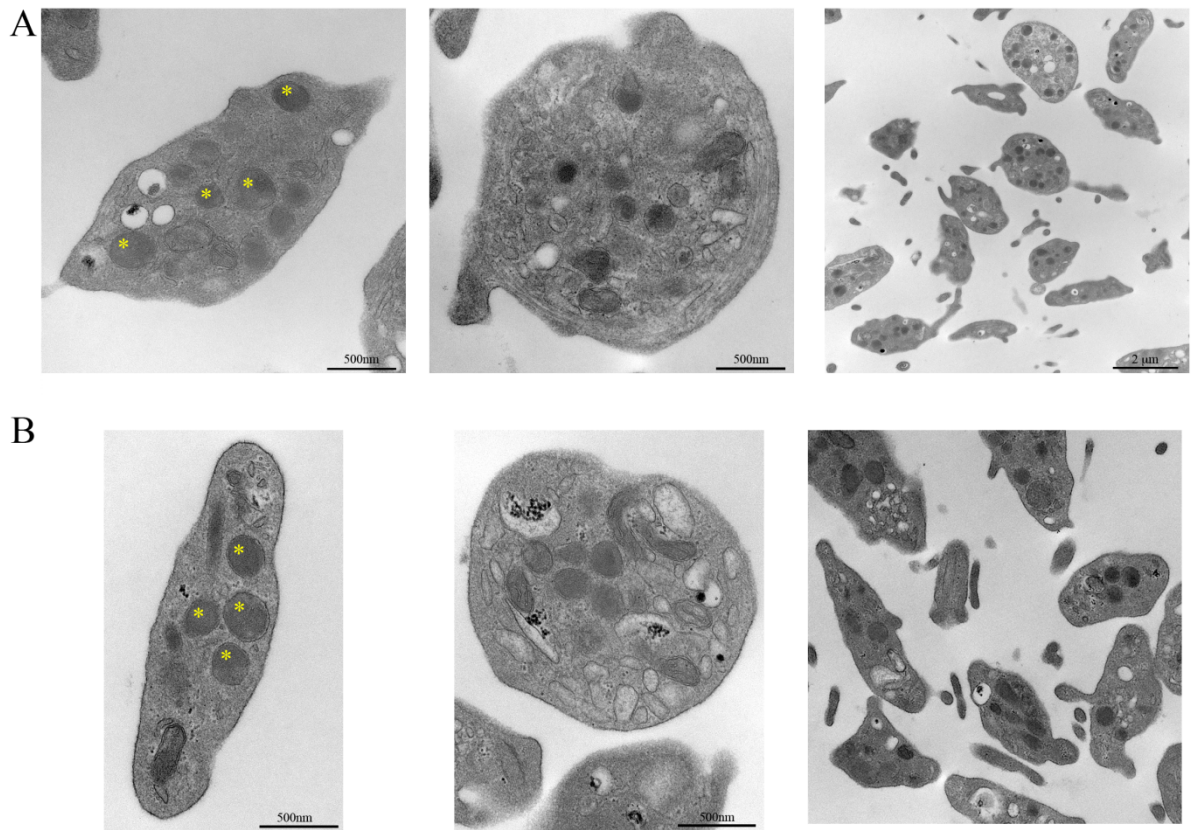
### **6.3.3 Electron microscopy of platelets**

Platelets were prepared for EM and sent for analysis to Walter Kahr, Hospital for Sick Children, Toronto.  $\alpha$ -granules were present in the *Vps33b<sup>fl/fl</sup>*-*Pf4Cre* mouse platelets (figure 6.2). To quantitatively determine if there was a difference in  $\alpha$ -granule number between control *Vps33b<sup>fl/fl</sup>* and *Vps33b<sup>fl/fl</sup>*-*Pf4Cre* platelets, 50 platelets from each sample were counted. As platelet sections were analysed only a proportion of the total number of  $\alpha$ -granules within the platelets were counted. *Vps33b<sup>fl/fl</sup>*-*Pf4Cre* platelets had  $4.5 \pm 0.38$   $\alpha$ -granules per platelet section in comparison to  $6.4 \pm 0.4$  in *Vps33b<sup>fl/fl</sup>* control. Data was analysed using a two-tailed Student t-test and identified a significant reduction,  $p=0.0018$ .

### **6.3.4 Bleeding time test**

In order to assess whether bleeding time was extended in the mice, bleeding time tests were carried out. Control *Vps33b<sup>fl/fl</sup>* mice and *Vps33b<sup>fl/fl</sup>*-*Pf4Cre* mice were tested using a standard bleeding time assay (see section 2.18.2 for methods). Blood loss was measured after removal of the tail tip. No significant difference was observed between the two groups of mice (figure 6.3).



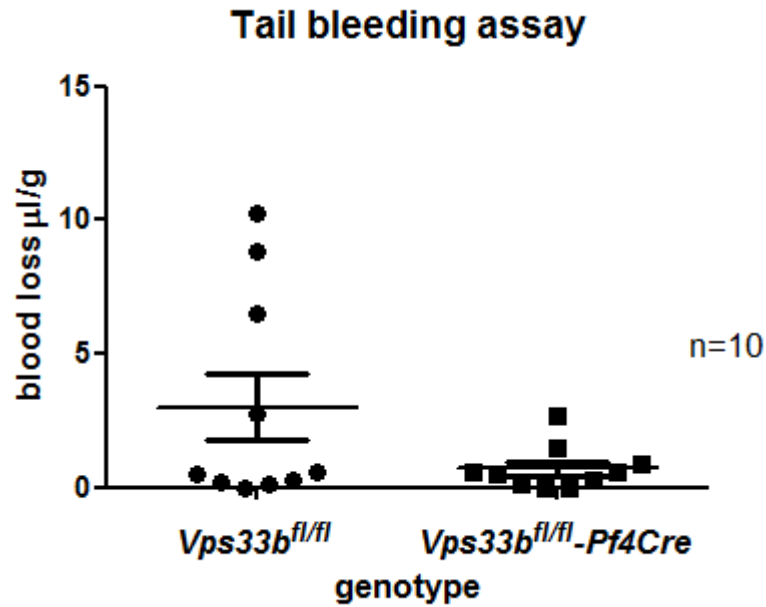


### **Figure 6.2 Ultrastructural analysis of platelets**

A. Electron microscopy images of control *Vps33b<sup>fl/fl</sup>* platelets, left- sagittal image with  $\alpha$ -granules marked with yellow asterisks, centre-horizontal section and right-field of view.

B. Electron microscopy images of *Vps33b<sup>fl/fl</sup>-Pf4Cre* platelets. left- sagittal image with  $\alpha$ -granules marked with yellow asterisks, centre-horizontal section and right-field of view. No obvious morphological differences were observed.

Images taken by Walter Kahr, Sick Kids, Toronto



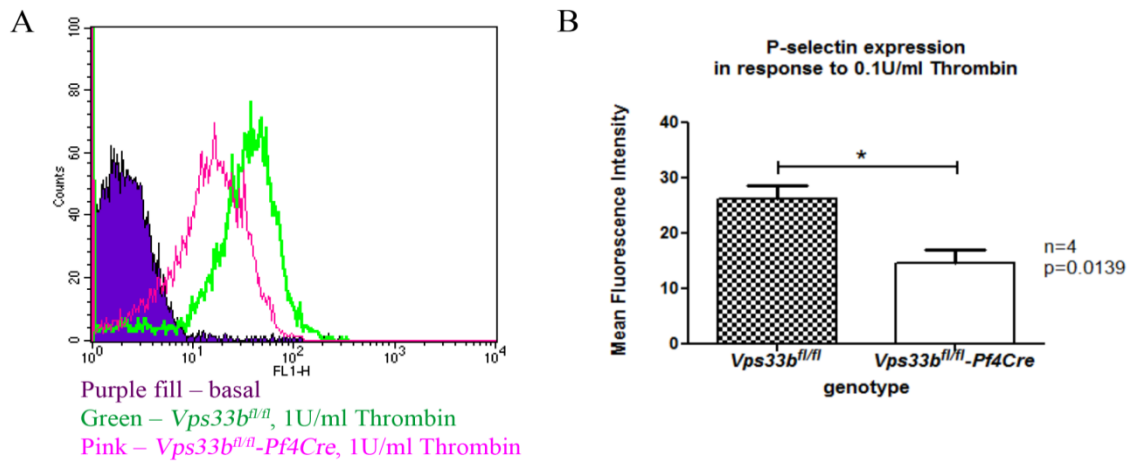
**Figure 6.3 Bleeding time test**

Total volume of blood lost in 20 minutes normalised to body mass. Test was stopped after 5 minutes if no droplet fell, n=10. No significant difference was observed between control *Vps33b<sup>fl/fl</sup>* and *Vps33b<sup>fl/fl</sup>-Pf4Cre* mice.

Data points for each mouse are presented, and the mean value depicted by a bar. Data was analysed using the Wilcoxon rank-sum test.

### 6.3.5 Flow cytometry to assess P-selectin expression

P-selectin is a protein found on the membranes of platelet  $\alpha$ -granules. Upon stimulation with thrombin,  $\alpha$ -granules fuse with the platelet outer-membrane allowing the release of their contents. As a result, P-selectin is relocated to the outer membrane of the platelet and thus is used as a marker for  $\alpha$ -granule presence and secretion. It must be noted that P-selectin has also been reported present on dense granule membranes (Israels et al. 1992). A FITC-conjugated anti-mouse CD-62 antibody was used to detect levels of P-selectin on the surface of the mouse platelets. No significant difference was observed between the  $Vps33b^{fl/fl}$  and  $Vps33b^{+/+}$ -*Pf4Cre* controls, data not shown. P-selectin levels were reduced by approximately 44% in the  $Vps33b^{fl/fl}$ -*Pf4Cre* mice compared to  $Vps33b^{fl/fl}$  control (figure 6.4).



**Figure 6.4 Flow cytometry to assess P-selectin expression on the platelet membrane**

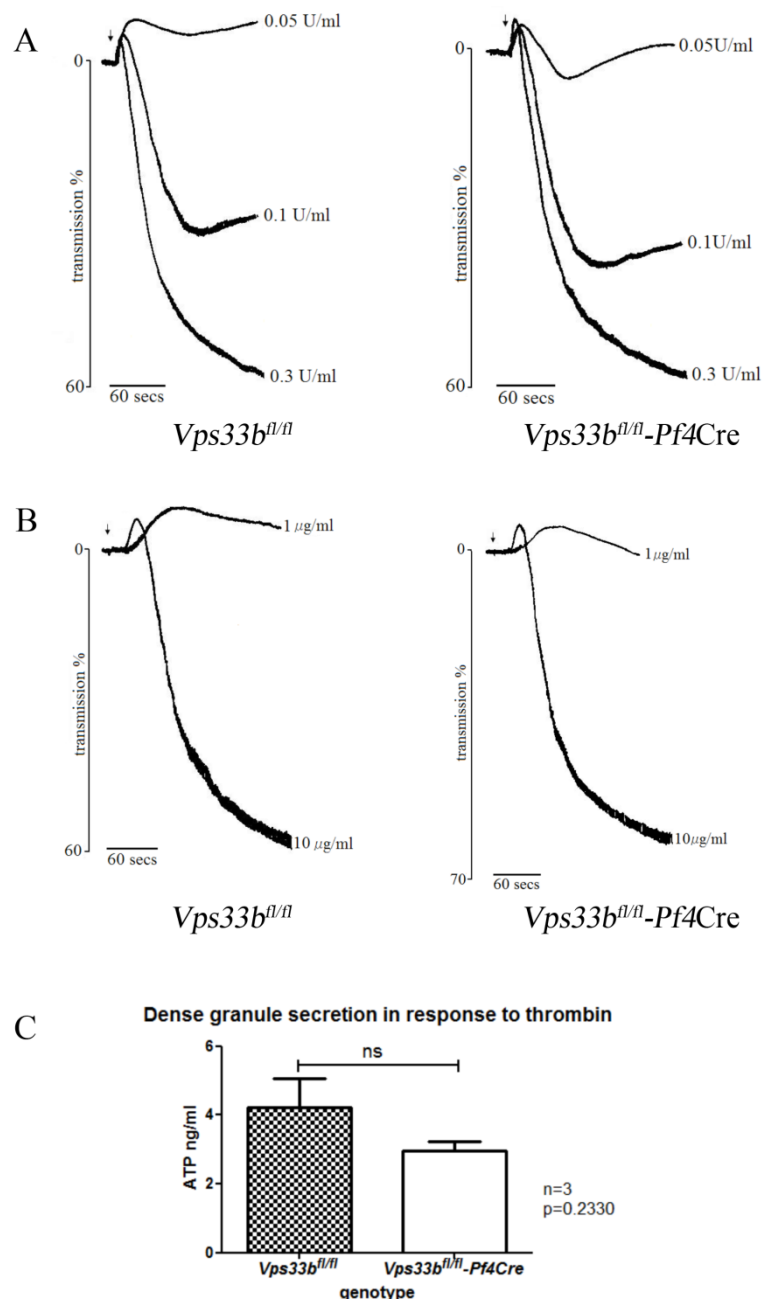
A. Basal (unstimulated) platelets or stimulated platelets (1U/ml thrombin) were labelled with FITC-conjugated anti-mouse CD62P (P-selectin). Flow cytometry results, represented by a histogram, show fluorescence intensity against platelet count. *Vps33b<sup>fl/fl</sup>-Pf4Cre* platelets showed a reduced level of fluorescence and therefore reduced P-selectin expression on the platelet surface.

B. Geometric mean fluorescence intensity of platelets was calculated from flow cytometry data, n=4. The mean value and standard error of mean error bars are presented. Data was analysed using a two-tailed Student t-test and a significant reduction in P-selectin levels on the *Vps33b<sup>fl/fl</sup>-Pf4Cre* platelets was observed.

### 6.3.5 Aggregation and dense granule secretion

In order to assess aggregation and dense granule secretion, low, threshold and high concentrations of thrombin, a strong platelet activator, were used to activate platelets. For aggregation in response to thrombin in washed platelets, fibrinogen, an  $\alpha$ -granule protein, must be present to allow cross-linking of platelets via the integrin  $\alpha$ IIb $\beta$ 3 receptor. Platelets were washed twice to remove all plasma proteins, thus the only available fibrinogen would be within the platelet. Aggregation was followed by monitoring light transmission in a stirred platelet suspension. No differences between the control *Vps33b*<sup>fl/fl</sup> mice, *Vps33b*<sup>+/+</sup>-*Pf4Cre* control mice (data not shown) and *Vps33b*<sup>fl/fl</sup>-*Pf4Cre* were observed in aggregation in response to thrombin or collagen (figure 6.4A and B).

Dense granule secretion by thrombin stimulation was also monitored by measuring ATP secretion using the reagent Chronolume. Chronolume contains luciferin, a pigment which is catalysed to oxyluciferin by the enzyme luciferase with a resultant emission of light. This energy for this reaction is provided by ATP, and the light given off is directly proportional to the quantity of ATP present. Therefore by recording luminescence ATP secretion from dense granules can be monitored. No significant difference was observed (figure 6.4C).



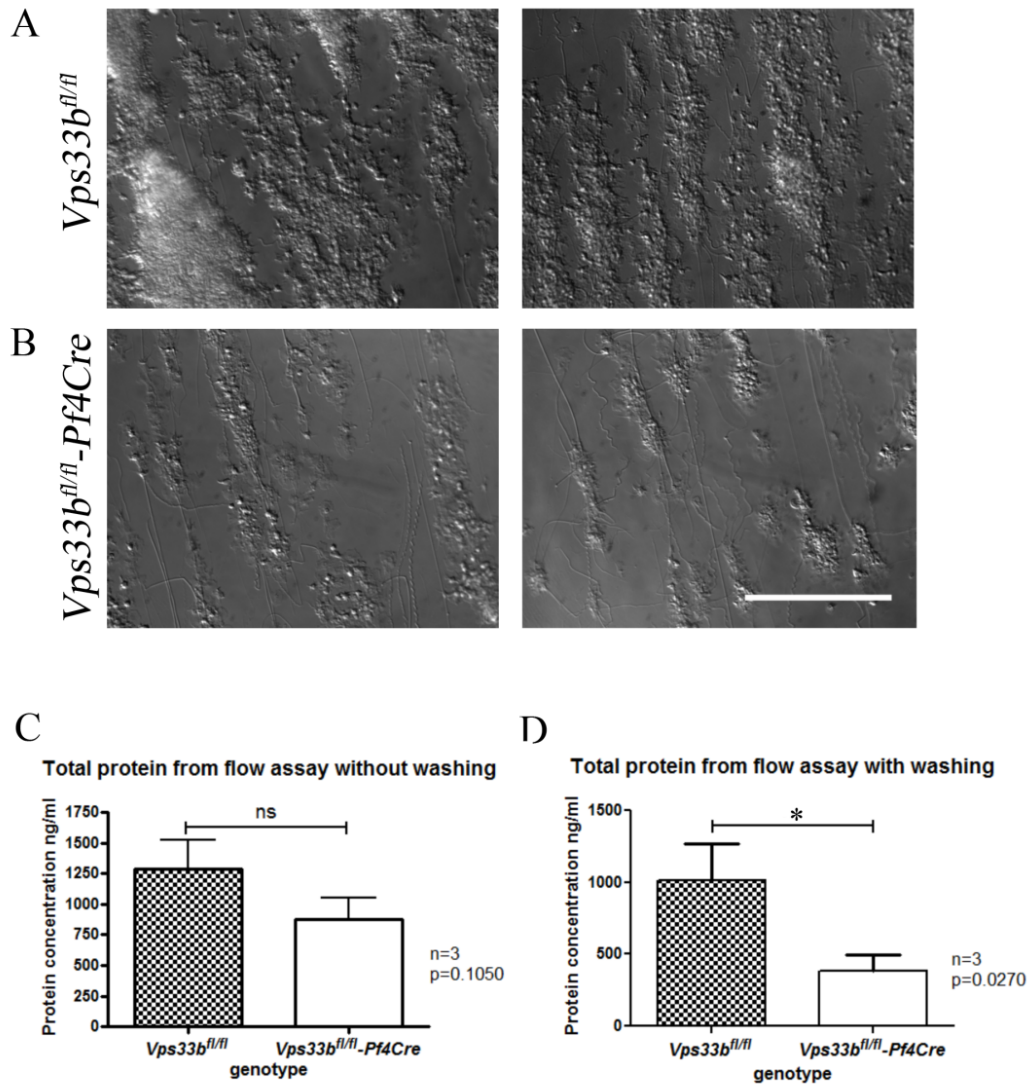
**Figure 6.5 Aggregation and dense granule secretion in response to thrombin and collagen**

(A-B) Traces showing aggregation in response to different concentrations of (A) thrombin or (B) collagen, n=3. No difference was observed.

(C) Graph showing ATP secretion in response to 0.3U/ml thrombin stimulation. ATP secretion from dense granules was monitored using Chronolume and measuring light emission. Data was analysed using a two-tailed Student t-test and the mean with standard error of mean error bars presented. No significant difference was observed, n=3.

### 6.3.6 Shear assay to assess thrombus formation under stress

Platelets are constantly exposed to shear forces due to the mechanical forces created by blood flow through the various blood vessels. It is therefore necessary to test platelet aggregation under shear conditions using an in vitro flow-based platelet aggregation assay in addition to the standard method of studying aggregation in a stirred platelet suspension. It is a more representative assay for the function of mouse platelets in vivo due to the mimicking of physiological conditions experienced by the platelets upon vascular injury. Two variations of the shear assay were carried out, one without washing and one with 5 minutes of washing upon termination of blood flow over the capillary. In this way, aggregate formation and aggregate stability could be assessed. There was a trend towards reduced aggregate formation in the *Vps33b<sup>fl/fl</sup>-Pf4Cre* mouse (figure 6.6C) assessed by total protein obtained from the flow assay capillary, however the difference was not significant. When the capillary was washed for 5 minutes following the flow assay, aggregates appeared to be unstable and washed off in the *Vps33b<sup>fl/fl</sup>-Pf4Cre* samples (figure 6.6B), when compared to control (figure 6.6A). This is supported by the significant reduction of total protein by approximately 62% in *Vps33b<sup>fl/fl</sup>-Pf4Cre* aggregates compared to control (figure 6.6D). These findings suggest that initial aggregate formation was not affected but that the aggregates formed were not stable, thus breaking down upon washing.



### Figure 6.6 In vitro shear assay images and protein quantification

A – Representative DIC images of *Vps33b<sup>fl/fl</sup>* control mouse platelet aggregations on collagen with 5 minutes wash, shear rate  $1000\text{s}^{-1}$ , 63x magnification, n=3

B – Representative DIC images of *Vps33b<sup>fl/fl</sup>-Pf4Cre* mouse platelet aggregations on collagen with 5 minutes wash, shear rate  $1000\text{s}^{-1}$ , 63x magnification, n=3, Scale bar = 50 $\mu\text{m}$ . Aggregates were much reduced in *Vps33b<sup>fl/fl</sup>-Pf4Cre* platelets after washing in comparison to *Vps33b<sup>fl/fl</sup>* control mouse platelets.

C – Protein quantification on lysates collected from the capillaries of shear aggregation studies on mouse platelets from A and B, n=3.

D - Protein quantification on lysates collected from the capillaries of shear aggregation studies without 5 minutes washing, n=3.

Data from C and D was analysed using a two-tailed Student t-test, and the mean with standard error of mean error bars are presented.

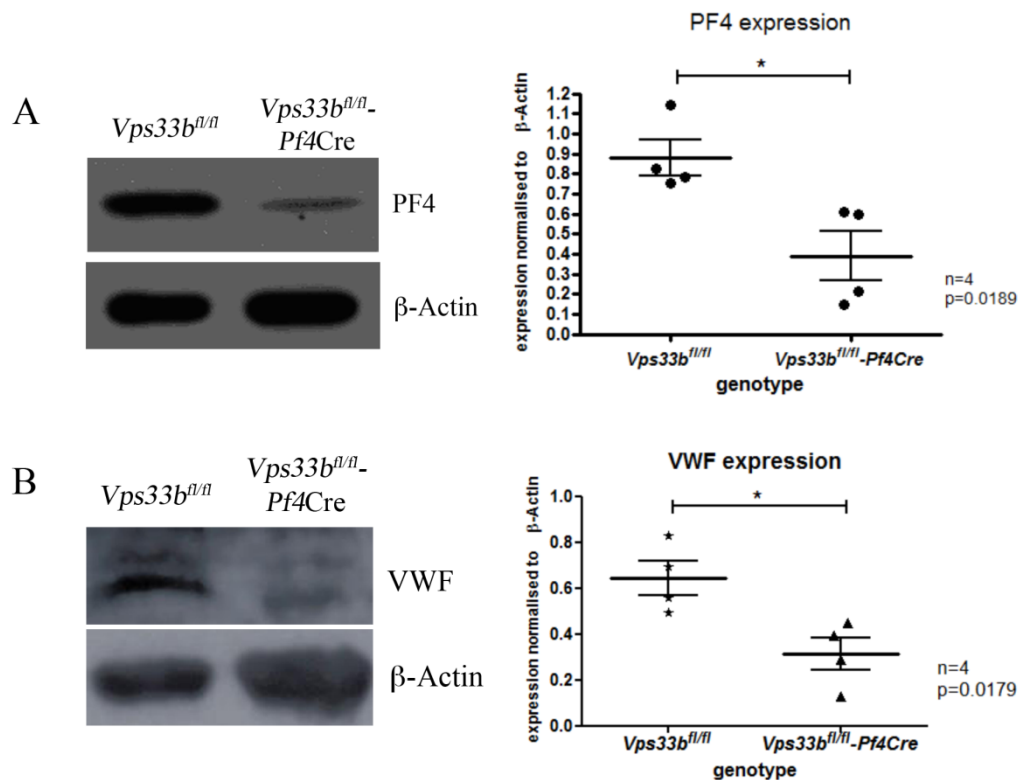
Flow assay carried out with Jocelyn Auger and Danai Bem



### 6.3.7 Immunoblotting for the presence of $\alpha$ -granule proteins

In order to determine if  $\alpha$ -granule contents within the platelet were altered the levels of  $\alpha$ -granule proteins PF4 and VWF were evaluated. Immunoblotting indicated that PF4 levels were reduced in *Vps33b<sup>fl/fl</sup> -Pf4Cre* mice (figure 6.7A). Densitometry revealed that there was a significant reduction of PF4 by approximately 56% compared to *Vps33b<sup>fl/fl</sup>* control levels.

VWF was also shown to be reduced by immunoblotting (figure 6.7B) in the *Vps33b<sup>fl/fl</sup>-Pf4Cre* mice, and densitometry revealed a significant reduction of approximately 51% in comparison to control platelets. These results demonstrate that *Pf4-cre* mediated *Vps33b* excision in the mouse megakaryocyte results in the reduction of PF4 and VWF,  $\alpha$ -granule proteins, in the mouse platelet.



**Figure 6.7 Immunoblotting and densitometry of  $\alpha$ -granule proteins.**

(A) Immunoblot for PF4 in platelets, rabbit anti-PF4 primary antibody (Accurate Chemical and Scientific Corp) at a concentration of 1:1000, and goat anti-rabbit HRP-conjugated secondary antibody (Invitrogen) at a concentration of 1:1000 was used. Loading was confirmed by immunoblotting for  $\beta$ -Actin, n=4.

(B) Immunoblot for VWF in platelets, rabbit anti-VWF primary antibody (Santa Cruz) at a concentration of 1:500, and goat anti-rabbit HRP-conjugated secondary antibody (Invitrogen) at a concentration of 1:500 was used. Loading was confirmed by immunoblotting for  $\beta$ -Actin, n=4.

Densitometry was carried out on immunoblots for PF4 and VWF and expression normalised to  $\beta$ -Actin. All data points are presented, the mean values represented as a bar and standard error of mean error bars plotted. Data was analysed using a two-tailed Student t-test.

## **6.4 Discussion**

### **6.4.1 Characterisation of the platelets from *Vps33b<sup>fl/fl</sup>*-*Pf4*Cre mouse**

The aim of this work was to develop a megakaryocyte and platelet-specific *Vps33b* conditional knockout mouse in the hope to create a model of ARC syndrome platelets. ARC platelets lack  $\alpha$ -granules, therefore characterisation of the *Vps33b<sup>fl/fl</sup>*-*Pf4*Cre platelets and more specifically the  $\alpha$ -granules was required.

Platelet count was unaffected in the *Vps33b<sup>fl/fl</sup>*-*Pf4*Cre mouse. Morphologically the platelets also did not have any gross abnormality, with a small increase of 4.4% in MPV and only a marginally reduced  $\alpha$ -granule count in comparison to control. The expression of P-selectin, an  $\alpha$ -granule membrane protein, on the plasma membrane was measured by flow cytometry. Levels were found to be reduced by approximately 44% compared to *Vps33b<sup>fl/fl</sup>* control. A reduction in P-selectin platelet surface expression by flow cytometry could be indicative of several different platelet defects: a reduced number of  $\alpha$ -granules, an  $\alpha$ -granule secretion defect, or a reduction in P-selectin protein levels within the platelet. These defects are not mutually exclusive and the reason for P-selectin level reduction could be a combination of these.

In vivo bleeding time test revealed that the mice did not suffer from a bleeding diathesis and aggregation experiments revealed no defect in aggregation or dense granule secretion when the platelets were stimulated with thrombin or collagen in stirred suspension. This suggests that fibrinogen is present within the platelet, as the platelets were washed twice for removal of all plasma proteins. Fibrinogen is required for platelets to aggregate in stirred suspension, as demonstrated by the use of fibrinogen-deficient mice (Suh et al. 1995) and in cases of afibrinogenemia (Xu et al. 2006).

The most notable defect in platelet function was revealed by an in vitro shear assay, the most physiologically relevant assay for platelet aggregation. Platelet aggregates formed; however, when washing was carried out the platelets were removed indicating that the aggregates formed were not stable. The reason for this instability may be due to reduced VWF within the  $\alpha$ -granules. The group of Dr Shaun Jackson have demonstrated in shear assay tests using von Willebrands disease platelets, that platelets lacking VWF are unable to support platelet tethering and translocation under shear conditions, with only 20% platelet tethering in comparison to control despite normal plasma VWF levels (Kulkarni et al. 2000). In addition thrombus formation was affected with only small thrombi formed when von Willebrands disease platelets were passed over a monolayer of control platelets (thrombus formation was restored to 50% with addition of purified VWF). This suggests that VWF contained within  $\alpha$ -granules is important for normal thrombus formation. As the *Vps33b<sup>fl/fl</sup>-Pf4Cre* mouse platelet VWF levels are reduced by approximately 51% they may not be able to as efficiently support platelet tethering, translocation and thrombus formation.

#### 6.4.2 Development of the mouse model - a good model for ARC platelets?

The aim of this work was to produce a mammalian ARC platelet model. Therefore a *Pf4*-Cre mouse was used in order to model the disease. It has been concluded that although the *Vps33b<sup>fl/fl</sup>*-*Pf4*Cre mouse had a mild  $\alpha$ -granule defect demonstrated by the shear assay, P-selectin expression and immunoblotting, it has not allowed generation of mice that are a model for ARC syndrome platelets. This may be due to the cre recombinase transgene selected, which is discussed in section 6.4.3.

ARC patients have a severe bleeding diathesis due to most platelets being devoid of platelet  $\alpha$ -granules. The *Vps33b<sup>fl/fl</sup>*-*Pf4*Cre mouse showed no such bleeding diathesis in bleeding time tests. Morphologically, *Vps33b<sup>fl/fl</sup>*-*Pf4*Cre mice do not resemble ARC platelets. ARC platelets are typically large and most platelets lack  $\alpha$ -granules (Lo et al. 2005). Compared to control platelets, there was only a marginal increase of 4.4% in mean platelet volume in *Vps33b<sup>fl/fl</sup>*-*Pf4*Cre platelets, and ultrastructural analysis revealed that  $\alpha$ -granules are present if at slightly reduced numbers. The  $\alpha$ -granule protein deficiency seen in ARC patients by immunoblotting indicates that PF4 and VWF are markedly reduced if not absent (Lo et al. 2005). In contrast, *Vps33b<sup>fl/fl</sup>*-*Pf4*Cre platelets showed reductions of approximately 56% and 51% in PF4 and VWF respectively, indicating only a partial defect.

#### 6.4.3 Why a mild phenotype in *Vps33b<sup>fl/fl</sup>*-*Pf4*Cre platelets?

Recently it has been identified that  $\alpha$ -granules are heterogeneous and that platelets contain different subsets of these granules, a controversial topic in the field of platelets.  $\alpha$ -granules have been found to contain VEGF, a pro-angiogenic molecule, and endostatin, an anti-

angiogenic molecule (Italiano et al. 2008). It was shown that they appear to be in different  $\alpha$ -granules and the secretion of these granules is different depending on the agonist used. One hypothesis for the partial  $\alpha$ -granule defect observed may be that in mice that only one subset of  $\alpha$ -granules is affected by removal of Vps33b.

A more likely explanation for a partial defect may be the nature of the *Pf4*-Cre recombinase transgene. When testing the efficiency of Cre-mediated excision, Tiedt et al found that the *Pf4*-Cre x *integrin  $\beta 1^{fl/fl}$*  mice still had reduced but detectable levels of integrin  $\beta 1$  (Tiedt et al. 2007). As Vps33b likely plays a role in  $\alpha$ -granule synthesis in megakaryocytes, it may be that there is sufficient Vps33b produced in *Vps33b<sup>fl/fl</sup>* *Pf4*-Cre megakaryocytes for the formation of  $\alpha$ -granules before the *pf4* promoter is activated and the Cre recombinase can carry out its function. Work has now begun on using an inducible cre, CreER<sup>T2</sup> to remove Vps33b at an earlier timepoint in megakaryocyte development.

## **CHAPTER 7 – DISCUSSION**

### **7.1 Development of an ARC-LOVD database provides a central resource for researchers and clinicians**

An ARC-LOVD database has been developed to provide a central resource for ARC, allowing easy access to a central log of updated information, and to provide the opportunity to share data. It is the hope that as data is added, opportunities for epidemiological investigations and meta-analysis will increase. The identification of a range of phenotypic severity in ARC underlines the importance of such a database to help accurately advise patient families on prognosis. In addition, advances in knowledge of ARC pathogenesis and clinical course may lead to novel therapies and improved management of patients with ARC.

### **7.2 Mutation analysis in *VPS33B* and *VIPAR* identifies a genotype-phenotype correlation**

For the first time patients with attenuated ARC phenotype have been identified and characterised as compound heterozygotes. Patients with attenuated phenotype have a common splice site mutation, *VPS33B*(c.1225+5G>C) which results in truncated VPS33B. VPS33B and VIPAR have previously been shown to interact (Cullinane et al. 2010), and this work demonstrates that in severe ARC syndrome mutations this interaction is disrupted, suggesting that VPS33B-VIPAR interaction is necessary for correct cellular functioning. VPS33B and VIPAR have been shown to co-localise with RAB11A positive endosomes (Cullinane et al. 2010). In keeping with this finding, ultrastructural analysis confirmed that VPS33B and VIPAR co-localised on endosome-associated tubular-vesicular membranes also positive for transferrin receptor. It was noted that the attenuated *VPS33B*(c.1225+5G>C) and VIPAR remain able to interact but form cytoplasmic aggregates and no longer associate with membranes. It suggests that VPS33B-VIPAR interaction is necessary but not sufficient for its



correct cellular functioning, and that correct cellular localisation of the complex is also required.

The yeast HOPS and CORVET subunit composition is well defined (Seals et al. 2000b)(Peplowska et al. 2007) and the organisation of these subunits have recently been a topic of great interest. Work by Ostrowicz et al. and Plemel et al. have led to models of HOPS subunit organisation (Ostrowicz et al. 2010)(Plemel et al. 2011), with Vps18 and Vps11 central to the interactions of the remaining subunits, and Vps33 interacting with these proteins via Vps16. At present the metazoan HOPS complex composition and structure is unclear. Zhu et al 2009 reported that Spe-39 (VIPAR homologue) in *C. elegans* interacted with both Vps33a and Vps33b (Zhu et al. 2009). Cullinane et al. and Pulipparacharuvil et al. found that Vipar interacted with Vps33b but not Vps33a in HEK293 cells and *Drosophila* respectively (Pulipparacharuvil et al. 2005)(Cullinane et al. 2010). Work in this thesis is insufficient to determine the likely composition of the metazoan HOPS complex, however, results suggest that VIPAR may interact with VPS18 only in the absence of VPS33B. This suggests that the VPS33B-VIPAR complex is unlikely to be involved in direct HOPS interaction in a wild-type situation.

It has been shown that patient mutations disrupt the interaction between VPS33B and VIPAR. However, it is not known how these two proteins interact. Future experiments should include the cloning of truncated VPS33B and VIPAR constructs. Co-transfection and subsequent co-immunoprecipitation experiments with these constructs will help map the regions required for their interaction. Additionally, producing purified VPS33B and VIPAR in complex, crystallisation of these proteins could help identify how the proteins interact, and may allow more accurate prediction of how patient mutations would disrupt the structure. The recombinant proteins could be used for pull-down experiments to identify possible interacting

partners by mass spectrometry. This approach would help to identify the downstream pathways affected in ARC syndrome for further investigation.

### **7.3 Vps33b and its homologue, Vps33a, are necessary for murine development**

Vps33a metazoan models have reported varying effects on development. In *Drosophila*, *carnation* is lethal at second instar stage (Sevrioukov et al. 1999). In contrast, the *buff* mouse with missense mutation in Vps33a, appear to develop normally and live to adulthood (Suzuki et al. 2003). In concordance with the findings in *Drosophila*, it has been determined that Vps33a is also required for murine development, and that a Vps33a deficiency results in embryonic lethality between E7.5 and E8.5. This highlights the importance of Vps33a in development and may help to explain why no mutations in human VPS33A have been discovered.

In contrast to Vps33a, no Vps33b model organisms previously reported have displayed a lethal phenotype during development (Matthews et al. 2005)(Zhu et al. 2009)(Akbar et al. 2011). By use of the ubiquitous *Pgk*-Cre recombinase it is shown that Vps33b is also required for murine development, and is also lethal at approximately E7.5-E8.5. Interestingly, the survival of ARC patients contradicts this finding. It suggests that humans are able to bypass lethality by a method that may only be postulated, for example by expressing alternative transcripts of *VPS33B*. It may also be that VPS33A in humans can compensate for the absence of VPS33B during human development.

At E7.5-E8.5 many important processes occur in murine development. In order to understand how Vps33a and Vps33b contribute to these processes full morphological analysis of embryos should be undertaken. Embryonic stem cells isolated from blastocysts of these mice could be

used to investigate pathways affected by Vps33a or Vps33b disruption, such as the trafficking of receptors required for signal transduction during development.

#### **7.4 Use of *Alfp*-Cre for removal of Vps33b from murine liver results in a suitable ARC phenocopy**

Intrahepatic cholestatic jaundice is a cardinal feature of ARC syndrome (Gissen et al. 2006). The molecular mechanism resulting in intrahepatic cholestasis is currently unknown. In this thesis, two liver specific Vps33b conditional knockout mice were developed using different Cre-recombinase transgenes in order to model the ARC liver. The mice with *Alb*-Cre recombinase transgene presented a more variable phenotype than those with the *Alfp*-Cre recombinase transgene, highlighting the importance of Cre-recombinase selection when considering the development of a disease model. The *Vps33b<sup>fl/fl</sup>*-*Alfp*Cre mice present with a good ARC phenocopy with the apical proteins CEA and BSEP being mislocalised, as seen in ARC livers (Gissen et al. 2004)(Cullinane et al. 2010). Additionally the bile acid taurocholate is increased in the mouse, indicative of a defect in bile acid secretion.

Morphological presentation of livers varies between ARC patients, as demonstrated by the original assumption that there were two different syndromes (Lutz-Richner & Landolt 1973)(Nezelof et al. 1979). Bile duct paucity is observed in patients and Zebrafish models (Matthews et al. 2005)(Gissen et al. 2006). In contrast in the *Vps33b<sup>fl/fl</sup>*-*Alfp*Cre mouse the reduced number of bile ducts was not detected so far. It has been suggested that bile duct formation is dependent on hepatocyte polarisation and correct apical trafficking of ABC transporters (Sakaguchi et al. 2008)(Wakabayashi et al. 2004). In mice it has been demonstrated that there is a compensatory mechanism for bile acid production when BSEP is absent (Wang et al. 2001), and may explain why the *Vps33b<sup>fl/fl</sup>*-*Alfp*Cre does not show bile

duct paucity. Future experiments should include a supplemented diet cholic acid which I expect will induce a more severe phenotype. By feeding *Vps33b<sup>fl/fl</sup>-AlfpCre* mice a cholic acid diet, histological observations made in ARC patients' livers such as giant cell transformation may be induced, in a response to increased conjugated hyperbilirubinaemia. Histological observations may be made with a wider variety of stains, a trichrome stain for example would indicate if there was fibrosis by inappropriate deposition of collagen. In addition, extraction and primary culture of hepatocytes from the liver of these mice using sandwich culture could therefore be used as a tool to investigate pathways affecting the trafficking in these cells by live cell imaging.

### **7.5 A megakaryocyte and platelet specific Vps33b conditional knockout mouse results in a mild $\alpha$ -granule defect**

ARC platelets are large and agranular, and have been reported to be absent of  $\alpha$ -granules (Lo et al. 2005). In contrast a mild  $\alpha$ -granule defect, characterised by present  $\alpha$ -granules at only a slightly reduced level, but reduced P-selectin levels (44%) by flow cytometry, reduced aggregate stability and reduced  $\alpha$ -granule protein content (56% reduction of PF4 and 51% reduction of VWF) was identified in *Vps33b<sup>fl/fl</sup>-Pf4cre* mice. VWF deficiency and aggregate instability in the *Vps33b<sup>fl/fl</sup>-Pf4Cre* is consistent with the proposal that VWF stored within the platelet is necessary for stable aggregate formation under shear conditions (Kulkarni et al. 2000). This may help to explain why ARC patients have a bleeding diathesis.

A mild phenotype in the *Vps33b<sup>fl/fl</sup>-Pf4Cre* mice may be explained by the nature of the Cre-recombinase transgene. Tiedtl et al. found detectable levels of their targeted protein, albeit at clearly reduced levels in cultured megakaryocytes. The suggestion was that it reflected a long half-life of their protein in megakaryocytes (Tiedt et al. 2007). This implies that although the

Cre-recombinase effectively reduces protein levels, excision may not occur early enough in the megakaryocyte to prevent the targeted protein from being produced. In the case of Vps33b, low levels of the protein may be sufficient for  $\alpha$ -granule formation.

## **7.6 Future Experiments**

The work presented provides many tools for the study of ARC syndrome and the proteins VPS33B and VIPAR. In addition to the further experiments discussed in sections 7.2-7.4, future experiments may include:

- Development of an inducible Vps33b ubiquitous knockout mouse. This would allow the induction of Vps33b after E9.5 to circumvent embryonic lethality, and allow all cell types to be targeted. As a result a more complete mouse model of ARC syndrome may be obtained for study of Vps33b deficiency in all organs, gene therapy and drug treatment trials.
- Platelet experiments should be repeated with the inducible Vps33b ubiquitous knockout mouse. Megakaryocyte precursors would express the Cre-recombinase allowing removal of Vps33b before the maturation to megakaryocytes. As a result a more accurate ARC platelet phenocopy may be observed due to the complete absence of Vps33b from megakaryocytes.

## **7.7 Final thoughts**

Defining the roles of VPS33B and VIPAR is a complex undertaking. These proteins have wide reaching functions demonstrated by the severe phenotype and multiple systems involved in ARC syndrome. By identifying and modelling patient mutations, the requirement for VPS33B-VIPAR complex formation in correct cellular functioning has been established. By

developing mammalian models the requirement of Vps33b in murine embryonic development has been identified. This knowledge has allowed subsequent progression to tissue specific and temporal Vps33b removal in the mouse providing ARC models for development of gene therapy and drug treatments in the future with the aim to eventually aid progression to clinical trials.

# **APPENDICES**

## **APPENDIX 1**

### **Primer pairs for *VPS33B* sequencing**

<i>Exon</i>	<b>Forward primer</b>	<b>Reverse primer</b>	<i>Product Size</i>
1	CCTTCTCAGAACGAAGGGC	GGAAGAAATGTGCATCCAATG	215
2	CTGCGGAAGCTCATGTGAC	TTGTTTCATCAAAAGAAAACTGC	196
3	TCTTCGTGTCACACTTTGTGC	AGATGAAAGGCAGACGTGC	202
4	GAGACCTGTAGGGCAAATGG	AGGGTCCTTATGGCCAAGG	237
5	GCAGCTTCCCTGTTTCTAGC	CCGGTCCTCAGTCCTGTTC	190
6	TTGTCTTTCACCTGGGTTTCGG	CCAGGAAAAGAAGGAGCTGG	276
7	TTCCCTCTTAACGTGGAGC	TGGTATTTCTAGCCCTCTGC	254
8	CTAGGGCTAGCCACTTTCC	CAGGGAAAACAGCGTCTGC	225
9	GGAAGTATCACGTGGAAAGG	TAGGGCTGAAAGATGACAGG	228
10	AAGCTGCCCTTGACATGC	GTCCATCTTGCCAAGATGC	189
11	GTAGGAGAAGTCCTCATTGG	CCCACAGCCTGGTATAAGC	187
12	GAACACCTGAGTACCCTTCC	CTGAGGCAACAAAACAGAGG	217
13	TGGTTTCTCGTGTCTGAGG	GGAGTAATGGTCCTCTGGA	540
14	AGAACCAGGAGTATGTCAGC	TAGAAGCGTGGGCAGTAGC	156
15-16	CCTGTTAGCATAGATGGCAGC	TCACTTCTTCTGTCCCTAAGGC	378
17	GTTTCGTTGCTGGTTGATCTG	TGCCCAATAACTGCCCTC	187
18	TGACAGTACTAGATGCTCTTTGGAC	ATGCTGCGTGTTGAGAGAAG	256
19	CTGTCGTGTCCTGAATGGTG	CTCCACAATGGAATGAACCC	212
20	TTTAAAGGGTTAGGGAGCTGAG	AAACATTGAGACACGCCAGG	239
21	TGCTGTGCCCTTCCTTTCC	AGGATCAGACCAGATTCAGC	246
22	CCCTTCCTTTCCCTAAGCCTG	GCCCAGCTGACACTTTGTTAC	427
23	TGGAGAGGCTCTATGGGTTG	TGCATCTCACTGAGGAATGTG	211
cDNA 1	CGGCCTTCTCAGAACGAA	AGCCAATTTGTCAGCATTGA	409
cDNA 2	GACCCCGCATCAAGAATATG	GGAGCAAAGTGCTGTCACAA	489
cDNA 3	GAAGGCCAGAGATTGGACAT	TTCTCAATGTAGCTGGTGCT	494
cDNA 4	GCAGGATTTCCAGGAGCTAA	CTTGGCCAGAGAACTGAAGG	370
cDNA 5	TCACAGCCGTGGAGAGTAAA	TGCTGTGTCGTCAGGAAAATGA	449
cDNA 6	GCCTCATCTTGGTGGTGTTC	AAAGTTGGAAGTGCGTGTCC	495



### Primer Pairs for *VIPAR* sequencing

<i>Exon</i>	Forward primer	Reverse primer
1	CCAGAAAGGGGCAATGTATG	GCCTAGTTACCCAGAATGCAA
2	GAGCACCTTAGCCTTGTGTC	TCTATCCCTGCCTAGGGACTC
3	TGTCAAGGCTTTATTGTGCTAT	GGACTTCCTATCCATTTAAG
4	CTTTAACCAAGCCTGGATGG	GTCCCCATAACTCCCCAGAC
5	GGAAGGAATGACAAGCAGGA	GGAAAATCAAGCCAGGTAACA
6	GGAGCGGGTATGCTGATAAA	TTCCCTGTGTGAACAAGCTG
7	TCCAGCAACAACAAAGGAATAAAGAA	TGATTGGATTTTCAGAAACTAGTGA
8	GGCATGACTCTGTGTTGGAA	CGCCCTCAGAGAGTGATTT
9	GGGAGACCAATTCACACTTG	TCCCTCAGAGTGCTTTGAAAC
10	GGCACTCGATTTTGTGAGGT	TGCCCAGCCTAGATTTCTGT
11	GCATGGGAAGTTCAGTTAATCA	CTTCCTGCCTATCCATTCCA
12	ATGCTGGCGATTGTTTAG	CCACGTGCAGAGCATAGAAA
13	TTTTCTCCTGCCTCTACTCCA	TTGTGCAATGAGAGTTTGTGG
14	AGAGCTTGGGTGGTACTTGG	CCCAAACCTCATTCTTTCCAA
15	TTAAGCACCCCCATTGATGT	AACCCTTCTGTCTCCCAAGG
16	GTTGAGTGTGCCTGGCCTA	GGGAAAACAAGAGCAGATCG
17	TGTGCCTTATGGGTGTTTGA	ACGGAGGACTCCCATTCTT
18	TGGGCAAAAAGAACCCTGTA	CTGTCTCCTGAGCCTGCTG
19	TGAGCCTTGTTTGTTGCAT	TTTCACAGGCAGGAGAGGAG
cDNA 1	CGCTGTCCTGAGAGGGAG	CAGGAAGATACAGGTGAGGCTT
cDNA 2	GGTAGATCCATGGCTTCCTG	ATACTTCCCACAGGTTCCCC
cDNA 3	TCGTGGATGATGATGACGAT	AGCTTTTGGCAGGTGTGTCT
cDNA 4	CCTACTCCCTGAGCAGCTTTT	AACTGCAGTAATGACGTTTCCA
cDNA 5	CCGCTCCTTACAGGACAAAC	AATGGCAAACCAACACAGGT
cDNA 6	ATTCAGGACCCTGACAAACG	TCTACATCATTCCAGGCTCG
cDNA 7	CCTGAAGAAGACATTTAAGATCCC	ATTCTTCCATCGAATTTGCG
cDNA 8	TTGATACCTACCGGGACCTG	TGTCAAGAGTAGCTGGCACTG

### Primers for genotyping of mice

Gene/ transgene	Forward	Reverse	Size
<i>Vps33b</i>	CCAACTGAATTGCTTGCTCAG	GTGTGACTCAGTGATACAGC	Wild-type ~350bp Floxed ~450bp
<i>Vps33b</i> excised allele	CCAACTGAATTGCTTGCTCAG	GTCCTGGTTTGATCTCCTGC	Cre + ~1000bp
<i>Vps33a</i>	TCCTGCTCTTCCAGAG	Ex 6R- GCATATGAGTGCAGTGACCAA Genetrap R- TCTAGGACAAGAGGGCGAGA	Wild-type ~200bp Genetrap ~300bp
<i>Pgk-Cre</i>	F COMM- TCGTTGCATCGACCGGTAAT PGK F-GCGCATCCTCTTCCTC	GACCAATGAAACGTGGGCG	Wild-type ~600bp Cre + ~100bp
<i>Alb-Cre</i>	GTAGTTATTCGGATCATCAGCTA CAC	GCTGCCACGACCAAGTGACAGCA ATG	Cre + ~400bp
<i>Alfp-Cre</i>	CCCGCAGAACCTGAAGATGTT	CCTGATCCTGGCAATTTCGGC	Cre + ~200bp
<i>Pf4-Cre</i>	CCCATACAGCACACCTTTTG	TGCACAGTCAGCAGGTT	Cre + ~400bp

### Antibodies and dilutions used for immunoblotting

Antibody	Supplier	Primary Dilution	Secondary Dilution
<b>Primary</b>			
Rabbit $\alpha$ -VPS33B	Protein Tech	1/500	1/500
Mouse $\alpha$ - $\beta$ -actin	Sigma	1/15000	1/20000
Rabbit $\alpha$ -PF4	Accurate chemical and scientific group	1/1000	1/1000
Rabbit $\alpha$ -VWF	Santa Cruz	1/500	1/500
<b>Secondary</b>			
HRP-conjugated goat $\alpha$ -rabbit	Dako		
HRP-conjugated rabbit $\alpha$ -mouse	Dako		

### Antibodies and dilutions used for immunofluorescence microscopy




Antibody	Supplier	Primary Dilution	Secondary Dilution
<b>Primary</b>			
mouse $\alpha$ -myc 9E10	Sigma	1/200	1/200
Chicken $\alpha$ -BSEP	Gift	1/300	1/200
<b>Secondary</b>			
Goat $\alpha$ -chicken Alexa 488	Invitrogen		
Goat $\alpha$ -mouse Alexa 633	Invitrogen		

### antibodies and dilutions used for immunohistochemistry

Antibody	Supplier	Primary Dilution	Secondary Dilution
<b>Primary</b>			
Rabbit $\alpha$ -CEA	Dako	1/100	1/100
Mouse $\alpha$ -E-cadherin	BD Transduction Laboratories	1/100	1/100
Mouse $\alpha$ -ZO-1	Invitrogen	1/100	1/100
Chicken $\alpha$ -BSEP	Gift	1/300	1/100
<b>Secondary</b>			
Biotinylated goat $\alpha$ - chicken	Vector Labs		
Biotinylated goat $\alpha$ - mouse	Vector Labs		
Biotinylated goat $\alpha$ - rabbit	Vector labs		


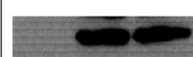
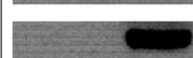
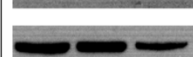
## APPENDIX 2

A

	IP: m $\alpha$ HA				
HA-Empty	+	+	+	+	
HA-VIPAR					+
myc-VPS11	+				+
myc-VPS18		+			
myc-VPS39			+		
myc-VPS41				+	
IP:					
WB: m $\alpha$ myc					
Input					
WB: m $\alpha$ HA					
Input					
WB: m $\alpha$ myc					

B

HA-Empty	+		
HA-VIPAR		+	+
YFP-Empty	+	+	
YFP-VPS33B			+
Myc-VPS18	+	+	+

IP: m $\alpha$ HA	
WB: m $\alpha$ myc	
Input	
WB: m $\alpha$ HA	
Input	
WB: Rb $\alpha$ VPS33B	
Input	
WB: m $\alpha$ myc	

### Supplementary figure 1. Co-immunoprecipitation of VIPAR with HOPS complex proteins.

(A) HEK293 cells were co-transfected with HA-empty or HA-VIPAR and myc tagged VPS11, VPS18, VPS39 or VPS41. Co-immunoprecipitation experiments revealed interaction between over-expressed VIPAR and HOPS complex proteins. More VPS18 than VPS11, VPS39 and VPS41 was pulled down. Although these proteins were present in the lysates, none were pulled down together with HA-empty.

(B) HEK293 cells were co-transfected with HA-empty or HA-VIPAR, YFP-empty or YFP-VPS33B and myc-VPS18. A co-immunoprecipitation experiment showed that VIPAR and VPS18 interacted when the over-expressed VPS33B was absent. In presence of over-expressed VPS33B substantially less VPS18 was pulled down.

Work done by Andrew Cullinane

## REFERENCES

- Abu-Sa'da, O. et al., 2005. Arthrogryposis, renal tubular acidosis and cholestasis (ARC) syndrome: two new cases and review. *Clinical Dysmorphology*, 14(4), pp.191–196.
- Akbar, M A, Ray, S. & Krämer, H., 2009. The SM protein Car/Vps33A regulates SNARE-mediated trafficking to lysosomes and lysosome-related organelles. *Molecular Biology of the Cell*, 20(6), pp.1705–1714.
- Akbar, Mohammed Ali et al., 2011. The full-of-bacteria gene is required for phagosome maturation during immune defense in *Drosophila*. *The Journal of Cell Biology*, 192(3), pp.383–390.
- Aktories, K. & Barbieri, J.T., 2005. Bacterial cytotoxins: targeting eukaryotic switches. *Nature Reviews. Microbiology*, 3(5), pp.397–410.
- Albers, C.A. et al., 2011. Exome sequencing identifies NBEAL2 as the causative gene for gray platelet syndrome. *Nature Genetics*, 43(8), pp.735–737.
- Angers, C.G. & Merz, A.J., 2009. HOPS interacts with Apl5 at the vacuole membrane and is required for consumption of AP-3 transport vesicles. *Molecular Biology of the Cell*, 20(21), pp.4563–4574.
- Anitua, E. et al., 2004. Autologous platelets as a source of proteins for healing and tissue regeneration. *Thrombosis and Haemostasis*, 91(1), pp.4–15.
- Arias, I. et al. eds., 2009. *The Liver: Biology and Pathobiology* 5th ed., Wiley-Blackwell.
- Au, J. et al., 2007. Myosin VI is required for sorting of AP-1B-dependent cargo to the basolateral domain in polarized MDCK cells. *The Journal of Cell Biology*, 177(1), pp.103–114.
- Axelrod, J.D., 2009. Progress and challenges in understanding planar cell polarity signaling. *Seminars in Cell & Developmental Biology*, 20(8), pp.964–971.
- Bach, H. et al., 2008. Mycobacterium tuberculosis virulence is mediated by PtpA dephosphorylation of human vacuolar protein sorting 33B. *Cell Host & Microbe*, 3(5), pp.316–322.
- Barbosa, M.D. et al., 1996. Identification of the homologous beige and Chediak-Higashi syndrome genes. *Nature*, 382(6588), pp.262–265.
- Barr, F.A. & Short, B., 2003. Golgins in the structure and dynamics of the Golgi apparatus. *Current Opinion in Cell Biology*, 15(4), pp.405–413.
- Baum, B. & Georgiou, M., 2011. Dynamics of adherens junctions in epithelial establishment, maintenance, and remodeling. *The Journal of Cell Biology*, 192(6), pp.907–917.
- Beck, J.A. et al., 2000. Genealogies of mouse inbred strains. *Nature Genetics*, 24(1), pp.23–25.

- Behnia, R. & Munro, S., 2005. Organelle identity and the signposts for membrane traffic. *Nature*, 438(7068), pp.597–604.
- Bock, J.B. et al., 2001. A genomic perspective on membrane compartment organization. *Nature*, 409(6822), pp.839–841.
- Bockamp, E. et al., 2002. Of mice and models: improved animal models for biomedical research. *Physiological Genomics*, 11(3), pp.115–132.
- van den Bogaart, G. et al., 2010. One SNARE complex is sufficient for membrane fusion. *Nature Structural & Molecular Biology*, 17(3), pp.358–364.
- Bolton-Maggs, P.H.B. et al., 2006. A review of inherited platelet disorders with guidelines for their management on behalf of the UKHCDO. *British Journal of Haematology*, 135(5), pp.603–633.
- Bonilha, V.L. et al., 1997. Apical sorting of influenza hemagglutinin by transcytosis in retinal pigment epithelium. *Journal of Cell Science*, 110 ( Pt 15), pp.1717–1727.
- Boyer, J.L., 1980. New concepts of mechanisms of hepatocyte bile formation. *Physiological Reviews*, 60(2), pp.303–326.
- Briggs, M.W. & Sacks, D.B., 2003. IQGAP proteins are integral components of cytoskeletal regulation. *EMBO Reports*, 4(6), pp.571–574.
- Brône, B. & Eggermont, J., 2005. PDZ proteins retain and regulate membrane transporters in polarized epithelial cell membranes. *American Journal of Physiology. Cell Physiology*, 288(1), pp.C20–29.
- Bull, L.N. et al., 1997. Genetic and morphological findings in progressive familial intrahepatic cholestasis (Byler disease [PFIC-1] and Byler syndrome): evidence for heterogeneity. *Hepatology (Baltimore, Md.)*, 26(1), pp.155–164.
- Burkhard, P., Stetefeld, J. & Strelkov, S.V., 2001. Coiled coils: a highly versatile protein folding motif. *Trends in Cell Biology*, 11(2), pp.82–88.
- Cagle, P.T., 2010. *Molecular Pathology of Liver Diseases* 1st ed. S. P. S. Monga, ed., Springer.
- Capaldo, C.T. & Macara, I.G., 2007. Depletion of E-cadherin disrupts establishment but not maintenance of cell junctions in Madin-Darby canine kidney epithelial cells. *Molecular Biology of the Cell*, 18(1), pp.189–200.
- Carim, L. et al., 2000. Cloning, mapping and expression analysis of VPS33B, the human orthologue of rat Vps33b. *Cytogenetics and Cell Genetics*, 89(1-2), pp.92–95.
- Carlton, V., Pawlikowska, L. & Bull, L., 2004. Molecular basis of intrahepatic cholestasis. *Annual Review of Medicine*, (36), pp.606–617.



- Carlton, V.E.H. et al., 2003. Complex inheritance of familial hypercholanemia with associated mutations in TJP2 and BAAT. *Nature Genetics*, 34(1), pp.91–96.
- Carmosino, M. et al., 2010. Polarized traffic towards the cell surface: how to find the route. *Biology of the Cell / Under the Auspices of the European Cell Biology Organization*, 102(2), pp.75–91.
- Caro, L. & Palade, G., 1964. Protein synthesis, storage, and discharge in the pancreatic exocrine cell. *The Journal of Cell Biology*, 20, pp.473–495.
- Carroll, K.S. et al., 2001. Role of Rab9 GTPase in facilitating receptor recruitment by TIP47. *Science (New York, N.Y.)*, 292(5520), pp.1373–1376.
- Casanova, J.E. et al., 1999. Association of Rab25 and Rab11a with the apical recycling system of polarized Madin-Darby canine kidney cells. *Molecular Biology of the Cell*, 10(1), pp.47–61.
- Casanova, J.E., Apodaca, G. & Mostov, K.E., 1991. An autonomous signal for basolateral sorting in the cytoplasmic domain of the polymeric immunoglobulin receptor. *Cell*, 66(1), pp.65–75.
- Cascorbi, I., 2011. P-glycoprotein: tissue distribution, substrates, and functional consequences of genetic variations. *Handbook of Experimental Pharmacology*, (201), pp.261–283.
- Chan, W. et al., 2005. Myosin II regulatory light chain is required for trafficking of bile salt export protein to the apical membrane in Madin-Darby canine kidney cells. *The Journal of Biological Chemistry*, 280(25), pp.23741–23747.
- Chintala, S. et al., 2009. The Vps33a gene regulates behavior and cerebellar Purkinje cell number. *Brain Research*, 1266, pp.18–28.
- Chinwalla, A.T. et al., 2002. Initial sequencing and comparative analysis of the mouse genome. *Nature*, 420(6915), pp.520–562.
- Ciferri, S. et al., 2000. Platelets release their lysosomal content in vivo in humans upon activation. *Thrombosis and Haemostasis*, 83(1), pp.157–164.
- Coico, R. & Sunshine, G., 2009. *Immunology: a short course*, Wiley-Blackwell.
- Collins, F.S., Rossant, J. & Wurst, W., 2007. A mouse for all reasons. *Cell*, 128(1), pp.9–13.
- Coppinger, J.A. et al., 2004. Characterization of the proteins released from activated platelets leads to localization of novel platelet proteins in human atherosclerotic lesions. *Blood*, 103(6), pp.2096–2104.
- Cramer, E M et al., 1985. Gray platelet syndrome: immunoelectron microscopic localization of fibrinogen and von Willebrand factor in platelets and megakaryocytes. *Blood*, 66(6), pp.1309–1316.

- Cullinane, A.R. et al., 2011. A BLOC-1 Mutation Screen Reveals that PLDN Is Mutated in Hermansky-Pudlak Syndrome Type 9. *The American Journal of Human Genetics*, 88(6), pp.778–787.
- Cullinane, A.R. et al., 2009. Molecular investigations to improve diagnostic accuracy in patients with ARC syndrome. *Human Mutation*, 30(2), pp.E330–337.
- Cullinane, A.R. et al., 2010. Mutations in VIPAR cause an arthrogryposis, renal dysfunction and cholestasis syndrome phenotype with defects in epithelial polarization. *Nature Genetics*, 42(4), pp.303–312.
- Davit-Spraul, A. et al., 2009. Progressive familial intrahepatic cholestasis. *Orphanet Journal of Rare Diseases*, 4, p.1.
- Deal, J.E., Barratt, T.M. & Dillon, M.J., 1990. Fanconi syndrome, ichthyosis, dysmorphism, jaundice and diarrhoea ? a new syndrome. *Pediatric Nephrology*, 4, pp.308–313.
- Dell'Angelica, E C et al., 1999. Altered trafficking of lysosomal proteins in Hermansky-Pudlak syndrome due to mutations in the beta 3A subunit of the AP-3 adaptor. *Molecular Cell*, 3(1), pp.11–21.
- Dulubova, I. et al., 2003. Convergence and divergence in the mechanism of SNARE binding by Sec1/Munc18-like proteins. *Proceedings of the National Academy of Sciences*, 100(1), pp.32–37.
- Dulubova, I. et al., 2007. Munc18-1 binds directly to the neuronal SNARE complex. *Proceedings of the National Academy of Sciences of the United States of America*, 104(8), pp.2697–2702.
- Durrbach, A. et al., 2000. Truncated brush border myosin I affects membrane traffic in polarized epithelial cells. *Traffic (Copenhagen, Denmark)*, 1(5), pp.411–424.
- Eastham, K.M. et al., 2001. ARC syndrome: an expanding range of phenotypes. *Archives of Disease in Childhood*, 85(5), pp.415–420.
- Elferink, O.R.P. & Beuers, U., 2011. Targeting the ABCB4 gene to control cholesterol homeostasis. *Expert Opinion on Therapeutic Targets*, 15(10), pp.1173–1182.
- Etienne-Manneville, S., 2008. Polarity proteins in migration and invasion. *Oncogene*, 27(55), pp.6970–6980.
- Falcón-Pérez, J.M. et al., 2002. BLOC-1, a novel complex containing the pallidin and muted proteins involved in the biogenesis of melanosomes and platelet-dense granules. *The Journal of Biological Chemistry*, 277(31), pp.28191–28199.
- Falik-Zaccai, T.C. et al., 2001. A new genetic isolate of gray platelet syndrome (GPS): clinical, cellular, and hematologic characteristics. *Molecular Genetics and Metabolism*, 74(3), pp.303–313.

- Felici, A. et al., 2003. TLP, a novel modulator of TGF-beta signaling, has opposite effects on Smad2- and Smad3-dependent signaling. *The EMBO Journal*, 22(17), pp.4465–4477.
- Ferguson, M.A. & Williams, A.F., 1988. Cell-surface anchoring of proteins via glycosyl-phosphatidylinositol structures. *Annual Review of Biochemistry*, 57, pp.285–320.
- Fokkema, I.F.A.C. et al., 2011. LOVD v.2.0: the next generation in gene variant databases. *Human Mutation*, 32(5), pp.557–563.
- Fölsch, H. et al., 1999. A novel clathrin adaptor complex mediates basolateral targeting in polarized epithelial cells. *Cell*, 99(2), pp.189–198.
- Fölsch, H., Mattila, P.E. & Weisz, O.A., 2009. Taking the Scenic Route: Biosynthetic Traffic to the Plasma Membrane in Polarized Epithelial Cells. *Traffic (Copenhagen, Denmark)*, 10(8), pp.972–981.
- Förster, C., 2008. Tight junctions and the modulation of barrier function in disease. *Histochemistry and Cell Biology*, 130(1), pp.55–70.
- Fristrom, D., 1988. The cellular basis of epithelial morphogenesis. A review. *Tissue & Cell*, 20(5), pp.645–690.
- Furgason, M.L.M. et al., 2009. The N-terminal peptide of the syntaxin Tlg2p modulates binding of its closed conformation to Vps45p. *Proceedings of the National Academy of Sciences of the United States of America*, 106(34), pp.14303–14308.
- Furth, P.A. et al., 1994. Temporal control of gene expression in transgenic mice by a tetracycline-responsive promoter. *Proceedings of the National Academy of Sciences of the United States of America*, 91(20), pp.9302–9306.
- Furuse, M. et al., 2002. Claudin-based tight junctions are crucial for the mammalian epidermal barrier: a lesson from claudin-1-deficient mice. *The Journal of Cell Biology*, 156(6), pp.1099–1111.
- Gabaldón, T., 2010. Peroxisome diversity and evolution. *Philosophical Transactions of the Royal Society of London. Series B, Biological Sciences*, 365(1541), pp.765–773.
- Gallwitz, D. & Jahn, Reinhard, 2003. The riddle of the Sec1/Munc-18 proteins - new twists added to their interactions with SNAREs. *Trends in Biochemical Sciences*, 28(3), pp.113–116.
- Giacomini, K.M. et al., 2010. Membrane transporters in drug development. *Nature Reviews Drug Discovery*, 9(3), pp.215–236.
- Gissen, P. et al., 2006. Clinical and molecular genetic features of ARC syndrome. *Human Genetics*, 120(3), pp.396–409.
- Gissen, P. et al., 2005. Comparative evolutionary analysis of VPS33 homologues: genetic and functional insights. *Human Molecular Genetics*, 14(10), pp.1261–1270.

- Gissen, P. et al., 2004. Mutations in VPS33B, encoding a regulator of SNARE-dependent membrane fusion, cause arthrogryposis-renal dysfunction-cholestasis (ARC) syndrome. *Nature Genetics*, 36(4), pp.400–404.
- Gossen, M. & Bujard, H., 1992. Tight control of gene expression in mammalian cells by tetracycline-responsive promoters. *Proceedings of the National Academy of Sciences of the United States of America*, 89(12), pp.5547–5551.
- Groen, A. et al., 2011. Complementary functions of the flippase ATP8B1 and the floppase ABCB4 in maintaining canalicular membrane integrity. *Gastroenterology*, 141(5), pp.1927–1937.e1–4.
- Grosse, B. et al., 2011. Claudin-1 involved in neonatal ichthyosis - sclerosing cholangitis syndrome, regulates hepatic paracellular permeability. *Hepatology (Baltimore, Md.)*. Available at: <http://www.ncbi.nlm.nih.gov/pubmed/22030598> [Accessed January 6, 2012].
- Grozovsky, R., Hoffmeister, K.M. & Falet, H., 2010. Novel clearance mechanisms of platelets. *Current Opinion in Hematology*, 17(6), pp.585–589.
- Gualdi, R. et al., 1996. Hepatic specification of the gut endoderm in vitro: cell signaling and transcriptional control. *Genes & Development*, 10(13), pp.1670–1682.
- Di Guglielmo, G.M. et al., 2003. Distinct endocytic pathways regulate TGF-beta receptor signalling and turnover. *Nature Cell Biology*, 5(5), pp.410–421.
- Gunay-Aygun, M. et al., 2011. NBEAL2 is mutated in gray platelet syndrome and is required for biogenesis of platelet  $\alpha$ -granules. *Nature Genetics*, 43(8), pp.732–734.
- Guo, X. et al., 2009. Involvement of vps33a in the fusion of uroplakin-degrading multivesicular bodies with lysosomes. *Traffic (Copenhagen, Denmark)*, 10(9), pp.1350–1361.
- Gupta, I.R. & Ryan, A.K., 2010. Claudins: unlocking the code to tight junction function during embryogenesis and in disease. *Clinical Genetics*, 77(4), pp.314–325.
- Hadj-Rabia, S. et al., 2004. Claudin-1 gene mutations in neonatal sclerosing cholangitis associated with ichthyosis: a tight junction disease. *Gastroenterology*, 127(5), pp.1386–1390.
- Hales, C.M., Vaerman, J.-P. & Goldenring, J.R., 2002. Rab11 family interacting protein 2 associates with Myosin Vb and regulates plasma membrane recycling. *The Journal of Biological Chemistry*, 277(52), pp.50415–50421.
- Hammel, I., Lagunoff, D. & Galli, S.J., 2010. Regulation of secretory granule size by the precise generation and fusion of unit granules. *Journal of Cellular and Molecular Medicine*, 14(7), pp.1904–1916.

- Handagama, P. et al., 1993. Kistrin, an integrin antagonist, blocks endocytosis of fibrinogen into guinea pig megakaryocyte and platelet alpha-granules. *The Journal of Clinical Investigation*, 91(1), pp.193–200.
- Harland, R.M., 1994. The transforming growth factor beta family and induction of the vertebrate mesoderm: bone morphogenetic proteins are ventral inducers. *Proceedings of the National Academy of Sciences of the United States of America*, 91(22), pp.10243–10246.
- Harris, T.J.C. & Tepass, U., 2010. Adherens junctions: from molecules to morphogenesis. *Nat Rev Mol Cell Biol*, 11(7), pp.502–514.
- Harrison, P & Cramer, E M, 1993. Platelet alpha-granules. *Blood Reviews*, 7(1), pp.52–62.
- Harrison, S.D. et al., 1994. Mutations in the Drosophila Rop gene suggest a function in general secretion and synaptic transmission. *Neuron*, 13(3), pp.555–566.
- Hartsock, A. & Nelson, W.J., 2008. Adherens and tight junctions: structure, function and connections to the actin cytoskeleton. *Biochimica Et Biophysica Acta*, 1778(3), pp.660–669.
- Hashizume, K. et al., 2009. Yeast Sec1p functions before and after vesicle docking. *Molecular Biology of the Cell*, 20(22), pp.4673–4685.
- Hata, Y., Slaughter, C.A. & Südhof, T.C., 1993. Synaptic vesicle fusion complex contains unc-18 homologue bound to syntaxin. *Nature*, 366(6453), pp.347–351.
- Hayes, G.L. et al., 2009. Multiple Rab GTPase binding sites in GCC185 suggest a model for vesicle tethering at the trans-Golgi. *Molecular Biology of the Cell*, 20(1), pp.209–217.
- Hayward, C.P. et al., 1996. An autosomal dominant, qualitative platelet disorder associated with multimerin deficiency, abnormalities in platelet factor V, thrombospondin, von Willebrand factor, and fibrinogen and an epinephrine aggregation defect. *Blood*, 87(12), pp.4967–4978.
- Hayward, C.P., 1997. Inherited disorders of platelet alpha-granules. *Platelets*, 8(4), pp.197–209.
- Hoebeeck, J. et al., 2005. Rapid detection of VHL exon deletions using real-time quantitative PCR. *Laboratory Investigation; a Journal of Technical Methods and Pathology*, 85(1), pp.24–33.
- Hofmann, A.F., 1999. Bile Acids: The Good, the Bad, and the Ugly. *Physiology*, 14(1), pp.24–29.
- Horazdovsky, B.F. & Emr, S.D., 1993. The VPS16 gene product associates with a sedimentable protein complex and is essential for vacuolar protein sorting in yeast. *The Journal of Biological Chemistry*, 268(7), pp.4953–4962.

- Horslen, S.P., Quarrell, O.W. & Tanner, M.S., 1994. Liver histology in the arthrogryposis multiplex congenita, renal dysfunction, and cholestasis (ARC) syndrome: report of three new cases and review. *Journal of Medical Genetics*, 31(1), pp.62–64.
- Hosobuchi, M., Kreis, T. & Schekman, Randy, 1992. SEC21 is a gene required for ER to Golgi protein transport that encodes a subunit of a yeast coatmer. *Nature*, 360(6404), pp.603–605.
- Hosono, R. et al., 1992. The unc-18 gene encodes a novel protein affecting the kinetics of acetylcholine metabolism in the nematode *Caenorhabditis elegans*. *Journal of Neurochemistry*, 58(4), pp.1517–1525.
- Huizing, M. et al., 2008. Disorders of lysosome-related organelle biogenesis: clinical and molecular genetics. *Annual Review of Genomics and Human Genetics*, 9, pp.359–386.
- Hutagalung, A.H. & Novick, P.J., 2011. Role of Rab GTPases in membrane traffic and cell physiology. *Physiological Reviews*, 91(1), pp.119–149.
- Ishibashi, H. et al., 2009. Liver architecture, cell function, and disease. *Seminars in Immunopathology*, 31(3), pp.399–409.
- Israels, S.J. et al., 1992. Platelet dense granule membranes contain both granulophysin and P-selectin (GMP-140). *Blood*, 80(1), pp.143–152.
- Italiano, J.E., Jr et al., 2008. Angiogenesis is regulated by a novel mechanism: pro- and antiangiogenic proteins are organized into separate platelet alpha granules and differentially released. *Blood*, 111(3), pp.1227–1233.
- Iyanagi, T., Emi, Y. & Ikushiro, S., 1998. Biochemical and molecular aspects of genetic disorders of bilirubin metabolism. *Biochimica Et Biophysica Acta*, 1407(3), pp.173–184.
- Jacquemin, E., 2001. Role of Multidrug Resistance 3 Deficiency in Pediatric and Adult Liver Disease: One Gene for Three Diseases. *Seminars in Liver Disease*, 21(04), pp.551–562.
- Jahn, R & Scheller, R.H., 2006. SNAREs--engines for membrane fusion. *Nature Reviews. Molecular Cell Biology*, 7(9), pp.631–643.
- Jaisser, F., 2000. Inducible gene expression and gene modification in transgenic mice. *Journal of the American Society of Nephrology: JASN*, 11 Suppl 16, p.S95–S100.
- Jansen, P.L.M. & Sturm, E., 2003. Genetic cholestasis, causes and consequences for hepatobiliary transport. *Liver International: Official Journal of the International Association for the Study of the Liver*, 23(5), pp.315–322.
- Jung, T., Bader, N. & Grune, T., 2007. Lipofuscin: formation, distribution, and metabolic consequences. *Annals of the New York Academy of Sciences*, 1119, pp.97–111.

- Kent, L., 2007. Chapter 13 - Gene-Specific Mutagenesis. In *The Mouse in Biomedical Research (Second Edition)*. Burlington: Academic Press, pp. 261–266. Available at: <http://www.sciencedirect.com/science/article/pii/B978012369454650025X> [Accessed December 13, 2011].
- Kahr, W.H. et al., 2011. Mutations in NBEAL2, encoding a BEACH protein, cause gray platelet syndrome. *Nature Genetics*, 43(8), pp.738–740.
- Kanaseki, T. & Kadota, K., 1969. The ‘vesicle in a basket’. A morphological study of the coated vesicle isolated from the nerve endings of the guinea pig brain, with special reference to the mechanism of membrane movements. *The Journal of Cell Biology*, 42(1), pp.202–220.
- Kaplan, J., De Domenico, I. & Ward, D.M., 2008. Chediak-Higashi syndrome. *Current Opinion in Hematology*, 15(1), pp.22–29.
- Kellendonk, C. et al., 2000. Hepatocyte-specific expression of Cre recombinase. *Genesis (New York, N.Y.: 2000)*, 26(2), pp.151–153.
- Kennedy, M.B., 1995. Origin of PDZ (DHR, GLGF) domains. *Trends in Biochemical Sciences*, 20(9), p.350.
- Kim, B.Y. et al., 2001. Molecular characterization of mammalian homologues of class C Vps proteins that interact with syntaxin-7. *The Journal of Biological Chemistry*, 276(31), pp.29393–29402.
- Kim, S.M. et al., 2010. Agranular platelets as a cardinal feature of ARC syndrome. *Journal of Pediatric Hematology/Oncology*, 32(4), pp.253–258.
- King, S.M. & Reed, G.L., 2002. Development of platelet secretory granules. *Seminars in Cell & Developmental Biology*, 13(4), pp.293–302.
- Kistner, A. et al., 1996. Doxycycline-mediated quantitative and tissue-specific control of gene expression in transgenic mice. *Proceedings of the National Academy of Sciences of the United States of America*, 93(20), pp.10933–10938.
- Kloepper, T.H., Kienle, C.N. & Fasshauer, D., 2007. An elaborate classification of SNARE proteins sheds light on the conservation of the eukaryotic endomembrane system. *Molecular Biology of the Cell*, 18(9), pp.3463–3471.
- Kulkarni, S. et al., 2000. A revised model of platelet aggregation. *The Journal of Clinical Investigation*, 105(6), pp.783–791.
- Lafont, F., Burkhardt, J.K. & Simons, K., 1994. Involvement of microtubule motors in basolateral and apical transport in kidney cells. *Nature*, 372(6508), pp.801–803.
- Lam, P., Wang, Renxue & Ling, V., 2005. Bile acid transport in sister of P-glycoprotein (ABCB11) knockout mice. *Biochemistry*, 44(37), pp.12598–12605.

- Le, T.L., Yap, A.S. & Stow, J L, 1999. Recycling of E-cadherin: a potential mechanism for regulating cadherin dynamics. *The Journal of Cell Biology*, 146(1), pp.219–232.
- Lee, M.C.S. et al., 2004. Bi-directional protein transport between the ER and Golgi. *Annual Review of Cell and Developmental Biology*, 20, pp.87–123.
- Leung-Hagesteijn, C. et al., 2005. Integrin-Linked Kinase Mediates Bone Morphogenetic Protein 7-Dependent Renal Epithelial Cell Morphogenesis. *Molecular and Cellular Biology*, 25(9), pp.3648–3657.
- Li, M. et al., 2010. NHERF-1 binds to Mrp2 and regulates hepatic Mrp2 expression and function. *The Journal of Biological Chemistry*, 285(25), pp.19299–19307.
- Li, R. & Gundersen, G.G., 2008. Beyond polymer polarity: how the cytoskeleton builds a polarized cell. *Nature Reviews. Molecular Cell Biology*, 9(11), pp.860–873.
- Lisanti, M.P. et al., 1989. A glycopospholipid membrane anchor acts as an apical targeting signal in polarized epithelial cells. *The Journal of Cell Biology*, 109(5), pp.2145–2156.
- Lo, B. et al., 2005. Requirement of VPS33B, a member of the Sec1/Munc18 protein family, in megakaryocyte and platelet alpha-granule biogenesis. *Blood*, 106(13), pp.4159–4166.
- Lock, J.G. & Stow, Jennifer L, 2005. Rab11 in recycling endosomes regulates the sorting and basolateral transport of E-cadherin. *Molecular Biology of the Cell*, 16(4), pp.1744–1755.
- Low, S.H. et al., 1996. Differential localization of syntaxin isoforms in polarized Madin-Darby canine kidney cells. *Molecular Biology of the Cell*, 7(12), pp.2007–2018.
- Lubarsky, B. & Krasnow, M.A., 2003. Tube morphogenesis: making and shaping biological tubes. *Cell*, 112(1), pp.19–28.
- Lutz-Richner, A. & Landolt, R., 1973. Familiäre Gallengangsmissbildungen mit tubularer Niereninsuffizienz. *Helv Paediatr Acta*, 28, pp.1–12.
- Mansuy, I.M. et al., 1998. Inducible and reversible gene expression with the rtTA system for the study of memory. *Neuron*, 21(2), pp.257–265.
- Matter, K. & Mellman, I., 1994. Mechanisms of cell polarity: sorting and transport in epithelial cells. *Current Opinion in Cell Biology*, 6(4), pp.545–554.
- Matthews, R.P. et al., 2005. Zebrafish vps33b, an ortholog of the gene responsible for human arthrogryposis-renal dysfunction-cholestasis syndrome, regulates biliary development downstream of the onecut transcription factor hnf6. *Development (Cambridge, England)*, 132(23), pp.5295–5306.
- Mayer, A, Wickner, W. & Haas, A., 1996. Sec18p (NSF)-driven release of Sec17p (alpha-SNAP) can precede docking and fusion of yeast vacuoles. *Cell*, 85(1), pp.83–94.



- Maynard, D.M. et al., 2007. Proteomic analysis of platelet alpha-granules using mass spectrometry. *Journal of Thrombosis and Haemostasis: JTH*, 5(9), pp.1945–1955.
- McBurney, M. et al., 1994. Murine PGK-1 promoter drives widespread but not uniform expression in transgenic mice. *Developmental dynamics : an official publication of the American Association of Anatomists*, 200(4), p.278.
- Meehan, R.R. et al., 1984. Pattern of serum protein gene expression in mouse visceral yolk sac and foetal liver. *The EMBO Journal*, 3(8), pp.1881–1885.
- Mellman, I. & Nelson, W.J., 2008. Coordinated protein sorting, targeting and distribution in polarized cells. *Nature Reviews. Molecular Cell Biology*, 9(11), pp.833–845.
- Messler, S. et al., 2011. The TGF- $\beta$  signaling modulators TRAP1/TGFBRAP1 and VPS39/Vam6/TLP are essential for early embryonic development. *Immunobiology*, 216(3), pp.343–350.
- Metzger, D. & Feil, R., 1999. Engineering the mouse genome by site-specific recombination. *Current Opinion in Biotechnology*, 10(5), pp.470–476.
- Mima, J. et al., 2008. Reconstituted membrane fusion requires regulatory lipids, SNAREs and synergistic SNARE chaperones. *The EMBO Journal*, 27(15), pp.2031–2042.
- Misura, K.M., Scheller, R.H. & Weis, W.I., 2000. Three-dimensional structure of the neuronal-Sec1-syntaxin 1a complex. *Nature*, 404(6776), pp.355–362.
- Mitchell, H. et al., 2004. Ligand-dependent and -independent transforming growth factor-beta receptor recycling regulated by clathrin-mediated endocytosis and Rab11. *Molecular Biology of the Cell*, 15(9), pp.4166–4178.
- Mochizuki, K. et al., 2007. Two N-linked glycans are required to maintain the transport activity of the bile salt export pump (ABCB11) in MDCK II cells. *American Journal of Physiology. Gastrointestinal and Liver Physiology*, 292(3), pp.G818–828.
- Mori, K. et al., 1986. Morphological changes of platelets during the process of platelet aggregation in gray platelet syndrome. *The Tohoku Journal of Experimental Medicine*, 149(4), pp.425–436.
- Mori, K., Suzuki, S. & Sugai, K., 1984. Electron microscopic and functional studies on platelets in gray platelet syndrome. *The Tohoku Journal of Experimental Medicine*, 143(3), pp.261–287.
- Mostov, K.E., de Bruyn Kops, A. & Deitcher, D.L., 1986. Deletion of the cytoplasmic domain of the polymeric immunoglobulin receptor prevents basolateral localization and endocytosis. *Cell*, 47(3), pp.359–364.
- Moustakas, A. & Heldin, C.-H., 2008. Dynamic control of TGF-beta signaling and its links to the cytoskeleton. *FEBS Letters*, 582(14), pp.2051–2065.

- Müller, B. & Grossniklaus, U., 2010. Model organisms--A historical perspective. *Journal of Proteomics*, 73(11), pp.2054–2063.
- Müller, T. et al., 2008. MYO5B mutations cause microvillus inclusion disease and disrupt epithelial cell polarity. *Nature Genetics*, 40(10), pp.1163–1165.
- Müsch, A., 2004. Microtubule organization and function in epithelial cells. *Traffic (Copenhagen, Denmark)*, 5(1), pp.1–9.
- Mushtaq, I. et al., 1999. Screening of newborn infants for cholestatic hepatobiliary disease with tandem mass spectrometry. *BMJ (Clinical Research Ed.)*, 319(7208), pp.471–477.
- Nagle, D.L. et al., 1996. Identification and mutation analysis of the complete gene for Chediak-Higashi syndrome. *Nature Genetics*, 14(3), pp.307–311.
- Nakamura, N. et al., 1997. Vam2/Vps41p and Vam6/Vps39p are components of a protein complex on the vacuolar membranes and involved in the vacuolar assembly in the yeast *Saccharomyces cerevisiae*. *The Journal of Biological Chemistry*, 272(17), pp.11344–11349.
- Nakatsu, F. & Ohno, H., 2003. Adaptor protein complexes as the key regulators of protein sorting in the post-Golgi network. *Cell Structure and Function*, 28(5), pp.419–429.
- Neumann, C. & Cohen, S., 1997. Morphogens and pattern formation. *BioEssays: News and Reviews in Molecular, Cellular and Developmental Biology*, 19(8), pp.721–729.
- Nezelof, C. et al., 1979. A lethal familial syndrome associated with arthrogryposis multiplex congenita, renal dysfunction, and a cholestatic and pigmentary liver disease. *J Pediatr*, 94, p.258–60.
- Nickerson, D.P., Brett, C.L. & Merz, A.J., 2009. Vps-C complexes: gatekeepers of endolysosomal traffic. *Current Opinion in Cell Biology*, 21(4), pp.543–551.
- Nicolaou, M. et al., 2012. Canalicular ABC transporters and liver disease. *The Journal of Pathology*, 226(2), pp.300–315.
- Novick, P., Field, C. & Schekman, R., 1980. Identification of 23 complementation groups required for post-translational events in the yeast secretory pathway. *Cell*, 21(1), pp.205–215.
- Novick, P. & Schekman, R., 1979. Secretion and cell-surface growth are blocked in a temperature-sensitive mutant of *Saccharomyces cerevisiae*. *Proceedings of the National Academy of Sciences of the United States of America*, 76(4), pp.1858–1862.
- Nurden, A.T. & Nurden, P., 2007. The gray platelet syndrome: clinical spectrum of the disease. *Blood Reviews*, 21(1), pp.21–36.
- Ohno, H. et al., 1999. Mu1B, a novel adaptor medium chain expressed in polarized epithelial cells. *FEBS Letters*, 449(2-3), pp.215–220.

- Ohya, T. et al., 2009. Reconstitution of Rab- and SNARE-dependent membrane fusion by synthetic endosomes. *Nature*, 459(7250), pp.1091–1097.
- Ordonez, C. et al., 2007. GPI-anchored CEA family glycoproteins CEA and CEACAM6 mediate their biological effects through enhanced integrin  $\alpha 5 \beta 1$ -fibronectin interaction. *Journal of Cellular Physiology*, 210(3), pp.757–765.
- Ostrowicz, C.W. et al., 2010. Defined subunit arrangement and rab interactions are required for functionality of the HOPS tethering complex. *Traffic (Copenhagen, Denmark)*, 11(10), pp.1334–1346.
- Paganelli, M. et al., 2011. Neonatal ichthyosis and sclerosing cholangitis syndrome: extremely variable liver disease severity from claudin-1 deficiency. *Journal of Pediatric Gastroenterology and Nutrition*, 53(3), pp.350–354.
- Palade, G., 1975. Intracellular aspects of the process of protein synthesis. *Science (New York, N.Y.)*, 189(4200), pp.347–358.
- Paulick, M.G. & Bertozzi, C.R., 2008. The glycosylphosphatidylinositol anchor: a complex membrane-anchoring structure for proteins. *Biochemistry*, 47(27), pp.6991–7000.
- Peplowska, K. et al., 2007. The CORVET tethering complex interacts with the yeast Rab5 homolog Vps21 and is involved in endo-lysosomal biogenesis. *Developmental Cell*, 12(5), pp.739–750.
- Perwaiz, S. et al., 2003. Appearance of atypical 3  $\alpha$ ,6  $\beta$ ,7  $\beta$ ,12  $\alpha$ -tetrahydroxy-5  $\beta$ -cholan-24-oic acid in spgp knockout mice. *Journal of Lipid Research*, 44(3), pp.494–502.
- Pevsner, J. et al., 1996. Mammalian homologues of yeast vacuolar protein sorting (vps) genes implicated in Golgi-to-lysosome trafficking. *Gene*, 183(1-2), pp.7–14.
- Pieren, M., Schmidt, A. & Mayer, Andreas, 2010. The SM protein Vps33 and the t-SNARE H(abc) domain promote fusion pore opening. *Nature Structural & Molecular Biology*, 17(6), pp.710–717.
- Pinkert, C.A. et al., 1987. An albumin enhancer located 10 kb upstream functions along with its promoter to direct efficient, liver-specific expression in transgenic mice. *Genes & Development*, 1(3), pp.268–276.
- Plemel, R.L. et al., 2011. Subunit organization and Rab interactions of Vps-C protein complexes that control endolysosomal membrane traffic. *Molecular Biology of the Cell*, 22(8), pp.1353–1363.
- Postic, C & Magnuson, M.A., 2000. DNA excision in liver by an albumin-Cre transgene occurs progressively with age. *Genesis (New York, N.Y.: 2000)*, 26(2), pp.149–150.
- Postic, Catherine et al., 1999. Dual Roles for Glucokinase in Glucose Homeostasis as Determined by Liver and Pancreatic  $\beta$  Cell-specific Gene Knock-outs Using Cre Recombinase. *Journal of Biological Chemistry*, 274(1), pp.305–315.

- Powell, D.W., 1981. Barrier function of epithelia. *The American Journal of Physiology*, 241(4), pp.G275–288.
- Preston, R.A. et al., 1991. Isolation and characterization of PEP3, a gene required for vacuolar biogenesis in *Saccharomyces cerevisiae*. *Molecular and Cellular Biology*, 11(12), pp.5801–5812.
- Pulipparacharuvil, S. et al., 2005. *Drosophila* Vps16A is required for trafficking to lysosomes and biogenesis of pigment granules. *Journal of Cell Science*, 118(16), pp.3663–3673.
- Raccuglia, G., 1971. Gray platelet syndrome. A variety of qualitative platelet disorder. *The American Journal of Medicine*, 51(6), pp.818–828.
- Rand, J. et al., 1987. Localization of surface vWF on resting and stimulated platelets. *Blood*, 70(5), pp.1297–1302.
- Raymond, C.K. et al., 1992. Morphological classification of the yeast vacuolar protein sorting mutants: evidence for a prevacuolar compartment in class E vps mutants. *Molecular Biology of the Cell*, 3(12), pp.1389–1402.
- Ren, Q., Ye, S. & Whiteheart, S.W., 2008. The platelet release reaction: just when you thought platelet secretion was simple. *Current Opinion in Hematology*, 15(5), pp.537–541.
- Rendu, F. et al., 1983. Evidence that abnormal platelet functions in human Chédiak-Higashi syndrome are the result of a lack of dense bodies. *The American Journal of Pathology*, 111(3), pp.307–314.
- Rendu, F. & Brohard-Bohn, B., 2001. The platelet release reaction: granules' constituents, secretion and functions. *Platelets*, 12(5), pp.261–273.
- Rieder, S.E. & Emr, S.D., 1997. A novel RING finger protein complex essential for a late step in protein transport to the yeast vacuole. *Molecular Biology of the Cell*, 8(11), pp.2307–2327.
- Rindler, M.J., Ivanov, I.E. & Sabatini, D.D., 1987. Microtubule-acting drugs lead to the nonpolarized delivery of the influenza hemagglutinin to the cell surface of polarized Madin-Darby canine kidney cells. *The Journal of Cell Biology*, 104(2), pp.231–241.
- Robinson, M.S., 2004. Adaptable adaptors for coated vesicles. *Trends in Cell Biology*, 14(4), pp.167–174.
- Robinson, M.S. & Bonifacino, J.S., 2001. Adaptor-related proteins. *Current Opinion in Cell Biology*, 13(4), pp.444–453.
- Di Rocco, M. et al., 1990. Arthrogryposis, cholestatic pigmentary liver disease and renal dysfunction: report of a second family. *American Journal of Medical Genetics*, 37(2), pp.237–240.

- Roland, J.T. et al., 2011. Rab GTPase-Myo5B complexes control membrane recycling and epithelial polarization. *Proceedings of the National Academy of Sciences of the United States of America*, 108(7), pp.2789–2794.
- Rosa, J.P. et al., 1987. Gray platelet syndrome. Demonstration of alpha granule membranes that can fuse with the cell surface. *The Journal of Clinical Investigation*, 80(4), pp.1138–1146.
- Ruggeri, Z.M. & Mendolicchio, G.L., 2007. Adhesion Mechanisms in Platelet Function. *Circulation Research*, 100(12), pp.1673–1685.
- Sachse, M. et al., 2002. Bilayered Clathrin Coats on Endosomal Vacuoles Are Involved in Protein Sorting toward Lysosomes. *Molecular Biology of the Cell*, 13(4), pp.1313–1328.
- Sai, Y., Nies, A. t. & Arias, I. m., 1999. Bile acid secretion and direct targeting of mdrl-green fluorescent protein from Golgi to the canalicular membrane in polarized WIF-B cells. *Journal of Cell Science*, 112(24), pp.4535–4545.
- Sakaguchi, T.F. et al., 2008. Endothelial signals modulate hepatocyte apicobasal polarization in zebrafish. *Current Biology: CB*, 18(20), pp.1565–1571.
- Salles, I.I. et al., 2008. Inherited traits affecting platelet function. *Blood Reviews*, 22(3), pp.155–172.
- Sauer, B., 1998. Inducible gene targeting in mice using the Cre/lox system. *Methods (San Diego, Calif.)*, 14(4), pp.381–392.
- Schlüter, M.A. & Margolis, B., 2009. Apical Lumen Formation in Renal Epithelia. *Journal of the American Society of Nephrology*, 20(7), pp.1444–1452.
- Schober, A. et al., 2002. Deposition of platelet RANTES triggering monocyte recruitment requires P-selectin and is involved in neointima formation after arterial injury. *Circulation*, 106(12), pp.1523–1529.
- Schuck, S. & Simons, K., 2004. Polarized sorting in epithelial cells: raft clustering and the biogenesis of the apical membrane. *Journal of Cell Science*, 117(Pt 25), pp.5955–5964.
- Seals, D.F. et al., 2000a. A Ypt/Rab effector complex containing the Sec1 homolog Vps33p is required for homotypic vacuole fusion. *Proceedings of the National Academy of Sciences of the United States of America*, 97(17), pp.9402–9407.
- Seals, D.F. et al., 2000b. A Ypt/Rab effector complex containing the Sec1 homolog Vps33p is required for homotypic vacuole fusion. *Proceedings of the National Academy of Sciences of the United States of America*, 97(17), pp.9402–9407.
- Seemann, J., Jokitalo, E.J. & Warren, G., 2000. The role of the tethering proteins p115 and GM130 in transport through the Golgi apparatus in vivo. *Molecular Biology of the Cell*, 11(2), pp.635–645.

- Sevrioukov, E.A. et al., 1999. A role for the deep orange and carnation eye color genes in lysosomal delivery in *Drosophila*. *Molecular Cell*, 4(4), pp.479–486.
- Sharma, N. et al., 2006. Apical targeting of syntaxin 3 is essential for epithelial cell polarity. *The Journal of Cell Biology*, 173(6), pp.937–948.
- Shenolikar, S. et al., 2002. Targeted disruption of the mouse NHERF-1 gene promotes internalization of proximal tubule sodium-phosphate cotransporter type IIa and renal phosphate wasting. *Proceedings of the National Academy of Sciences of the United States of America*, 99(17), pp.11470–11475.
- Sherry, S.T. et al., 2001. dbSNP: the NCBI database of genetic variation. *Nucleic Acids Research*, 29(1), pp.308–311.
- Shorter, J. et al., 2002. Sequential tethering of Golgins and catalysis of SNAREpin assembly by the vesicle-tethering protein p115. *The Journal of Cell Biology*, 157(1), pp.45–62.
- Sinka, R. et al., 2008. Golgi coiled-coil proteins contain multiple binding sites for Rab family G proteins. *The Journal of Cell Biology*, 183(4), pp.607–615.
- Söllner, T. et al., 1993. SNAP receptors implicated in vesicle targeting and fusion. *Nature*, 362(6418), pp.318–324.
- Son, S. et al., 2009. Knockdown of tight junction protein claudin-2 prevents bile canalicular formation in WIF-B9 cells. *Histochemistry and Cell Biology*, 131(3), pp.411–424.
- Song, K.S. et al., 2003. *Korean Journal of Hematology*, 23, pp.68–72.
- Sönnichsen, B. et al., 1998. A role for giantin in docking COPI vesicles to Golgi membranes. *The Journal of Cell Biology*, 140(5), pp.1013–1021.
- Sriram, V., Krishnan, K.S. & Mayor, S., 2003. deep-orange and carnation define distinct stages in late endosomal biogenesis in *Drosophila melanogaster*. *The Journal of Cell Biology*, 161(3), pp.593–607.
- St. Croix, B. et al., 1998. E-Cadherin-dependent Growth Suppression is Mediated by the Cyclin-dependent Kinase Inhibitor p27KIP1. *The Journal of Cell Biology*, 142(2), pp.557–571.
- Starcevic, M. & Dell'Angelica, Esteban C, 2004. Identification of snapin and three novel proteins (BLOS1, BLOS2, and BLOS3/reduced pigmentation) as subunits of biogenesis of lysosome-related organelles complex-1 (BLOC-1). *The Journal of Biological Chemistry*, 279(27), pp.28393–28401.
- Stenmark, H. & Olkkonen, V.M., 2001. The Rab GTPase family. *Genome Biology*, 2(5), p.REVIEWS3007.
- Sternberg, N. & Hamilton, D., 1981. Bacteriophage P1 site-specific recombination. I. Recombination between loxP sites. *Journal of Molecular Biology*, 150(4), pp.467–486.

- Stevenson, B.R. et al., 1986. Identification of ZO-1: a high molecular weight polypeptide associated with the tight junction (zonula occludens) in a variety of epithelia. *The Journal of Cell Biology*, 103(3), pp.755–766.
- Strautnieks, S.S. et al., 1998. A gene encoding a liver-specific ABC transporter is mutated in progressive familial intrahepatic cholestasis. *Nature Genetics*, 20(3), pp.233–238.
- Stroupe, C. et al., 2009. Minimal membrane docking requirements revealed by reconstitution of Rab GTPase-dependent membrane fusion from purified components. *Proceedings of the National Academy of Sciences of the United States of America*, 106(42), pp.17626–17633.
- Stroupe, C. et al., 2006. Purification of active HOPS complex reveals its affinities for phosphoinositides and the SNARE Vam7p. *The EMBO Journal*, 25(8), pp.1579–1589.
- Stryke, D. et al., 2003. BayGenomics: a resource of insertional mutations in mouse embryonic stem cells. *Nucleic Acids Research*, 31(1), pp.278–281.
- Subramanian, S., Woolford, Carol A & Jones, E.W., 2004. The Sec1/Munc18 protein, Vps33p, functions at the endosome and the vacuole of *Saccharomyces cerevisiae*. *Molecular Biology of the Cell*, 15(6), pp.2593–2605.
- Südhof, T.C. & Rothman, J.E., 2009. Membrane fusion: grappling with SNARE and SM proteins. *Science (New York, N.Y.)*, 323(5913), pp.474–477.
- Suh, T.T. et al., 1995. Resolution of spontaneous bleeding events but failure of pregnancy in fibrinogen-deficient mice. *Genes & Development*, 9(16), pp.2020–2033.
- Suzuki, T. et al., 2003. The mouse organellar biogenesis mutant buff results from a mutation in Vps33a, a homologue of yeast vps33 and *Drosophila* carnation. *Proceedings of the National Academy of Sciences of the United States of America*, 100(3), pp.1146–1150.
- Sztul, E. & Lupashin, V., 2006. Role of tethering factors in secretory membrane traffic. *American Journal of Physiology. Cell Physiology*, 290(1), pp.C11–26.
- Tai, A.W. et al., 1999. Rhodopsin's Carboxy-Terminal Cytoplasmic Tail Acts as a Membrane Receptor for Cytoplasmic Dynein by Binding to the Dynein Light Chain Tctex-1. *Cell*, 97(7), pp.877–887.
- Takahashi, D. et al., 2011. The epithelia-specific membrane trafficking factor AP-1B controls gut immune homeostasis in mice. *Gastroenterology*, 141(2), pp.621–632.
- Takahashi, K. & Suzuki, K., 1996. Density-dependent inhibition of growth involves prevention of EGF receptor activation by E-cadherin-mediated cell-cell adhesion. *Experimental Cell Research*, 226(1), pp.214–222.
- Takeda, T., Hosokawa, M. & Higuchi, K., 1997. Senescence-accelerated mouse (SAM): a novel murine model of senescence. *Experimental Gerontology*, 32(1-2), pp.105–109.

- Tanaka, M. et al., 2011. Liver stem/progenitor cells: their characteristics and regulatory mechanisms. *Journal of Biochemistry*, 149(3), pp.231–239.
- Tchernev, V.T. et al., 2002. The Chediak-Higashi protein interacts with SNARE complex and signal transduction proteins. *Molecular Medicine (Cambridge, Mass.)*, 8(1), pp.56–64.
- Theiler, K., 1989. The House Mouse, Atlas of Embryonic Development pg26-34. In *The House Mouse, Atlas of Embryonic Development*.
- Thomas, K.R. & Capecchi, M.R., 1987. Site-directed mutagenesis by gene targeting in mouse embryo-derived stem cells. *Cell*, 51(3), pp.503–512.
- Tiedt, R. et al., 2007. Pf4-Cre transgenic mice allow the generation of lineage-restricted gene knockouts for studying megakaryocyte and platelet function in vivo. *Blood*, 109(4), pp.1503–1506.
- Trauner, M. & Boyer, J.L., 2003. Bile salt transporters: molecular characterization, function, and regulation. *Physiological Reviews*, 83(2), pp.633–671.
- Tremblay, P. et al., 1998. Doxycycline control of prion protein transgene expression modulates prion disease in mice. *Proceedings of the National Academy of Sciences of the United States of America*, 95(21), pp.12580–12585.
- Vagin, O., Kraut, J.A. & Sachs, G., 2009. Role of N-glycosylation in trafficking of apical membrane proteins in epithelia. *American Journal of Physiology. Renal Physiology*, 296(3), pp.F459–469.
- Verhage, M. et al., 2000. Synaptic assembly of the brain in the absence of neurotransmitter secretion. *Science (New York, N.Y.)*, 287(5454), pp.864–869.
- de Vree, J.M. et al., 1998. Mutations in the MDR3 gene cause progressive familial intrahepatic cholestasis. *Proceedings of the National Academy of Sciences of the United States of America*, 95(1), pp.282–287.
- Wada, Y., Ohsumi, Y. & Anraku, Y., 1992. Genes for directing vacuolar morphogenesis in *Saccharomyces cerevisiae*. I. Isolation and characterization of two classes of vam mutants. *The Journal of Biological Chemistry*, 267(26), pp.18665–18670.
- Wakabayashi, Y., Kipp, H. & Arias, I.M., 2006. Transporters on Demand: Intracellular Reservoirs and Cycling of Bile Canalicular ABC Transporters. *Journal of Biological Chemistry*, 281(38), pp.27669–27673.
- Wakabayashi, Y., Lippincott-Schwartz, J. & Arias, I.M., 2004. Intracellular trafficking of bile salt export pump (ABCB11) in polarized hepatic cells: constitutive cycling between the canalicular membrane and rab11-positive endosomes. *Molecular Biology of the Cell*, 15(7), pp.3485–3496.
- Wanders, R.J.A. & Waterham, H.R., 2006. Biochemistry of Mammalian Peroxisomes Revisited. *Annual Review of Biochemistry*, 75(1), pp.295–332.



- Wang, Q. & Margolis, B., 2007. Apical junctional complexes and cell polarity. *Kidney International*, 72(12), pp.1448–1458.
- Wang, R et al., 2001. Targeted inactivation of sister of P-glycoprotein gene (spgp) in mice results in nonprogressive but persistent intrahepatic cholestasis. *Proceedings of the National Academy of Sciences of the United States of America*, 98(4), pp.2011–2016.
- Wang, Renxue et al., 2009. Compensatory role of P-glycoproteins in knockout mice lacking the bile salt export pump. *Hepatology (Baltimore, Md.)*, 50(3), pp.948–956.
- Wang, Renxue et al., 2003. Severe cholestasis induced by cholic acid feeding in knockout mice of sister of P-glycoprotein. *Hepatology (Baltimore, Md.)*, 38(6), pp.1489–1499.
- Wang, X. et al., 2000. Regulation of vesicle trafficking in madin-darby canine kidney cells by Rab11a and Rab25. *The Journal of Biological Chemistry*, 275(37), pp.29138–29146.
- Ward, D.M. et al., 2003. Use of expression constructs to dissect the functional domains of the CHS/beige protein: identification of multiple phenotypes. *Traffic (Copenhagen, Denmark)*, 4(6), pp.403–415.
- Watanabe, T. et al., 2004. Interaction with IQGAP1 links APC to Rac1, Cdc42, and actin filaments during cell polarization and migration. *Developmental Cell*, 7(6), pp.871–883.
- Waters, M.G., Clary, D.O. & Rothman, J.E., 1992. A novel 115-kD peripheral membrane protein is required for intercisternal transport in the Golgi stack. *The Journal of Cell Biology*, 118(5), pp.1015–1026.
- Waters, M.G. & Hughson, F M, 2000. Membrane Tethering and Fusion in the Secretory and Endocytic Pathways. *Traffic*, 1(8), pp.588–597.
- Watson, S.P. & Harrison, Paul, 2007. The Vascular Function of Platelets. In pp. 772–792. Available at:  
<http://onlinelibrary.wiley.com.ezproxyd.bham.ac.uk/doi/10.1002/9781444323160.ch40/summary> [Accessed February 15, 2012].
- Wei, M.L., 2006. Hermansky-Pudlak syndrome: a disease of protein trafficking and organelle function. *Pigment Cell Research / Sponsored by the European Society for Pigment Cell Research and the International Pigment Cell Society*, 19(1), pp.19–42.
- Weimbs, T. et al., 1997. Apical targeting in polarized epithelial cells: There's more afloat than rafts. *Trends in Cell Biology*, 7(10), pp.393–399.
- Weisend, C.M. et al., 2009. Cre activity in fetal albCre mouse hepatocytes: Utility for developmental studies. *genesis*, 47(12), pp.789–792.
- Weisz, O.A. & Rodriguez-Boulan, E., 2009. Apical trafficking in epithelial cells: signals, clusters and motors. *Journal of Cell Science*, 122(Pt 23), pp.4253–4266.

- White, J.G., 1979. Ultrastructural studies of the gray platelet syndrome. *The American Journal of Pathology*, 95(2), pp.445–462.
- Wickner, W., 2010. Membrane fusion: five lipids, four SNAREs, three chaperones, two nucleotides, and a Rab, all dancing in a ring on yeast vacuoles. *Annual Review of Cell and Developmental Biology*, 26, pp.115–136.
- Wildeman, &#32;Martin et al., 2008. Improving sequence variant descriptions in mutation databases and literature using the Mutalyzer sequence variation nomenclature checker. *Human Mutation*, 29(1), pp.6–13.
- Wilton, J.C. & Matthews, G.M., 1996. Polarised membrane traffic in hepatocytes. *BioEssays*, 18(3), pp.229–236.
- Woolford, C A et al., 1990. Isolation and characterization of PEP5, a gene essential for vacuolar biogenesis in *Saccharomyces cerevisiae*. *Genetics*, 125(4), pp.739–752.
- Xu, X. et al., 2006. A novel fibrinogen B $\beta$  chain frameshift mutation in a patient with severe congenital hypofibrinogenemia. *Thrombosis and Haemostasis*. Available at: [http://www.schattauer.de/index.php?id=1214&doi=10.1160/TH06-01-0020&no\\_cache=1](http://www.schattauer.de/index.php?id=1214&doi=10.1160/TH06-01-0020&no_cache=1) [Accessed February 15, 2012].
- Yamaguchi, T. et al., 2002. Sly1 binds to Golgi and ER syntaxins via a conserved N-terminal peptide motif. *Developmental Cell*, 2(3), pp.295–305.
- Yamamoto, A., Hen, R. & Dauer, W.T., 2001. The Ons and Offs of Inducible Transgenic Technology: A Review. *Neurobiology of Disease*, 8(6), pp.923–932.
- Youssefian, T. & Cramer, Elisabeth M., 2000. Megakaryocyte dense granule components are sorted in multivesicular bodies. *Blood*, 95(12), pp.4004 –4007.
- Yu, I.-M. & Hughson, Frederick M, 2010a. Tethering factors as organizers of intracellular vesicular traffic. *Annual Review of Cell and Developmental Biology*, 26, pp.137–156.
- Yu, I.-M. & Hughson, Frederick M, 2010b. Tethering factors as organizers of intracellular vesicular traffic. *Annual Review of Cell and Developmental Biology*, 26, pp.137–156.
- Zhang, H. et al., 2007. Lysosomal membranes from beige mice contain higher than normal levels of endoplasmic reticulum proteins. *Journal of Proteome Research*, 6(1), pp.240–249.
- Zhu, G. et al., 2009. SPE-39 family proteins interact with the HOPS complex and function in lysosomal delivery. *Molecular Biology of the Cell*, 20(4), pp.1223–1240.
- Zhu, G.-D. & L'Hernault, S.W., 2003. The *Caenorhabditis elegans* spe-39 gene is required for intracellular membrane reorganization during spermatogenesis. *Genetics*, 165(1), pp.145–157.
- Zink, S. et al., 2009. A link between ER tethering and COP-I vesicle uncoating. *Developmental Cell*, 17(3), pp.403–416.

Zlatic, S.A., Tornieri, K., L'Hernault, S.W., et al., 2011. Clathrin-dependent mechanisms modulate the subcellular distribution of class C Vps/HOPS tether subunits in polarized and nonpolarized cells. *Molecular Biology of the Cell*, 22(10), pp.1699–1715.

Zlatic, S.A., Tornieri, K., L'hernault, S.W., et al., 2011. Metazoan cell biology of the HOPS tethering complex. *Cellular Logistics*, 1(3), pp.111–117.

# **MANUSCRIPTS AND PEER REVIEWED PAPERS**

1. Smith, H. et al. Associations among genotype, clinical phenotype and intracellular localization of trafficking proteins in ARC syndrome.  
Human Mutation (2012).doi:10.1002/humu.22155
2. Unsworth, A. J., Smith, H., Gissen, P., Watson, S. P. & Pears, C. J. Submaximal inhibition of protein kinase C restores ADP-induced dense granule secretion in platelets in the presence of  $\text{Ca}^{2+}$ .  
J. Biol. Chem. 286, 21073–21082 (2011).